Development of a discrete numerical approach to the Fredholm Integral Method for evaluating microwave scattering by irregular hydrometeors

Felix Opuama Ngobigha

A thesis submitted for the degree of *Doctor of Philosophy*

School of Computer Science and Electronic Engineering

University of Essex

Date of Submission: December, 2015

Dedication

To my family

Abstract

A new approach to the implementation of Fredholm Integral Method (FIM) was developed to evaluate microwave scattering by irregular hydrometeors in the melting layer where snowflakes aggregate. These contain air, ice and liquid water and therefore complex to model. In this study, the particles were modelled discretizing their volume, filling it with cubic or spherical cells according to their weighted contents. The FIM presented represents a departure from earlier work where the numerical integration is no longer based on expansion in a set of polynomials but based on direct spatial integration. The strength of our approach is that the computations are performed in the spatial frequency domain. As a result, the angular scattering pattern is strongly connected to the Spatial Fourier Transform of the scatterer; hence, for electrically small particles the angular spectrum is relatively smooth and the number of pivots required for integration is relatively low. The theoretical analysis of the first Born term is comparatively simple. Comparisons show a good agreement between the first Born term using our approach and the exact method by Holt. However, the theory of the second Born term is relatively difficult. The approach taken by Hankel cannot be applied essentially because of the power of p in the integrand being odd. An alternative approach which still involves contour integration method uses quandrantal contour in combination with a conditioning weighting function to control the magnitude of the integrand. The numerical evaluation of the scattering functions are performed and compared. The results suggested similar pattern in comparison with the Mie theory and other established numerical algorithms for homogeneous spherical or ellipsoidal dielectric scatterers. This technique has a good potential to be applied to irregular hydrometeors since only the distribution of the dielectric constants need to be changed.

Acknowledgements

I would like to thank Almighty God and everyone that helped exceedingly in completing this thesis.

A special gratitude goes to my supervisor David H.O. Bebbington, who gave me the opportunity to start this adventure and introduced me to the field of electromagnetic waves propagation and scattering by small particles and numerical analysis method. He supported me tremendously and unconditionally offered me his wealth of experience, and outstanding guidance at all stages of this work; without him I believe this thesis would have been very different.

I am very thankful to Laura Carrea for her continued interest, comments, suggestions and kindness for always being available for fruitful exchanges on the mathematical aspects of this thesis and with whom I had very insightful discussions on theoretical physics, also for proof-reading this thesis.

I gratefully acknowledge the financial support of my sponsor; Petroleum Trust Development Fund (PTDF), for making my dreams come true.

I would like to express my deepest gratitude to my wife: Ebiere; children: Naomi, Taripredo and Preye; mum: Hausaere; siblings: Ebiye, Ukiye, Werenipre and Donkumo for their dedication, love, and support in all my endeavours.

To Philips E. Orubide and John T. Afa for their words of encouragement inspired me to undertake doctoral programme.

I am thankful to all of my colleagues in the School of Computer Science and Electronic Engineering for the enjoyable atmosphere and for their help, with particular

mention to: Peter Damuut, Adewale Abe, Bostanci Gazi and Arief Setyanto.

Thanks also to the school IT service team with special mention to: Bob Self for his excellent computer support, and Robin Dowling when I needed other technical support.

Acronyms and abbreviations

BB	Bright Band
DDA	Discrete Dipole Approximation
DDRM	Debye Double Relaxation Method
EBCM	Extended Boundary Condition Method
EM	Electromagnetic
EMTs	Effective Medium Theories
FIE	Fredholm Integral Equation
FIM	Fredholm Integral Method
GGM	Generalized Multiparticle Method
IE	Integral Equation
LU	Lower and Upper triangular matrices
MG	Maxwell-Garnett
MMEs	Macroscopic Maxwell's Equations
MMw	Millimetre Waves
MP	Marshall and Palmer
RTT	Radiative Transfer Theory
TMM	T-Matrix Method
PSD	Particle Size Distribution
VoIE	Volume Integral Equation
VSWF	Vector Spherical Wave Function

CONTENTS

LIST OF FIGURES

LIST OF TABLES

LIST OF ALGORITHMS

CHAPTER 1

INTRODUCTION

The aim of this study is to evaluate scattering amplitude functions of dielectric particles modelled as irregular scatterer consisting of different homogeneous inclusions using the approach of Volume Integral Equation (VoIE) known as Fredholm Integral Method (FIM) to characterise scattering properties of inhomogeneous hydrometeors. Characterisation of particles without making physical or direct contact can be broadly described as remote sensing [1]. Thus this is in contrast to in-situ observation . In weather radar parlance, the term generally refers to the use of sensor technologies to detect and classify objects on Earth (both on the surface and atmosphere) by means of propagated and scattered waves [2]. The concept is actually not new, as every living creature practice the act unknowingly on daily basis through a very important sensor called the eye, intended for detecting op-

tical waves. This process is the oldest and perhaps the primary remote sensing technique employed in many applications, such as Earth atmosphere observation. A big part of the EM spectrum can be used for these purposes. In this thesis, the scattering characteristics of precipitation such as melting irregular hydrometeors in weather radars frequency range [3] are studied.

Recent studies have explored the possibility to use weather radar at high frequency bands to obtain the properties of irregular hydrometeors. The region of short microwave have been studied due to availability of large bandwidth at these frequencies. Nevertheless, the challenge in using these bands to describe the scattering properties of irregular hydrometeors is that strong interactions (absorption and scattering) may occur between such waves and the atmospheric hydrometeors (such as rain, snow, hail and ice crystals) [4] and [5].

In general, there are two approaches to the problem of scattering by small particles: (1) wave theory and (2) radiative transport theory. In the wave theory method, solutions are obtained directly by solving Macroscopic Maxwell Equations (MMEs) for the fields, while the radiative transport technique is formulated on the basis of energy equilibrium [6]. The relationship between the radiative transfer approach and the wave theory method using MMEs has been explicitly given in [7]. The application of the transport theory and related studies have also been explored in great details in [8]. In this thesis, the wave theory method has been explored since we are interested in studying the single scattering.

The wave theory method stems from the way electromagnetic waves propagate in a medium by change in magnetic field will induce a change in the electric field and vice-visa. These fields coexist and they are linked through Maxwell equations. The interaction of the EM waves with the medium can be grouped

into two categories: (a) scattering and absorption of a wave from a medium and (b) line-of-sight propagation of a wave through a medium. For each of these two cases, waves are somehow distorted when travelling through the medium. The degree of influence and the way they are affected often depends upon the frequency and other factors [8, 9]. The mechanisms behind the fields interaction with these media are diverse, however, can generally be attributed to the following: diffraction, refraction, and reflection (diffused and specular).

The reflection mechanism is the most important in this study and it plays a significant role in EM waves scattering by irregular bodies. Assuming a plane electromagnetic wave incident on a scatterer, the energy is reflected in two possible ways:

- Specular reflection : The mirror-like reflection of wave from a surface, in which radiation from a source is reflected into a single outgoing direction. Specular reflection is described by the law of reflection, which states that the direction of the incoming wave (the incident field), and the direction of the outgoing wave (the reflected field) make the same angle with respect to the surface normal, thus the angle of incidence equals the angle of reflection ($\theta_i = \theta_r$). Moreover the incident, the normal to the surface, and the reflected directions are coplanar [10].

- Diffuse reflection: EM waves is radiated from a surface such that an incident wave is scattered in many angles rather than just one angle as in the case of specular reflection.

The diffused reflection does not simply involve the surface only, the contribution to the total reflected field basically involved the scattering centres beneath and

the surface of the particles. This description is very general, because the majority of the naturally occurring bodies are made of microscopic irregular structures held together which give rise to a diffuse process. In this thesis, we take into account this factor and we study the microwave diffuse reflection also known as electromagnetic scattering by particles in the microwave region.

1.1 Motivation

Most of the hydrometeors have more than two dielectric constants including air. Effective medium theories for two-part dielectrics have been fully developed where one of the dielectrics can be regarded as an inclusion in the other (host or background). There is yet no known unique effective medium mixing formula or Effective Medium Theory (EMTs) for three or more dielectric components. However, naturally occurring scatterer (irregular hydrometeors) are characterised by more than two dielectric components. It has been suggested that estimation of their effective dielectric constant could be done by average the optical properties of the composite materials (two-part effective medium mixing formula) and subsequently evaluating the scattering characteristics. Nevertheless, this is not fully consistent with the complex nature of the scatterer. Moreover, for weather radar, the melting layer in which melting snowflakes aggregates contain air, ice and wet-water and therefore it is difficult to model. In [11], an assumption to simplify the problem has been made: melting hydrometeors are described to assume no change in geometrical and electrical characteristics in the transition region (a region between the dry ice crystal particles and raindrops). Nevertheless, this assumption has been found to be unsatisfactory owing to the complex nature of these scatterers within this layer and the problem has not been fully investigated either experimentally

or theoretically.

Few methods have been explored such as the Discrete Dipole Approximation (DDA) by DeVoe [12] and the FIM by Holt et. al [13]. In the DDA, the particle is replaced with interacting dipoles. With this approach the number of matrix equations to be solved increases if the particle is electrically large and the problem becomes computationally difficult. The FIM approach of Holt uses an integral equation to calculate the scattering characteristic of the particle. However, as also stated by the author the main limitation is that the evaluation of the second Born matrix elements is limited for inhomogeneous scatterer. Consequently, these techniques are inadequate to describe the scattering properties of irregular hydrometeors.

In this work we consider a new perspective still based on the FIM but in contrast with the approach of Holt. Instead of using an expansion in a set of polynomials we apply a direct spatial integration. However, our approach retains the property of having second order accuracy owing to the variational properties of the integral. The scatterer is modelled within a finite regular lattice field of cubic or spherical cells. The first and second Born terms are evaluated for a cell at the origin, while the contributions for all other cells are evaluated efficiently using the Fourier Shift Theorem.

We have named our numerical approach to the Fredholm Integral Method (FIM) as the Discrete Method (DM) where we expressly evaluate scattering amplitude functions of irregular hydrometeors by relatively avoiding any of the established effective medium theories or empirical methods.

1.2 Thesis outline

The remainder of this chapter describes the layout of the thesis, which is organised into a further five chapters.

Chapter 2 starts with Macroscopic Maxwell equations to describe electromagnetic fields and wave equations in dielectric media. A brief description of micro-physics of melting snowflakes within the Bright Band layer is presented. Then, a concise survey of scattering particle characteristics at this layer is given. In addition, numerical and empirical formulae for evaluating dielectric properties of complex mixture constituents are presented with emphasis on the single relaxation method known as Debye formula. Few effective medium theories are reviewed, with focus on widely used methods such as Maxwell-Garnett, Bruggeman and Coherent Potential. Finally, a theoretical overview of electromagnetic waves scattering problems by small particles is briefly presented with emphasis on Mie Theory, T-Matrix Method and Discrete Dipole Approximation, since they can be used to validate the new implementation of the FIM approach.

Chapter 3 presents a concise analysis of volume integral equations with special attention to Fredholm linear Integral Equation of the second kind used in previous work for the solution of electromagnetic waves scattering by homogeneous dielectric ellipsoids and spheroids. Our approach, the Discrete Method is introduced and fully developed.

Chapter 4 presents the code level implementation of the Discrete Method. The algorithm is developed using Fortran programming language and separated into sub-programs or modules. Block diagram which summarizes the program structure and logic flow are given. In addition, the algorithm is designed to give the user

some flexibility to select different program mode such as variable angles, fixed angle for forward and back scattered radiation. The validity, stability and accuracy of core parts of the algorithm are validated.

Chapter 5 begins with the modelling of scattering particles using standard ellipsoid equation inscribed in a discretized finite lattice field. Then the validity of the proposed Discrete Method is verified by computing the scattering amplitude functions of homogeneous dielectric spherical particle. The numerical results for specific particle's characteristic length are compared with Rayleigh and Mie theories. Further tests were made using the same scatterer including compliance with the reciprocity and the scattered field obtained. The validity check was extended to mixed phase hydrometeors such as ice aggregate or dry snowflakes.

Finally, in *Chapter* 6, the main contributions of the thesis are highlighted, certain limitations of the work are identified, and areas for possible further study are suggested.

CHAPTER 2

BACKGROUND STUDY AND LITERATURE REVIEW

2.1 Introduction

The Maxwell macroscopic equations are used to describe the interaction of the fields with different media and to define wave equations with particular interest in irregular hydrometeors which can be modelled as inhomogeneous dielectric medium. The physical processes that lead to the formation, growth and precipitation of cloud inhomogeneous dielectric particles in the atmosphere with emphasis on melting hydrometeors consisting of liquid water, ice and air in the melting layer also known as the bright band is discussed. The melting layer is defined

as a transition region between the dry snow particles and raindrops. Modelling of the irregular hydrometeors in this region is difficult due to the complexity of the electric and geometrical properties. Thereafter, outline of study carried out on melting irregular hydrometeors is presented. Furthermore, the refractive index of water based irregular hydrometeors in the bright band are highlighted. A concise review of effective medium theories to evaluate or estimate the average optical constants of inhomogeneous materials are discussed with emphasis on Maxwell-Garnett (MG) mixing formula [14] and Bruggeman or Polder-van-Santen in remote sensing parlance [15].

A brief review of work done on electromagnetic scattering by small particles (single or fixed aggregate) in relation to their electric and geometrical properties is presented. The Mie theory or solution given in [16, 17] in the case of dielectric spheroids and ellipsoids, T-matrix method developed by P.C. Waterman [18] for solving problem of arbitrary scatterers, Discrete dipole approximation [12] also known as couple dipole method involve replacing the scatterers with dipoles to evaluate the scattering functions, and Fredholm integral equation method introduced by Holt et.al [13] with specific application to the electromagnetic waves scattering by dielectric ellipsoids and spheroids are highlighted and chosen as the axiomatic basis for the reminder of this study.

Application of the scattering characteristics are required in many areas of science and engineering, such as investigation and calculation of the scattering and absorption of electromagnetic (EM) waves by small scattering bodies [19], small chemical particles [20], biological blood cells [21] and in quantum theory [22]. The idea of scattering by small-sized particle was developed by Lord Rayleigh in 1871 to describe why scattering of sunlight in the atmosphere causes the diffuse sky

radiation, which is the reason for the blue colour of the sky [23, 24, 25]. However, if the dielectric constant is high, the Rayleigh scattering theory can become inadequate even if the characteristic length (radius) of particles are significantly less than the wavelength. The electrical properties of particles are generally defined in terms of the conductivity σ, the permeability μ, and its dielectric constant or permittivity ε. However, most of the naturally occurring particles such as dielectric materials are non-magnetic and conductivity is zero, since our study is based on these categories of particles which have inclusions of different dielectric properties; hence electromagnetic waves interaction is mainly characterised by only the dielectric constant in this study. Detailed understanding of EM waves scattering by scatterers similar to, or larger than the wavelength of EM radiation and other computational techniques are treated in [8] and [26].

2.2 Electromagnetic fields and wave equations

Maxwell's equations are a set of relations linking the values of a number of quantities that describe electric $\mathbf{E}$ and magnetic $\mathbf{H}$ fields [27] and [28]. Therefore, the foundation of our theoretical approach in this study are the Maxwell macroscopic equations that describe the origin of fields propagating in space and time where the physical properties of the material medium (characterized by ε and μ) are continuous. We use the Gaussian units given in [29] unless stated otherwise:

$$\nabla \cdot \mathbf{D} = 4\pi\rho, \tag{2.1}$$

$$\nabla \times \mathbf{E} = -\frac{1}{c}\frac{\partial \mathbf{B}}{\partial t}, \tag{2.2}$$

$$\nabla \cdot \mathbf{B} = 0, \tag{2.3}$$

$$\nabla \times \mathbf{H} = \frac{4\pi}{c}\mathbf{J} + \frac{1}{c}\frac{\partial \mathbf{D}}{\partial t}, \tag{2.4}$$

where $\mathbf{E}$ is the electric field, $\mathbf{D}$ the electric displacement, $\mathbf{H}$ the magnetic field, $\mathbf{B}$ the magnetic induction, t denotes time and c the speed of light in free space. Likewise $\mathbf{J}$ and ρ denote the current density and charge of the medium respectively. The varnishing of the magnetic induction may be interpreted as saying that there exist no free magnetic poles. The expression of the various fields are assumed to be dielectric medium for simplicity that the medium is homogeneous, linear, isotropic, and non-dispersive, so that the permittivity is a simple constant. The electric displacement $\mathbf{D}$ and magnetic field $\mathbf{H}$ are given in [30]

$$\mathbf{D} = \varepsilon_0 \mathbf{E} + 4\pi \mathbf{P}, \tag{2.5}$$

$$\mathbf{H} = \frac{\mathbf{B}}{\mu} - 4\pi \mathbf{M}, \tag{2.6}$$

where $\mathbf{P}$ is the electric polarization (average electric dipole moment per unit volume), $\mathbf{M}$ the magnetization (average magnetic dipole moment per unit volume), $\varepsilon = \varepsilon_0(1 + \chi_e)$ dielectric constant of the medium, and μ the permeability of the medium. In practice, the magnetic properties of the dielectric medium is so weak that the permeability is assumed to be equal to that of the vacuum, thus $\mu \approx 1$. To allow a unique determination of the field vectors from a given distribution of current and charges, equations (2.1) - (2.6) are not sufficient in themselves, they must be supplemented by constitutive relations describing the medium under the influence of the fields. These relations are given in [30]

$$\mathbf{J} = \sigma \mathbf{E}, \tag{2.7}$$

$$\mathbf{B} = \mu \mathbf{H}, \tag{2.8}$$

$$\mathbf{P} = \varepsilon_0 \chi_e \mathbf{E}, \tag{2.9}$$

where σ is the conductivity, μ the permeability, ε_0 the free space permittivity, and χ_e the electric susceptibility. The phenomenological coefficients σ, μ, and χ_e depend on the material medium under consideration.

The wave equation for electric field

We restrict ourselves to derive the wave equations for the electric field vector $\mathbf{E}$ in a volume with no charge density $\rho = 0$, and current density $\mathbf{J} = 0$. In the case of homogeneous wave equation for $\mathbf{E}$, we take the curl of (2.2) and using (2.4) to obtain

$$\nabla \times (\nabla \times \mathbf{E}) = -\frac{1}{c}\frac{\partial}{\partial t}(\nabla \times \mathbf{B}) = -\frac{1}{c}\frac{\partial}{\partial t}\left(n^2 \frac{1}{c}\frac{\partial}{\partial t}\mathbf{E}\right), \tag{2.10}$$

by assuming $\mu \approx 1$ and $\varepsilon = n^2$. Using the following vector identity

$$\nabla \times (\nabla \times \mathbf{A}) = \nabla(\nabla \cdot \mathbf{A}) - \nabla^2 \mathbf{A}. \tag{2.11}$$

Furthermore, since $\rho = 0$, equation (2.1) becomes

$$\nabla \cdot \mathbf{D} = 0, \tag{2.12}$$

we find that rearranging Equation (2.10) and applying the operator triple product given in (2.11), equation (2.10) becomes

$$\nabla^2 \mathbf{E} - n^2 \frac{1}{c^2}\frac{\partial^2 \mathbf{E}}{\partial t^2} = 0. \tag{2.13}$$

Now looking for a solution of the wave equation (2.13) in the form of a time harmonic wave. We therefore make the following Fourier component Ansatz given in [30]

$$\mathbf{E} = \mathbf{E}(r)\exp(-i\omega t), \tag{2.14}$$

and insert (2.14) into (2.13). This yields

$$\begin{aligned} \nabla^2\mathbf{E}(r)e^{-i\omega t} - n^2\frac{1}{c^2}\frac{\partial^2}{\partial t^2}\mathbf{E}(r)e^{-i\omega t} &= 0, \\ &= \nabla^2\mathbf{E} - n^2\frac{1}{c^2}(-i\omega)^2\mathbf{E}(r)e^{-i\omega t}, \\ &= \nabla^2\mathbf{E} + n^2\,\frac{\omega^2}{c^2}\mathbf{E}, \\ \nabla^2\mathbf{E} + k_0^2n^2\mathbf{E} &= 0, \end{aligned} \tag{2.15}$$

where k_0 is the vacuum wavenumber and (2.15) is the homogeneous Helmholtz wave equation for $\mathbf{E}$.

Following the same order of derivation of the $\mathbf{E}$ wave equation, we can also express the homogeneous $\mathbf{H}$ wave equation in the same form

$$\nabla^2\mathbf{H} + k_0^2n^2\mathbf{H} = 0. \tag{2.16}$$

In the case of inhomogeneous material medium and using (2.14), the field equations (2.2) and (2.4) then become

$$\begin{aligned} \nabla\times\mathbf{E} &= ik_0\mathbf{B} = i\mu k_0\mathbf{H}, \\ \mu^{-1}\nabla\times\mathbf{E} &= ik_0\mathbf{H}, \\ \nabla\times\mathbf{H} &= -ik_0n^2\mathbf{E}. \end{aligned} \tag{2.17}$$

Taking the curl of the second equation (2.17) leads to

$$\begin{aligned} \nabla \times \left(\mu^{-1}\nabla \times \mathbf{E}\right) &= ik_0 \nabla \times \mathbf{H}, \\ &= k_0^2\, n^2\, \mathbf{E}, \\ \nabla \times \left(\mu^{-1}\nabla \times \mathbf{E}\right) - k_0^2\mathbf{E} &= k_0^2(n^2-1)\mathbf{E}. \end{aligned} \tag{2.18}$$

Adding the left hand side of the vector identity given in (2.11) into both sides of the third part of equation (2.18) yields

$$\nabla \times \nabla \times \mathbf{E} + \nabla \times \left(\mu^{-1}\nabla \times \mathbf{E}\right) - k_0^2\mathbf{E} = \nabla \times \nabla \times \mathbf{E} + k_0^2(n^2-1)\mathbf{E}, \tag{2.19}$$

we find that (2.19) can be rearranged and expressed as

$$\begin{aligned} \nabla \times \nabla \times \mathbf{E} - k_0^2\mathbf{E} &= \nabla \times \nabla \times \mathbf{E} - \nabla \times \left(\mu^{-1}\nabla \times \mathbf{E}\right) + k_0^2(n^2-1)\mathbf{E}, \\ &= k_0^2(n^2-1)\mathbf{E} + \nabla \times \left[\left(1-\mu^{-1}\right)\nabla \times \mathbf{E}\right], \end{aligned} \tag{2.20}$$

where n is the refractive index and the permeability μ may be tensors. In the case where μ is not a tensor, then (2.20) can be rewritten as

$$\nabla \times \nabla \times \mathbf{E} - k_0^2\mathbf{E} = k_0^2(n^2-1)\mathbf{E} + \mu^{-1}\left(\nabla\mu\right) \times \nabla \times \mathbf{E}. \tag{2.21}$$

Besides, the presumption that μ is not a tensor, and making further assumption that the material medium is non magnetic i.e. permeability $\mu = 1$. Thus simplify equation (2.20) and can be expressed

$$\nabla \times \nabla \times \mathbf{E} - k_0^2\mathbf{E} = k_0^2(n^2-1)\mathbf{E}, \tag{2.22}$$

which is the inhomogeneous dielectric wave equation used in chapter 3 as the basis

to formulate the theoretical analysis of the research problem.

The **E** and **H** fields must also satisfy the following boundary conditions, where $\hat{\mathbf{n}}$ is a unit vector normal to the boundary as summarized in Table 2.1 [10].

Table 2.1: Electromagnetic boundary conditions for linear dielectric medium.

	Component	Linear materials
Electric displacement	Perpendicular	$D_2, \perp -D_1, \perp = \rho_f$
	Parallel	$D_2, \parallel -D_1, \parallel = 0$
Electric field	Perpendicular	$\varepsilon_2 E_2, \perp -\varepsilon_1 E_1, \perp = \rho_f$
	Parallel	$E_2, \parallel = E_1, \parallel$
H-field	Perpendicular	$\mu_1 H_1, \perp -\mu_2 H_2, \perp = 0$
	Parallel	$H_1, \parallel -H_2, \parallel = J_f$
Magnetic field	Perpendicular	$B_1, \perp -B_2, \perp = 0$
	Parallel	$\frac{1}{\mu_1} B_1, \parallel -\frac{1}{\mu_2} B_2, \parallel = J_f$

where ρ_f and J_f are any existing surface charge and current densities, where $J_f = 0$ for dielectric scattering particles.

2.3 Melting snowflakes formation in the cloud

The description of the physical processes that lead to the formation, growth and precipitation of cloud particles in the atmosphere with emphasis on irregular hydrometeors such as melting snowflakes is presented in this section. The formation of individual snow crystal is a complex process, where the crystal can have different length scales, shapes and sizes [31, 32]. An in-depth understanding of the

growth process is given in [33, 34]. The crystal can consist of a single ice particles or an aggregate of many ice particle inside the cold cloud. The ice crystal process involves mainly the interaction of supercooled water droplets and tiny ice crystal but also involves other interactions as discussed in the following [35]:

- Accretion: Growth of an ice particle when it captures supercooled liquid droplets.

- Aggregation: Merging of multiple ice particles to form one main snowflake (snowflakes sticking together). The surfaces of ice crystals become sticky at temperatures above -5^0 C , and this process maximizes near 0^0 C.

- Deposition: Growth by water vapour depositing on the ice particle in a liquid form and immediately freezing, or directly depositing as a solid. This is the dominant method of snow growth process.

Tiny water droplets and ice crystals coexist in cold clouds at a fixed temperature [31]. The coexistence is dynamic due to the fact that the saturation vapour pressure over the droplets is slightly greater than that over the ice crystals. Thus, the interaction between them causes the ice crystals to grow at the expense of the droplets. This process is referred to as Bergeron process [35] and the crystals can grow in clouds as long as there is sufficient vapour. The type and shape of ice crystals formed by this process is primarily a function of the temperature and secondarily a function of the degree of saturation in the clouds. It is also interesting to note that crystals can grow due to the interaction with other crystals but also due to the contacts with supercooled water droplets to create dry snowflakes.

The ice crystals eventually grow to a size and mass that allow them to fall as a result of coalescence and gravity. As the snowflakes fall, they pass through a level

where the temperature rises above freezing [35]. The snowflakes due to a change in temperature, start to melt and initially develop a water coating. As the wet flakes continue to fall and melt, a more complicated mixture is developed consisting of water, ice and air with different electrical properties and the resulting complex particle is known herein as melting snowflakes. The amount of the water content in the irregular hydrometeors at this stage is about nine times more reflective than dry ice in the region of microwave [34], so these melting snowflakes produce a much higher radar reflectivity than dry snowflakes. All of these processes lead to the formation of a narrow ring of high reflectivity at the melting layer. This layer is also known as the Bright Band (BB) and is highlighted in § 2.4.

2.4 Melting layer model

The melting layer can be described as a transition region between the dry snow particles and raindrops. It can also be observed in stratiform rain condition as described in [36]. The radar reflectivity of this region is relatively high because of the fast increase in dielectric constant of the melting particles compared to those of snow or dry ice at the beginning of the melting process. As melting progresses, the increase in the fall velocity of wet snowflakes reduces the concentration, and decreases the particle size. This results in a rapid reduction in the reflectivity at a lower part of the melting layer [37], [38]. Figure 2.1 shows the height versus the reflectivity factor Z_e highlighting the height of the reflectivity in the Bright Band [39].

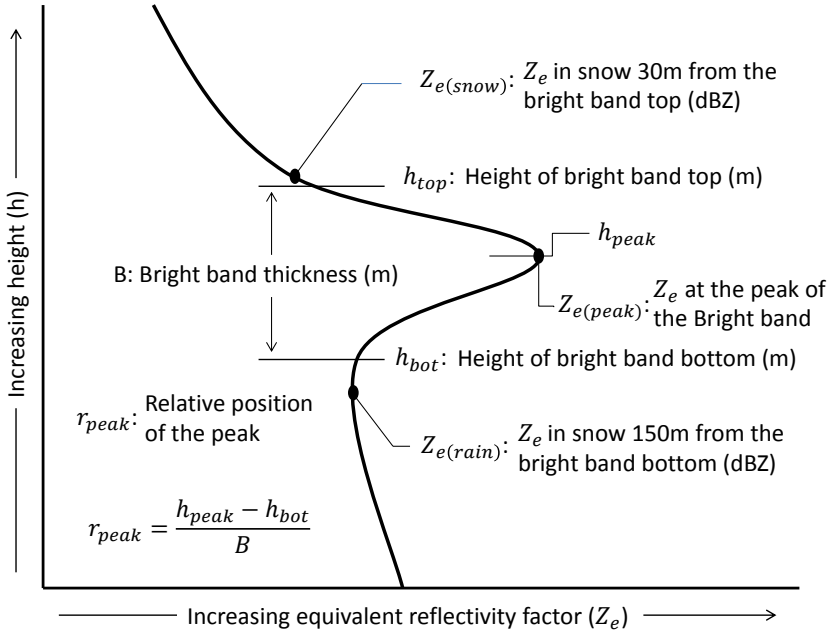

Figure 2.1: Schematic diagram illustrating various parameters extracted from the vertical reflectivity profile.

Describing adequately the particle's characteristics in this regime is quite difficult due to change in geometrical and electrical properties [40]. As discussed in [38], the complex nature of the melting process and lack of accurate experimental/measured data on the effective dielectric constant of the melting flakes make computations of the scattering properties of partly wet irregular hydrometeors relying mainly on particle Bright Band models.

The melting layer models developed for remote sensing of irregular hydrometeors in this region proposed no collision coalescence and breakup processes during the transition process [11]. These assumptions were employed in [41] and [42] to describe a dry snowflake of the size D_s above the freezing level melting into a raindrop of the size D_r below the Bright Band. A further assumption made in [11]

and [43] was that the mass and density of the dry snow particle remain constant during melting. However, this assumption are too strong and not consistent with the physics of the formation of process. This means the vertical flux of the hydrometeors concentrations is preserved throughout the melting layer [37] and this can be expressed as

$$\eta_s(D_s)V_s(D_s) = \eta_m(D_m)V_m(D_m) = \eta_r(D_r)V_r(D_r) = \text{Constant}, \tag{2.23}$$

where η_s, η_m, and η_r are concentrations of the snowflakes above the freezing level,of the melting hydrometeors in the bright band, and of the raindrops below BB respectively, V_s, V_m, and V_r are their fall velocities, while D_s, D_m, and D_r are the equal-volume spherical diameters of dry snowflakes, melting hydrometeors, and raindrops respectively.

Another melting layer model focus directly on the shape of the hydrometeors which is assumed to be spherical or spheroidal in [38], [40] and [11]. However, this obviously depends on the axial ratio of the maximum horizontal dimension to the height of the scatterer. The size of the raindrop radius a_r is used to directly evaluate the size of the dry snow particle radius a_s and is given in [11]

$$a_s^3 = a_r^3 \left[Q + (1-Q)\frac{\rho_r}{\rho_s} \right], \tag{2.24}$$

where $Q = \dfrac{M_r}{M}$ is the mass fraction, M_r is the mass melted into water in the wet snow particle, M the mass of the hydrometeors, ρ_r is the density of the melted hydrometeors below the melting layer, and ρ_s is the density of dry snow particles on the top of the melting layer.

Bright Band models are used to establish the scattering model which quantifies the

reflectivity factor of hydrometeors as a function of their size, of the proportion of melted snow, of the melting snow density, and of the radar wavelength. Given the particle sizes, another key ingredient of the Bright Band model is the Particle Size Distribution (PSD) based on the Marshall and Palmer (MP) also known as the simpler MP exponential approximation [34] and [44]. The Marshall and Palmer model has been implemented in [45] with the observation of Law and Parsons. The Marshall-Palmer PSD model expresses the concentration of the particles as a function of their diameter D as an exponential function [34]

$$\eta(D) = \eta_0 \exp(-\Lambda D), \tag{2.25}$$

where $\Lambda = 4.1R^{-0.21}\text{mm}^{-1}$ is the size parameter, $\eta_0 = 8 \times 10^3\text{m}^{-3}\text{mm}^{-1}$ is the concentration parameter, and R is the rain rate in $\text{mm}h^{-1}$. The MP distribution was later discovered not to be sufficient to describe most of the observed raindrop spectra accurately [34]. Thus, the Gamma PSD was introduced. In particular it offers practical advantages and was shown to be more appropriate to describe raindrops than the MP. Since a factor taking into account the distribution shape μ was introduced [44]

$$\eta(D) = \eta_0 D^{\mu} \exp(-\Lambda D), \tag{2.26}$$

where η_0 and Λ are concentration, and size parameters respectively. For $\mu = 0$ in (2.26) becomes the simpler MP exponential approximation (2.25). Given the particle size distribution $\eta(D)$, the unattenuated radar reflectivity factor can be calculated at any range within the melting layer as the integral of the backscattering cross section $\sigma_b(D, \lambda)$ weighted by the particle concentration $\eta(D)$ [5], [11], [38], [40]

$$Z = \frac{\lambda^4}{\pi^5 \left|K_w\right|^2} \int_0^{\infty} \eta(D)\sigma_b(D, \lambda) dD, \tag{2.27}$$

where λ is the radar wavelength. In order to be able to evaluate the radar reflectivity Z of the irregular hydrometeors, scattering models are needed to define σ_b and mixing formulas are required to adequately model the effective dielectric constant of particle with different constituting materials. K_w is the complex dielectric factor and gives some indication of the particle during backscattering. It can be defined as $(n^2-1)/(n^2+2)$ or $(\varepsilon-1)/(\varepsilon+2)$, where n is the complex refractive index or ε complex dielectric constant. It is discussed in [38] that $|K_w|^2$ is taken to be 0.93 for water, and 0.197 for ice. The evaluation of σ_b depends upon the scattering model of hydrometeors and the mixing formulas used in the determination of the effective dielectric constant of the melting snow.

2.5 Refractive index of melting hydrometeors

Few models have been developed to describe particles which are mixture of ice, water and air. In [46], Matthew Sadiku presented a systematic procedure for calculating refractive index of snow at microwave using Peter Debye formula introduced in 1912 at different temperatures and frequencies. This model is based on single relaxation time and is known as Debye dispersion formula.

In the theoretical treatment of the electrical properties of melting hydrometeors, it is assumed that the component materials are large enough to be assigned with their dielectric functions. The Debye single relaxation formula for the dielectric constant is given in [47] and [48]

$$\varepsilon = \varepsilon_\infty + \frac{\varepsilon_{st} - \varepsilon_\infty}{1 - i\omega\tau}, \tag{2.28}$$

or may be expressed in terms of its real and imaginary parts $\varepsilon = \varepsilon' + i\varepsilon''$ where:

$$\varepsilon^{'} = \varepsilon_{\infty} + \frac{\varepsilon_{st} - \varepsilon_{\infty}}{1 + (\omega\tau)^2}, \tag{2.29}$$

and

$$\varepsilon^{''} = \frac{(\varepsilon_{st} - \varepsilon_{\infty})(\omega\tau)}{1 + (\omega\tau)^2}, \tag{2.30}$$

where ω is the angular frequency, τ is the characteristic relaxation time, ε_{st} is the static dielectric constant, ε_{∞} is the infinite frequency dielectric constant.

Given the dielectric constant, the refractive index can be computed as

$$n = \sqrt{\varepsilon} = n_r + in_i, \tag{2.31}$$

where the real part $\varepsilon^{'} = n_r^2 - n_i^2$ is called relative permittivity and it describes how the electric field is stored. The imaginary part $\varepsilon^{''} = 2n_r in_i$ is the loss factor or rate of energy dissipated. The real part of n is related to the phase shift (or wave velocity), while the imaginary part is associated with wave attenuation. It should be noted that if the material has conductivity σ in addition, the dielectric constant of the particle becomes [49]

$$\varepsilon_r(\mathbf{r}, \omega) = \varepsilon(\mathbf{r}, \omega) + i\frac{\sigma(\mathbf{r}, \omega)}{\omega}. \tag{2.32}$$

The Debye model suffers in accuracy at intermediate temperatures and a more detailed understanding of this procedure is given in [50].

2.5.1 Refractive index of water

The Debye single model is commonly used for calculating the dielectric constant of water but it is unsuitable for frequency above 10 GHz [46]. This indicates that the single relaxation time is not valid at higher frequencies toward the millimetre and optical regions of the electromagnetic spectrum. Subsequently the Debye single relaxation time (2.28) was modified by Cole and Cole [51] by raising the $i\omega\tau$ term to the power of $(1-\alpha)$, where α is known as the spread parameter whose value lies between 0 and 1. This is expressed as

$$\varepsilon = \varepsilon_{\infty} + \frac{\varepsilon_{st} - \varepsilon_{\infty}}{1 - i\omega\tau^{(1-\alpha)}}. \tag{2.33}$$

For $\alpha = 0$ becomes (2.28) in Debye form. The spread parameter for water is evaluated to be less than 0.03 [52], indicating that the Debye form for a single relaxation time is satisfactory. Further modification of equation (2.28) resulted in a frequency-independent conductivity model for the dielectric properties of ice and water over a large frequency spectrum and temperature range [46], [53].

There are no generally acceptable empirical or theoretical model for the calculation of the refractive index of water and ice for a wide range of frequency and temperature. D.H.O Bebbington used another model called Debye Double relaxation model employing observable data from P.S Ray to compute permittivity of water [54]. After performing a numerical comparison the Debye Double Relaxation Model behaves as the other models for lower frequencies. The real and imaginary parts of the Debye Double Relaxation Model (**DDRM**) are expressed as

$$\varepsilon_r = \varepsilon_2 + \frac{\varepsilon_0 - \varepsilon_1}{1 + f_n^2} + \frac{\varepsilon_1 - \varepsilon_2}{1 + f_s^2}, \tag{2.34}$$

and

$$\varepsilon_i = f_n \frac{\varepsilon_0 - \varepsilon_1}{1 + f_n^2} + f_s \frac{\varepsilon_1 - \varepsilon_2}{1 + f_s^2}, \tag{2.35}$$

where ε_0, ε_1 and ε_2 are the coefficients for the static term, f_n the normalise frequency based on double term coefficient and f_s the normalise frequency based on single term coefficient. The range of validity of the model is 0 to 1000 GHz in frequency and -10^0C to 30^0C temperature.

2.5.2 Refractive index of ice

The real part of refractive index of ice is known to be relatively constant at high frequency (microwaves and above) and simulations show that the real part of complex refractive index of ice, between 0^0C and 5^0C take a fairly constant value ≈ 1.78 independent of both frequency and temperature, and the imaginary part (the loss factor) takes an extremely small value but varies slightly throughout the centimetre and millimetre bands [46].

The result of empirical model of the complex refractive index of ice by P.S.Ray [4] agreed with the work of [46], and the procedure for the construction of the model is similar to that of water. The real part of the complex permittivity for pure ice is evaluated in [55] to be 3.15. When this value is substituted into equation (2.31) the same result is obtained [46].

2.5.3 Refractive index of air

It is customary to assume that the refractive index of air near Earth's surface is approximately $n \approx 1.0003$ throughout the radio spectrum, obviously, this value for

practical purposes is indistinguishable from those of free space or vacuum ($n \approx 1$) [56].

2.6 Effective medium theories

Given the dielectric constant of the constituent parts of the melting hydrometeors, homogenization is one approach to achieve a simplified description of the behaviour of a wet snowflakes. Effective medium theories (EMTs) achieve this purpose. Many different mixing rules can be found in the literature [47] and [57] but Maxwell-Garnett rule [14], Coherent Potential mixing rule [58] and the Bruggeman [15] have been considered for this work because of their applications in weather radar. A variety of EMTs have been developed for different internal structures of the medium and for a variety of shapes, size distributions and physical properties of the inhomogeneity.

The evaluation of the effective dielectric function of a complex mixture is a difficult problem since a large number of interactions can occur within the component materials [4]. Also the mixing techniques may vary considerably depending on the external conditions to which the particles are exposed.

The interaction of electromagnetic waves with the particles model of mixed dielectric material is a complex process. In order to model the interaction, the inhomogeneous materials of the mixture has to be taken into account. This increase the complexity of the description of scattering process. In order to reduce this effect, homogenization techniques can be employed to evaluate the effective or average dielectric constant. The more general family of mixing rules is based on matrix medium ε_e and inclusion or guest medium ε_i describing the effective medium ε_{eff}

of the inhomogeneous material with a fraction volume of the inclusion f linked by the following [47], [57], [59]

$$\frac{\varepsilon_{eff} - \varepsilon_e}{\varepsilon_{eff} + 2\varepsilon_e + \nu(\varepsilon_{eff} - \varepsilon_e)} = f\frac{\varepsilon_i - \varepsilon_e}{\varepsilon_i + 2\varepsilon_e + \nu(\varepsilon_{eff} - \varepsilon_e)}, \tag{2.36}$$

where ν is a dimensionless parameter. For different values of this dimensionless parameter ν, various mixing formula are recovered. For $\nu = 3$ into (2.36) becomes separated-grain effective medium theory called Coherent Potential mixing formula.

2.6.1 Maxwell-Garnett theory

The Maxwell-Garnett (MG) mixing method also regarded as separated-grain topology assumes a host or background homogeneous material where some parts are replaced by inclusions or guest of different relative permittivity material. The analytical relationship between the electrical and geometrical parameters of a bi-phasic dielectric material with a collection of spherical inclusions is given in [47], [60]

$$\varepsilon_{eff} = \varepsilon_e + 3f\varepsilon_e\frac{\varepsilon_i - \varepsilon_e}{\varepsilon_i + 2\varepsilon_e - f(\varepsilon_i - \varepsilon_e)}, \tag{2.37}$$

where ε_{eff} is the mixture effective permittivity, ε_e is the relative permittivity of the host material, ε_i is the relative permittivity of the spherical guest inclusions, and f is the fractional volume of the inclusions. A parallel derivation to the MG formula (2.37) for the magnetic permeability of mixed materials was proposed in [61]. This approach treats hydrometeors (such as melting snowflakes) as either a two-component (bi-phasic dielectric) or three-component (multi-phase dielectric) mixture of ice, air, and water. The two component formulation is usually applied to dry snow (mixture of air and ice) and sometimes to wet snow through the

additional application of the formula for dry snow and water.

A typical approach of using the MG mixing rule for the three components mix is to calculate the dielectric constant of the two components mix and then to consider the resultant dielectric constant as inclusions in the matrix of the third component or as the background with the third material as inclusions. This generally admits 12 different solutions depending on how the three constituents are ordered [38]. One physically reasonable way to tackle the problem is to calculate the dry snow dielectric constant assuming solid ice inclusions in an air matrix and then to calculate the dielectric constants of melting hydrometeors as dry snow inclusions in a water matrix or water inclusion in the dry snow matrix.

Maxwell-Garnett in 1904 was one of the very early formulation of this method that could be used for multi phased mixtures with different geometries of inclusions (such as ellipsoid and rods) [62]. This method has the advantage of including geometrical factors inside the formulation. However, it is not always easy to know the material geometries [63]. This method can be suitable for wet particle since the shape tends to be spherical [59]. The MG mixing formula has been used to determine the effective dielectric properties of water based particle (such as melting snowflake in terms of its constituent parts air, ice, and liquid water under certain conditions) but its validity at higher frequencies has not been fully established.

Limitations

The MG method has these limitations as highlighted below:

- It is important to mentioned that interchanging guest and host materials in (2.37) do not yield the same results. This asymmetry in the results is

particularly drastic when the difference in the dielectric constants of the two materials is large.

- Another shortcoming of the Maxwell-Garnett formula was found when attempts were made to generalise it to several components.

- A resonance effect can be found in the scattering description where a composite particle is homogenized using this method [64]. This causes oscillation in the backscattering cross sections for particles comparable in dimension to half a wavelength or larger.

We adopted the numerical results of refractive indices of ice $= 1.782 + 3.344 \times 10^{-3}i$ and water $= 8.227 + 2.341i$ at frequency of 6.0 GHz and temperature of 0^0C as stated in [46] to evaluate the average refractive index for three components mixture such as melting snowflakes assuming homogeneous inclusions using effective medium theories. In Table 2.2 we illustrate the problem of applying effective medium methods such as Maxwell-Garnett for non-binary media. Using MG formula for binary media, air inclusions in an ice matrix, (herein referenced as $\text{MG}_{ia} = 1.20947592 + 0.832705996 \times 10^{-3}i$) and ice inclusions in an air matrix, (herein referenced as $\text{MG}_{ai} = 1.19839930 + 0.0717479539 \times 10^{-3}i$).

Table 2.2: Numerical examples of non-binary media such as melting snowflakes with homogeneous inclusions (air, water, and ice)

Matrix	Inclusions	Binary EMTs	Matrix	Inclusions	Non-binary EMTs
70% of ice	30% of air	MG_{ia}	70% of MG_{ia}	30% of water	$MG_{(ia)w} = 4.41026029 + 0.644639288i$
70% of ice	30% of air	MG_{ia}	30% of water	70% of MG_{ia}	$MG_{w(ia)} = 5.60043131 + 1.43205165i$
30% of air	70% of ice	MG_{ai}	70% of MG_{ia}	30% of water	$MG_{(ai)w} = 4.37820859 + 0.642554374i$
30% of air	70% of ice	MG_{ai}	30% of water	70% of MG_{ia}	$MG_{w(ai)} = 5.59521969 + 1.43188028i$

2.6.2 Bruggeman mixing theory

Another competing effective permittivity formulation is Bruggeman mixing theory [15], which made a significant improvement to the Maxwell-Garnett mixing theory. He introduced an approximation that treats the two composites in symmetrical fashion regarded as aggregated-grain topology. The medium is treated as a set of randomly distributed cells of different materials.

This method is better known as Polder-van-Santen [6] in remote sensing applications. It can be used for two phased mixtures by substituting $\nu = 2$ into (2.36) leads to

$$\eta_1 \left(\frac{\varepsilon_e - \varepsilon_{eff}}{\varepsilon_e + 2\varepsilon_{eff}} \right) + \eta_2 \left(\frac{\varepsilon_i - \varepsilon_{eff}}{\varepsilon_i + 2\varepsilon_{eff}} \right) = 0, \tag{2.38}$$

where $\eta_1 = 1 - f$ is the volume fraction of dielectric constant ε_e, $\eta_2 = f$ represents volume fraction of dielectric constant ε_i and ε_{eff} is the effective permittivity of the medium. Mixing rules are symmetric relative to which component is called matrix and which makes inclusion. A more rigorous derivation of this mixing theory and some properties of Bruggeman mixing formula has been introduced by [57]. Unlike the Maxwell-Garnett formula, the Bruggeman mixing theory can be generalised to include any number of components.

2.7 Electromagnetic wave scattering

The concept of electromagnetic waves scattering by a material medium can be described as placing a particle with a dielectric constant or refractive index different from that of the surrounding medium. This would cause a change in the electric and magnetic fields that would otherwise exist in an unbounded homogeneous

space. Thus, the difference in the total field with the presence of the object and the original field that would exist in the absence of the object can be thought of as the scattered field space . In other words, the total field is equal to the vector sum of the incident (original) field and the scattered field [19].

The Mie theory (solution) for the special case of spherical particles [16], [17], [26], T- matrix method [18], [65], the Discrete dipole approximation [66, 67], and other approaches with emphasis on single or aggregate scatterer are reviewed in this section. An extensive literature of evaluating scattering problems by small particles are given in [16], [19], [26]. The problem of multiple scattering of EM waves by particles are treated in detail by [8, 9] and [68, 69, 70, 71], however, this is not the focus of this study and as such not considered.

2.7.1 Mie theory

Mie solution or theory has been the most usual theoretical tool to handle electromagnetic waves scattering by a simple geometry of sphere through solving of the Macroscopic Maxwell's Equations. The theory was developed by Gustav Mie in 1908 in order to understand the colours that resulted from light scattering from gold particles suspended in water. Sphere has been studied more extensively than has the scattering by any other particle shape. This is partly because, it has been the only three dimensional particle for which an analytical close form solution is readily available [16], [17], [26], [72], [73].

Although it is exact, only with the emergence of numerical techniques it has become more practical to extend the range of its applications [74]. Formulation of the theory begins with an object possessing a discrete boundary and optical con-

stants different from those of the surrounding medium, is incident by a linearly polarized plane electromagnetic wave, a scattered field is generated and is usually solved by separation of variable method described in some of the literature already highlighted, but the notation given in [26] is followed for the derivation of the Mie solution theory.

Solutions to the vector wave equations

The basic concepts of the wave theory directly from Macroscopic Maxwell's Equations (2.1) - (2.4) (MMEs) are the basis applied to formulate the vector wave equation in the Mie theory. Interestingly, the shape of the scatterer also bears an important relationship to a particular coordinate system to use and which enables the boundary conditions to be expressed in traceable form.

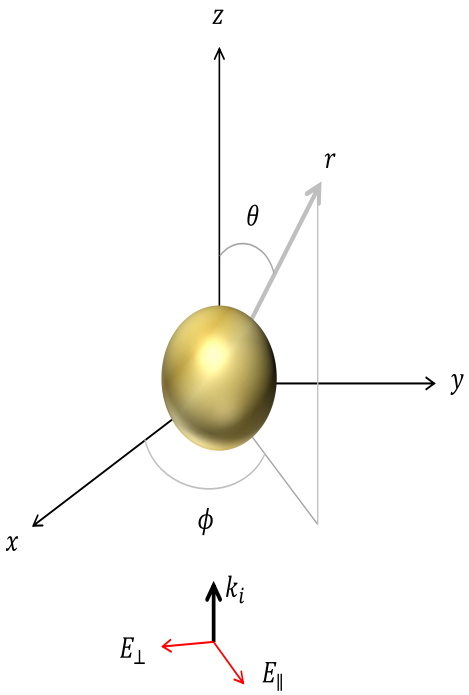

Figure 2.2: Geometry of the sphere of radius (r) illuminated by linearly polarized plane electromagnetic wave propagating in the +z direction.

For sphere, spherical coordinates r, θ, ϕ , as shown in Fig. 2.2 provide such a natural coordinate system for the theoretical overview. The general solution of the wave equation (2.15) is not straightforward but can be derived from a scalar function or potential ψ which satisfies the following wave equation treated in Appendix (A.2). Thereto, one can construct an intermediate vector function given in [26]

$$\mathbf{M} = \nabla \times (\mathbf{c}\psi), \tag{2.39}$$

where $\mathbf{c}$ is an arbitrary constant vector and ψ is any scalar function. Since the divergence of the curl of any vector function vanishes (i.e. $\nabla \cdot (\nabla \times \mathbf{v})$ for any vector function v), we can say that

$$\nabla \cdot \mathbf{M} = 0,$$

and

$$\nabla \times (\mathbf{A} \times \mathbf{B}) = \mathbf{A}(\nabla \cdot \mathbf{B}) - \mathbf{B}(\nabla \cdot \mathbf{A}) + (\nabla \cdot \mathbf{B})\mathbf{A} - (\nabla \cdot \mathbf{A})\mathbf{B}, \tag{2.40a}$$

$$\nabla(\mathbf{A} \cdot \mathbf{B}) = \mathbf{A} \times (\nabla \times \mathbf{B}) + \mathbf{B} \times (\nabla \times \mathbf{A}) + (\mathbf{B} \cdot \nabla)\mathbf{A} + (\mathbf{A} \cdot \nabla)\mathbf{B}. \tag{2.40b}$$

Using the vector identities in (2.40) and if the operator $\nabla^2 + k^2$ is applied to (2.39) we obtain

$$\nabla^2\mathbf{M} + k^2\mathbf{M} = \nabla \times [\mathbf{c}(\nabla^2\psi + k^2\psi)]. \tag{2.41}$$

Therefore, $\mathbf{M}$ satisfies the vector wave equation if ψ is a solution of the scalar wave equation. In [27], a second divergence free vector function is define which obeys all of the above equations for $\mathbf{M}$

$$\mathbf{N} = \frac{\nabla \times \mathbf{M}}{k}, \tag{2.42}$$

or equivalently

$$\nabla \times \mathbf{N} = k\mathbf{M}. \tag{2.43}$$

Now, changing our arbitrary constant vector $\mathbf{c}$ to the radius vector $\mathbf{r}$, we have solutions to the vector wave equation in spherical polar coordinates. Final forms of $\mathbf{M}$ and $\mathbf{N}$ as in [26] are given in Appendix (A.1). Seeking separable solutions, we say $\psi(r, \theta, \phi) = R(r)\Theta(\theta)\Phi(\phi)$, and obtain the well known separated equations in spherical form [17]

$$\frac{d^2\Phi}{d\phi^2} + m^2\Phi = 0, \tag{2.44a}$$

$$\frac{1}{\sin\theta}\frac{d}{d\theta}\left(\sin\theta\frac{d\Theta}{d\theta}\right) + \left[l(l+1) - \frac{m^2}{\sin^2\theta}\right]\Theta = 0, \tag{2.44b}$$

$$\frac{d}{dr}\left(r^2\frac{R}{dr}\right) + \left[k^2r^2 - l(l+1)\right]R = 0. \tag{2.44c}$$

Hence the complete solution of the scalar wave equation (2.44) is given as:

$$\psi_{eml} = \cos m\phi P_l^m(\cos\theta) z_l(kr), \tag{2.45a}$$

$$\psi_{oml} = \sin m\phi P_l^m(\cos\theta) z_l(kr), \tag{2.45b}$$

where e and o mean even and odd respectively, P_l^m is the associated Legendre functions of first kind of degree l and order m and z_l represents any of the four spherical Bessel functions: j_l, y_l, $h_l^{(1)}$ or $h_l^{(2)}$ and $l = 0, 1, 2, ...$, and m runs over integer values from $-l$ to l. Every solution of the scalar function ψ, may be expanded as an infinite series of the functions (2.45). The final vector solution can

be obtained from (2.41) with $\mathbf{c} = \mathbf{r}$

$$\mathbf{M}_{eml} = \nabla \times (\mathbf{r}\psi_{eml}), \qquad \mathbf{M}_{oml} = \nabla \times (\mathbf{r}\psi_{oml}), \tag{2.46a}$$

$$\mathbf{N}_{eml} = \frac{\nabla \times \mathbf{M}_{eml}}{k}, \qquad \mathbf{N}_{oml} = \frac{\nabla \times \mathbf{M}_{oml}}{k}. \tag{2.46b}$$

It is possible to conclude that any solution of the wave equation (2.22) can be written as an infinite series of the vector harmonics given by (2.46).

The incident wave in spherical harmonics

The incident field is considered to be a plane wave linearly polarized parallel to the x axis and propagating in the +z direction as shown in Figure 2.2 and is given in [27]

$$\mathbf{E}\, e^{ik_0 z} = \mathbf{E}_0\, e^{ik_0\, r\cos\theta}\hat{\mathbf{e}}_x, \tag{2.47}$$

where $\mathbf{E}_0$ is the amplitude of the electric field, k_0 is the wavenumber and $\hat{\mathbf{e}}_x$ is the unit vector in the polarization direction

$$\hat{\mathbf{e}}_x = \sin\,\theta\,\cos\,\phi\,\hat{\mathbf{e}}_r + \cos\,\theta\,\cos\,\phi\,\hat{\mathbf{e}}_\theta - \sin\,\theta\,\hat{\mathbf{e}}_\phi. \tag{2.48}$$

Given the incident field, it can be expanded as an infinite series into Vector Spherical Waves Functions VSWF, one can write

$$\mathbf{E}_i = \sum_{m=0}^{\infty}\sum_{l=m}^{\infty}\left(B_{eml}\mathbf{M}_{eml} + B_{oml}\mathbf{M}_{oml} + A_{eml}\mathbf{N}_{eml} + A_{oml}\mathbf{N}_{oml}\right), \tag{2.49}$$

B_{eml}, B_{oml}, A_{eml} and A_{oml} being the expansion coefficients. Using the orthogonality of the vector harmonics and the finiteness of the incident field at the origin,

the expansion leads to

$$\mathbf{E}_i = \sum_{l=0}^{\infty} \left(B_{oml}\mathbf{M}_{oml}^{(1)} + A_{eml}\mathbf{N}_{eml}^{(1)} \right). \tag{2.50}$$

In view of $\sin\phi$ and $\cos\theta$ found in the expansion of equation (2.47) not shown, only the terms with m = 1 survive. If there was no scattering object at the origin, the wave would have to be finite, so we reject spherical Bessel functions of the 2nd kind $y_l(\rho)$, since they have singularities and using only $j_l(\rho)$. We write the VSWF as $M_{o1l}^{(1)}$ and $N_{e1l}^{(1)}$, the (1) indicating that the radial components are $z_l(kr) = j_l(kr)$. After rigorous analysis and some manipulations, we obtain the final form of the expansion coefficients given in [26]

$$B_{o1l} = E_0 \frac{2l+1}{l(l+1)}\, i^l, \tag{2.51}$$

and

$$A_{e1l} = -i^{l+1} E_0 \, \frac{2l+1}{l(l+1)}, \tag{2.52}$$

hence, substituting (2.52) and (2.51) into (2.50) gives x-polarised incident wave expansion

$$\mathbf{E}_i = E_0 \sum_{l=0}^{\infty} i^l \, \frac{2l+1}{l(l+1)} \, (\mathbf{M}_{o1l}^{(1)} - i\mathbf{N}_{e1l}^{(1)}). \tag{2.53}$$

The same approach is adopted for the incident magnetic field $\mathbf{H}$ and the corresponding expansion is given as

$$\mathbf{H}_i = \frac{-k}{\omega\,\mu} E_0 \sum_{l=0}^{\infty} i^l \, \frac{2l+1}{l(l+1)} \, (\mathbf{M}_{e1l}^{(1)} + i\mathbf{N}_{o1l}^{(1)}). \tag{2.54}$$

The scattered field

In the same way that we expanded the incident field E_i, we can expand the scattered and internal fields, E_s and E_l . The form of the incident radiation and the orthogonality of the VSWF determine the form given in [27].

The internal field also has a different value of wave vector, since the refractive index is different from the surrounding medium. We use the size parameter x, which can be defined as a clearer means of measuring the size regime in which we are interested than an absolute measure of the particle. Hence, we can say that in the scattering medium, the wave vector can be written as $k_l = k_0(n_l/n_0) = nk_0$ so that the effective size parameter becomes nx. When working with the magnetic materials inclusive, the value of μ will also change.

The scattered field must be continuous at the origin so it allowed discontinuities. The correct radial function for the scattered field is the spherical Hankel functions of the first kind $h_n^{(1)}$. The VSWF for $\mathbf{R}_l = h_l^{(1)}$ are $\mathbf{M}_{o1l}^{(3)}$ and $\mathbf{N}_{e1l}^{(3)}$. The scattered field $(\mathbf{E}_s; \mathbf{H}_s)$ and the field inside the particle $(\mathbf{E}_l; \mathbf{H}_l)$ can be obtained from the incident field by enforcing the boundary conditions between the sphere and the surrounding medium [27]

$$(\mathbf{E}_i + \mathbf{E}_s - \mathbf{E}_l) \times \hat{\mathbf{e}}_r = (\mathbf{H}_i + \mathbf{H}_s - \mathbf{H}_l) \times \hat{\mathbf{e}}_r = 0, \tag{2.55}$$

and

$$E_l = E_0\, i^l\, \frac{2l+1}{l(l+1)},$$

we have

$$\mathbf{E}_s = \sum_{l=1}^{\infty} E_l\, (i a_l\, \mathbf{N}_{e1l}^{(3)} - b_l \mathbf{M}_{o1l}^{(3)}), \tag{2.56}$$

and

$$\mathbf{H}_s = \frac{k}{\omega\mu}\sum_{l=1}^{\infty} E_l\,(ib_l\,\mathbf{N}_{o1l}^{(3)} + ia_l\,\mathbf{M}_{e1l}^{(3)}), \tag{2.57}$$

where the superscript (3) refers to the radial dependence of the generating function, which is given by the spherical Hankel function $h_l^{(1)}$. The coefficients, a_l and b_l, are the so-called Mie coefficients for the scattered field. Again, by applying the boundary conditions at the surface of the sphere, we obtain four equations from which the analytical expressions for the Mie coefficients are obtained. Only two of these equations are presented and have been expressed in [26]

$$\begin{aligned} a_l = &\quad \frac{\mu\, n^2\, j_l(nx)[x\, j_l(x)]' - \mu_1\, j_l(x)\,[nx j_l(nx)]'}{\mu\, n^2 j_l(nx)[x\, h_l^1\,(x)]' - \mu_1\, h_l^1\,(x)[nx j_l(nx)]'}, \\ b_l = &\quad \frac{\mu_1\, j_l(nx)[x\, j_l(x)]' - \mu\, j_l(x)\,[nx j_l(nx)]'}{\mu_1\, j_l(nx)[x\, h_l^1\,(x)]' - \mu\, h_l^1\,(x)[n\, x\, j_l(nx)]'}. \end{aligned} \tag{2.58}$$

The scattering coefficients (2.58) can be simplified somewhat by introducing the Riccati-Bessel function

$$\psi_l(\rho) = \rho j_l(\rho), \qquad\qquad \xi\,(\rho) = \rho h_l^{(1)}(\rho).$$

If we assumed that the permeability of both mediums is the same, then

$$\begin{aligned} a_l = &\quad \frac{n\psi_l(nx)\,\psi_l'(x) - \psi_l(x)\,\psi_l'(nx)}{n\psi_l(nx)\,\xi_l'(x) - \xi_l(x)\,\psi_l'(nx)}, \\ b_l = &\quad \frac{\psi_l(nx)\,\psi_l'(x) - n\psi_l(x)\,\psi_l'(nx)}{\psi_l(nx)\,\xi_l'(x) - n\xi_l(x)\,\psi_l'(nx)}, \end{aligned} \tag{2.59}$$

where n in equations (2.58) and (2.59) represents the refractive index of the material medium. The addition of a prime to the Riccati-Bessel functions denotes

differentiation with respect to their arguments.

Cross section, efficiency factors and amplitude matrix

The important physical quantities of the scatterer such as scattering cross sections C_{sca}, describes the power scattered by the product of a cross-sectional area and the incident intensity, or power. The absorption cross-section C_{abs}, tells us how much of the incident radiation is converted to heat energy. For non-absorbing particles, the extinction cross section is equal to the scattering cross section. Efficiency or normalized factors are closely related to the cross-sections. Thus, describes what proportion of the incident beam on a particle is attributable to a certain process. Most particles have an obvious geometrical cross-section G. A sphere of radius r has for instance, $G = \pi r^2$. The scattering and extinction cross sections are given in [16] and [17]

$$C_{sca} = (\lambda^2/2\pi) \sum_{l=1}^{\infty} (2l+1) \left\{ |a_l|^2 + |b_l|^2 \right\}, \tag{2.60}$$

and

$$C_{ext} = (\lambda^2/2\pi) \sum_{l=1}^{\infty} (2l+1) \left\{ R_e \left(a_l + b_l \right) \right\}, \tag{2.61}$$

where (2.60) and (2.61) represent the scattering and extinction cross sections respectively. The corresponding efficiency factors for scattering and extinction are obtained by dividing with the geometrical cross section of the particle, and for the case of sphere is πa^2, given as

$$Q_{sca} = (2/x^2) \sum_{l=1}^{\infty} (2l+1) \left\{ |a_l|^2 + |b_l|^2 \right\}, \tag{2.62}$$

and

$$Q_{ext} = (2/x^2) \sum_{l=1}^{\infty} (2l+1) \left\{ R_e \left(a_l + b_l \right) \right\}. \tag{2.63}$$

The amplitude matrix relates the scattered electric field E_s to the incident amplitude of the electric field E_i, where the EM radiation is split into polarized parallel and perpendicular to the scattering plane for the case of the linearly polarized plane waves. The amplitude matrix S for spherical object is a diagonal matrix; due to symmetry it takes the form

$$\begin{pmatrix} E_{\parallel}^{s} \\ E_{\perp}^{s} \end{pmatrix} = \frac{e^{ikr}}{r} \begin{pmatrix} S_2 & 0 \\ 0 & S_1 \end{pmatrix} \begin{pmatrix} E_{\parallel}^{i} \\ E_{\perp}^{i} \end{pmatrix}, \tag{2.64}$$

where

$$S_1 = \sum_{l=1}^{\infty} \frac{2l+1}{l(l+1)} \left(a_l \, \pi_l(\cos\theta) + b_l \, \tau_l(\cos\theta) \right), \tag{2.65}$$

and

$$S_2 = \sum_{l=1}^{\infty} \frac{2l+1}{l(l+1)} \left(a_l \, \tau_l(\cos\theta) + b_l \, \pi_l(\cos\theta) \right), \tag{2.66}$$

hence, τ_l and π_l are called the angle-dependent function, because they introduce this dependence in the Mie coefficients through the scattering angle θ, and are defined as

$$\tau_l = \frac{dP_l^1}{\sin\theta}, \qquad\qquad \pi_l = \frac{dP_l^1}{d\theta}. \tag{2.67}$$

Note the somewhat odd choice of element numbering in (2.64) which is due to convention in solving spherical case. This is a far field solution where it can be assumed that the scattered field is transverse and the elements of S are complex. The definition of this quantity do vary slightly between different authors and this must be taken into due consideration. The derivation of C_{sca} is obtained differently

in [16] in a way that it provides a rather interesting physical insight into the process.

2.7.2 T-Matrix method

The T-matrix method supported by freely available codes is now found everywhere and one of the most powerful technique according to available literature in the weather radar and microwave propagation and scattering. The original theory was developed by P.C. Waterman in 1965 [18], [75, 76] and is one of the popular computational method used for solving electromagnetic waves scattering problems by arbitrarily shaped particles. Another important feature of the T-matrix technique is that it reduces exactly to the Mie theory discussed in § 2.7.1 when the scatterer is a solid or layered sphere composed of isotropic material.

The approach is described as null field method by [77] and [78] or Extended Boundary Condition Method (EBCM) in [79]. The EBCM technique was also used by [80, 81] for computing scattering properties of three-dimensional scattering problem using a system of magnetic and electric dipoles, with many more implementations for different scattering problems explained in [82, 83, 84]. The power of the T-matrix method lies in relating the expansion of the scattered waves expansion coefficients in matrix notation to the incident coefficients. Changing the incident field angle, or the angle of the scattered radiation, does not require recalculation of the T-matrix.

2.7.2.1 T-Matrix method formulation

The standard scheme for computing the T-matrix for simple single particle or fixed aggregate is based on the extended boundary condition method, it begins

with spherical harmonic expansions of the incident and scattered fields in conjunction with boundary conditions at the surface of the scattering particle to obtain a system of linear equations relating the unknown expansion coefficients of the scattered field to the known coefficients incident field. Details of the development can be found in [85] and other improvement to this approach is fully discussed elsewhere [19] and [79]. Hence, only description of specific equations of interest are given here.

The notation of [65] is followed in the brief mathematical analysis of the T-matrix method in this review. The incident electric field expansion is given in [65]

$$\mathbf{E}^i(k_0\mathbf{r}) = \mathbf{E}_0 \sum_{\nu=1}^{\infty} \mathbf{D}_\nu \left[a_\nu \mathbf{M}_\nu^1 (k_0\mathbf{r}) + b_\nu \mathbf{N}_\nu^1 (k_0\mathbf{r}) \right], \tag{2.68}$$

where $\mathbf{M}$ and $\mathbf{N}$ are vector spherical harmonic functions of the first kind are finite at the origin (Bessel function), υ is the spherical harmonic triple index σ (even or odd), m, n. The expansion coefficient a and b are assumed known for a specified incident field (plane waves). The argument of the vector spherical wave functions is $k_0\mathbf{r}$, where $k_0 = 2\pi/\lambda$ the wave number in the surrounding medium, λ is the incident wavelength, and $\mathbf{r}$ is the position vector which defines a point in three-dimensional space. The $\mathbf{E}_0$ is the amplitude of the incident electric field. The normalization constant $\mathbf{D}_\nu$ is given in [86]

$$\mathbf{D}_\nu = \frac{\epsilon_m (2n+1)(n-m)!}{4n (2n+1)(n-m)!}, \tag{2.69}$$

where ϵ_m is equal to 1 for $m = 0$ and equal to 2 for $m > 0$.

The field inside the particle is written as [65]

$$\mathbf{E}^{int}(mk_0\mathbf{r}) = \mathbf{E}_0 \sum_{\mu=1}^{\infty} \mathbf{D}_\mu \left[c_\mu \mathbf{M}_\mu^1 (mk_0\mathbf{r}) + d_\mu \mathbf{N}_\mu^1 (mk_0\mathbf{r}) \right], \tag{2.70}$$

where c_μ and d_μ are the unknown internal field expansion coefficients, μ is the spherical harmonic triple index σ', m', n', and m is the refractive index of the particle relative to that of the surrounding medium. The internal field expansion coefficients solution are given in [79]

$$\left[\begin{array}{c|c} K_{\nu\mu} + mJ_{\nu\mu} & L_{\nu\mu} + mI_{\nu\mu} \\ \hline I_{\nu\mu} + mL_{\nu\mu} & J_{\nu\mu} + mK_{\nu\mu} \end{array}\right] \left[\begin{array}{c} c_\mu \\ \hline d_\mu \end{array}\right] = \left[\begin{array}{c} -ia_\nu \\ \hline -ib_\nu \end{array}\right], \tag{2.71}$$

where I, J, K, and L are two-dimensional integrals which defined the scattering object and are numerically evaluated over the surface of the particle. For instance their integral are expressed in [86]

$$\begin{aligned} I_{\nu\mu} &= \frac{k_0^2}{\pi} \int_s i_n \cdot \mathbf{M}_\nu^3(k_0\mathbf{r}') \times \mathbf{M}_\mu^1(mk_0\mathbf{r}')\, dS, \\ J_{\nu\mu} &= \frac{k_0^2}{\pi} \int_s i_n \cdot \mathbf{M}_\nu^3(k_0\mathbf{r}') \times \mathbf{N}_\mu^1(mk_0\mathbf{r}')\, dS, \\ K_{\nu\mu} &= \frac{k_0^2}{\pi} \int_s i_n \cdot \mathbf{N}_\nu^3(k_0\mathbf{r}') \times \mathbf{M}_\mu^1(mk_0\mathbf{r}')\, dS, \\ L_{\nu\mu} &= \frac{k_0^2}{\pi} \int_s i_n \cdot \mathbf{N}_\nu^3(k_0\mathbf{r}') \times \mathbf{N}_\mu^1(mk_0\mathbf{r}')\, dS, \end{aligned} \tag{2.72}$$

where i_n is the unit vector normal to the surface and $\mathbf{r}'$ is the position vector from an internal origin to the particle surface S.

Evaluation of scattered field coefficient. The field is expanded similar to that of

the incident field [86], one can write

$$\mathbf{E}^s(k_0\mathbf{r}) = \mathbf{E}_0 \sum_{\nu=1}^{\infty} \mathbf{D}_\nu \left[f_\nu \mathbf{M}_\nu^3 (k_0\mathbf{r}) + g_\nu \mathbf{N}_\nu^3 (k_0\mathbf{r}) \right], \tag{2.73}$$

where f_ν and g_ν are the unknown expansion coefficients of the scattered field, and the superscript 3 on $\mathbf{M}$ and $\mathbf{N}$ indicates that these functions are of the type suitable for radiation or outgoing fields (Hankel function). The scattered field expansion coefficients solution are expressed in [79]

$$\left[\begin{array}{c} f_\nu \\ \hline g_\nu \end{array}\right] = -i \left[\begin{array}{c|c} K'_{\nu\mu} + mJ'_{\nu\mu} & L'_{\nu\mu} + mI'_{\nu\mu} \\ \hline I'_{\nu\mu} + mL'_{\nu\mu} & J'_{\nu\mu} + mK'_{\nu\mu} \end{array}\right] \left[\begin{array}{c} c_\mu \\ \hline d_\mu \end{array}\right], \tag{2.74}$$

The parameters I', J', K', and L' are the same two-dimensional integral as in (2.71) expect that the Bessel function are replaced by Hankel function. The internal field two-dimensional integral is written in matrix form $[A]$ and the scattered field surface integral as matrix $[B]$, the scattered field expansion coefficients can be obtained from the known incident field expansion coefficients given in [79]

$$\left[\begin{array}{c} f_\nu \\ g_\nu \end{array}\right] = -\left[\begin{array}{c} \\ B \\ \\ \end{array}\right] \left[\begin{array}{c} \\ A \\ \\ \end{array}\right]^{-1} \left[\begin{array}{c} i(-ia_\nu) \\ i(-ib_\nu) \end{array}\right]. \tag{2.75}$$

The quantities $[B]\,[A]^{-1}$ is the $[T]$ or transition matrix which means that the column vector of the expansion coefficients of the scattered field is obtained by multiplying the T matrix and the column vector of the incident field expansion coefficients.

The vector far-field scattering amplitude of the scattered field and other charac-

teristics of the scatterer are defined in [86]

$$\mathbf{E}^s(k\mathbf{r}) = \mathbf{F}\left(\theta_s,\, \phi_s/\theta_i,\, \phi_i\right) \frac{\exp(ikr)}{r}, \quad kr \longrightarrow \infty, \tag{2.76}$$

where $\mathbf{F}(\theta_s,\, \phi_s/\theta_i,\, \phi_i)$ is the vector far-field amplitude in the $(\theta_s,\, \phi_s)$ direction due to an incident field in a given $(\theta_i,\, \phi_i)$ direction. The differential scattering cross section is defined as

$$\sigma_D = \lim_{r \longrightarrow \infty} \left[4\pi r^2 \frac{S_s(\theta_s,\, \phi_s)}{S_i(\theta_i,\, \phi_i)} \right], \tag{2.77}$$

where $S_s(\theta_s,\, \phi_s)$ = the scattered power density

$$S_s(\theta_s,\, \phi_s) = \frac{|\mathbf{F}(\theta_s,\, \phi_s/\theta_i,\, \phi_i)|^2}{2Z_0 r^2}, \qquad Z_0 = \sqrt{\mu_0/\epsilon_0}, \tag{2.78}$$

and $S_i(\theta_i,\, \phi_i)$ = the incident power density

$$S_i(\theta_i,\, \phi_i) = \frac{\left|\mathbf{E}^i\right|^2}{2Z_0}. \tag{2.79}$$

The differential scattering cross section $(d\sigma/d\Omega)$ is a normalised measure of how the intensity of scattered EM field varies with scattering angle or specifies the electromagnetic power scattered into unit solid angle about a given direction per unit incident intensity. And it depends on the polarization state of the incident radiation as well as on the incidence and scattering directions. Assuming that the incident electric field $\mathbf{E}^i$ has unit amplitude and substituting the expressions of (2.78) and (2.79) into (2.77) leads to

$$d\sigma/d\Omega(\theta_s,\, \phi_s/\theta_i,\, \phi_i) = 4\pi \left|\mathbf{F}(\theta_s,\, \phi_s/\theta_i,\, \phi_i)\right|^2. \tag{2.80}$$

All other properties such as extinction, scattering, absorption cross sections and

efficiency factors can be obtained directly once the vector far-field scattering amplitude **F** is known.

2.7.3 Discrete Dipole Approximation

The Discrete Dipole Approximation (DDA) is another approach [87, 88, 89] of evaluating scattering and absorption of electromagnetic waves by particles of arbitrary geometry and composition. The idea of the DDA according to [12], was introduced in 1964 by DeVoe who applied it to study the optical properties of molecular aggregates, however, his treatment was limited, due to non inclusion of retardation effect. The concept was modified and improved further by the inclusion of the retardation effect, which was proposed in 1973 by Purcell and Pennypacker and used it to study interstellar dust grains as explained in [67].

Conceptually, one fundamental aspect of the DDA can be interpreted as replacing the target of interest by a set of interacting dipoles; these dipoles interact with each other and the incident field, so the DDA is also sometimes referred to as couple dipole approximation [90]. The formulation give rise to a system of linear equations, which is solved to obtain dipole polarizations. All the measured scattering quantities can be obtained from these polarizations. However, the size of the linear equation to be solved depends on the number of dipole points.

The complexity of the DDA increases for electrically large scattering particles due to the number of polarizable points required to represent the target, in effect increasing the number of linear equations required n^3.

2.7.3.1 General formulation of DDA

The general form of the integral equation governing the electric field inside the dielectric scatterer is provided in [67], whose notation and outline is used in this description. The $\exp(-i\omega\, t)$ harmonic time dependence of all fields is assumed and suppressed throughout the formulation. A dielectric scatterer is considered without magnetic properties (i.e. permeability $\mu \approx 1$). The electric permittivity is assumed isotropic to simplify the derivation given in [67]

$$\mathbf{E(r)} = \mathbf{E}^{inc}\mathbf{(r)} + \int_{V \setminus V_0} \mathrm{d}^3 r' \bar{\mathbf{G}}(\mathbf{r}, \mathbf{r}')\chi(\mathbf{r}')\mathbf{E}(\mathbf{r}') + \mathbf{M}(V_0, \mathbf{r}) - \bar{\mathbf{L}}(\partial V_0, \mathbf{r})\chi(\mathbf{r})\mathbf{E(r)}, \tag{2.81}$$

where $\mathbf{E}^{inc}(\mathbf{r})$ and $\mathbf{E(r)}$ are the incident and total electric field at location $\mathbf{r}$; $\chi(\mathbf{r}) = (\varepsilon(\mathbf{r} - 1))/4\pi$ is the susceptibility of the medium at point $\mathbf{r}$ and $\varepsilon(\mathbf{r})$ is the relative permittivity. V is the volume of the particle, i.e., the volume that contains all point where the susceptibility is not zero. V_0 is a smaller volume such that $V_0 \subset V$, $\mathbf{r} \in V_0 \setminus \delta V_0$. $\bar{\mathbf{G}}(\mathbf{r}, \mathbf{r}')$ is the free space dyadic Green's function, defined in Appendix B.1. $\mathbf{M}$ is the integral associated with the finiteness of the exclusion volume $\mathbf{V}_0$, and expressed as

$$\mathbf{M}(V_0, \mathbf{r}) = \int_{V_0} \mathrm{d}^3 r' \left(\bar{\mathbf{G}}(\mathbf{r}, \mathbf{r'})\chi(\mathbf{r}')\mathbf{E}(\mathbf{r}') - \bar{\mathbf{G}}^s(\mathbf{r}, \mathbf{r}')\chi(\mathbf{r}')\mathbf{E(r)} \right), \tag{2.82}$$

where $\bar{\mathbf{G}}^s(\mathbf{r}, \mathbf{r}')$ is the static limit ($k \longrightarrow 0$) of $\bar{\mathbf{G}}(\mathbf{r}, \mathbf{r}')$ and $\bar{\mathbf{L}}$ is the so called self-term dyadic given as

$$\bar{\mathbf{L}}(\partial V_0, \mathbf{r}) = -\oint_{\partial V_0} \mathrm{d}^2 r' \frac{\hat{\mathbf{n}}'\hat{\mathbf{R}}}{R^3}, \tag{2.83}$$

hence, $\hat{\mathbf{n}}'$ is an external normal to the surface δV_0 at point $\mathbf{r}'$. $\bar{\mathbf{L}}$ is always a real symmetric dyadic with trace equal to 4π. It is important to note that $\bar{\mathbf{L}}$ does not

depend on the size of the volume V_0, but only on its shape (and location of the point $\mathbf{r}$ inside it). On the contrary, $\mathbf{M}$ does depend on the size of the volume, moreover it approaches zero when the size of the volume decreases [67]. When deriving equation (2.81) the singularity of the Green's function has been treated explicitly for dielectric medium, therefore it is preferable to the commonly used formulation [29]

$$\mathbf{E}(\mathbf{r}) = \mathbf{E}^{inc}(\mathbf{r}) + \int_V \mathrm{d}^3 r' \bar{\mathbf{G}}(\mathbf{r}, \mathbf{r}') \chi(\mathbf{r}') \mathbf{E}(\mathbf{r}'). \tag{2.84}$$

Discretization of equation (2.81) yields the following expression

$$\mathbf{E}(\mathbf{r}) = \mathbf{E}^{inc}(\mathbf{r}) + \sum_{j \neq i} \int_{V_j} \mathrm{d}^3 r' \bar{\mathbf{G}}(\mathbf{r}, \mathbf{r}') \chi(\mathbf{r}') \mathbf{E}(\mathbf{r}') + \mathbf{M}(V_i, \mathbf{r}) - \bar{\mathbf{L}}(\partial V_i, \mathbf{r}) \chi(\mathbf{r}) \mathbf{E}(\mathbf{r}). \tag{2.85}$$

The set of equation (2.85) is exact. Further, one fixed point $\mathbf{r}_i$ inside each V_i (its centre) is chosen and $\mathbf{r} = \mathbf{r}_i$ is set. Based upon the analysis in [67], in many cases the following assumption are expressed by

$$\int_{V_j} \mathrm{d}^3 r' \bar{\mathbf{G}}(\mathbf{r}, \mathbf{r}') \chi(\mathbf{r}') \mathbf{E}(\mathbf{r}') = V_j \bar{\mathbf{G}_{ij}} \chi(\mathbf{r}_j) \mathbf{E}(\mathbf{r}_j), \tag{2.86}$$

and

$$\mathbf{M}(V_i, \mathbf{r}_i) = \bar{\mathbf{M}}_i \chi(\mathbf{r}_i) \mathbf{E}(\mathbf{r}_i), \tag{2.87}$$

which state that integrals in equation (2.85) linearly depend upon the values of χ and $\mathbf{E}$ at point $\mathbf{r}_i$. Equation (2.85) leads to

$$\mathbf{E}_i = \mathbf{E}_i^{inc} + \sum_{j \neq i} \bar{\mathbf{G}}_{ij} V_j \, \chi(\mathbf{r}_j) \mathbf{E}(\mathbf{r}_j) \, (\bar{\mathbf{M}}_i - \bar{\mathbf{L}}_i) \chi_i \mathbf{E}_i, \tag{2.88}$$

where $\mathbf{E}_i = \mathbf{E}(\mathbf{r}_i)$, $\mathbf{E}_i^{inc} = \mathbf{E}^{inc}(\mathbf{r}_i)$, $\chi_i = \chi(\mathbf{r}_i)$, $\bar{\mathbf{L}}_i = \bar{\mathbf{L}}(\delta V_i, \mathbf{r})$. The values of $\mathbf{E}$ and χ is consider constant inside each sub-volume and which automatically implies that equations (2.86) and (2.87) yield

$$\bar{\mathbf{M}}_i^{(0)} = \int_{V_i} \mathrm{d}^3 r' \, \left(\bar{\mathbf{G}}(\mathbf{r}_i, \mathbf{r}') - \bar{\mathbf{G}}^s(\mathbf{r}_i, \mathbf{r}') \right), \tag{2.89}$$

and

$$\bar{\mathbf{G}}_{ij}^{(0)} = \frac{1}{V_j} \int_{V_i} \mathrm{d}^3 r' \, \bar{\mathbf{G}}(\mathbf{r}_i, \mathbf{r}'). \tag{2.90}$$

Superscript (0) denotes approximate values of the dyadics. Further approximation of (2.90), which is used in almost all formulations of the DDA is given [67]

$$\bar{\mathbf{G}}_{ij}^{(0)} = \bar{\mathbf{G}}(\mathbf{r}_i, \mathbf{r}'). \tag{2.91}$$

This assumption is made implicitly by all formulations that start by replacing the scatterer with a set of point dipoles. Equation (2.88) is assumed as the distinctive feature of the DDA, i.e. a method is called the DDA if and only if its main equation is equivalent to (2.88) with any of V_i, χ_i, $\bar{\mathbf{M}}_i$, $\bar{\mathbf{L}}_i$ and $\bar{\mathbf{G}}_{ij}$.

After the internal electric fields are determined, the scattered field and cross sections can be calculated. The scattered field is obtained by taking the limit $r \longrightarrow \infty$ of the integral in equation (2.81) yields

$$\mathbf{E}^{sca}(\mathbf{r}) = \mathbf{F}(\mathbf{n}) \, \frac{exp(ikr)}{-ikr}, \tag{2.92}$$

where $\mathbf{n} = \mathbf{r}/r$ is the unit vector in the scattering direction, and $\mathbf{F}$ is the scattering

amplitude function

$$\mathbf{F}(\mathbf{n}) = -ik^3(\bar{\mathbf{I}} - \hat{\mathbf{n}}\,\hat{\mathbf{n}}) \sum_i \int_{V_i} \mathrm{d}^3 r' \exp\left(-ik\mathbf{r}' \cdot \mathbf{n}\right) \chi(\mathbf{r}')\mathbf{E}(\mathbf{r}'). \tag{2.93}$$

All other differential scattering properties, such as amplitude and Mueller scattering matrices, and asymmetry parameter $< \cos\theta >$ can be derived from $\mathbf{F}(\mathbf{n})$. Considering an incident polarized plane wave given as

$$\mathbf{E}^{inc}(\mathbf{r}) = \mathbf{e}^0 \exp\left(i\mathbf{k} \cdot \mathbf{r}\right), \tag{2.94}$$

where $\mathbf{k} = k\mathbf{a}$, $\mathbf{a}$ is the incident direction vector, and $|\mathbf{e}^0| = 1$. The scattering cross section C_{sca} is given [67]

$$C_{sca} = \frac{1}{k^2} \oint \mathrm{d}\Omega \left|\mathbf{F}(\mathbf{n})\right|^2. \tag{2.95}$$

The absorption and extinction cross sections can be derived [91] directly from the internal fields

$$C_{abs} = 4\pi k \sum_i \int_{V_i} \mathrm{d}^3 r' \mathbf{Im}\left(\chi(\mathbf{r}')\right) \left|\mathbf{E}(\mathbf{r}')\right|^2, \tag{2.96}$$

$$C_{ext} = 4\pi k \sum_i \int_{V_i} \mathrm{d}^3 r' \mathbf{Im}\left(\chi(\mathbf{r}')\mathbf{E}(\mathbf{r}') \cdot \left[\mathbf{E}^{inc}(\mathbf{r}')\right]^*\right) = \frac{4\pi}{k^2} \mathbf{Re}\left(\mathbf{F}(\mathbf{n}) \cdot e^{0*}\right), \tag{2.97}$$

where $*$ denotes a complex conjugate. Conservation of energy necessitates that $C_{sca} = C_{ext} - C_{abs}$.

2.7.4 Other techniques

Aside the above mentioned methods of solving EM radiation scattering by particles, other techniques have been developed to treat the problem of electromagnetic

scattering and absorption by non-spherical and inhomogeneous dielectric particles. Majority of these procedures still involved homogenization of the complex objects by applying effective medium theories.

The last decades have experience different methods for volume and surface integral equations formulated for evaluating scattering properties and other desire quantities of inhomogeneous dielectric particles ranging from high to low permittivity contrast from the host background as treated in [62], and [92, 93], however, their approach culminate in homogenization process using conventional effective medium theories or piecewise homogeneous method (predefine distribution of constituents).

Experimental approach of [94] employ an open resonator to measure scattering properties of ice particles, artificially produced and located in a radar beam, but knowing the exact dimensions and physical state of the remotely sensed particle at melting layer remains a major challenge.

The null approach of solving inhomogeneous scattering problem explained in [77], [95] using integral equations for piecewise homogeneous structures. This was accomplished by treating each homogeneous section separately in a manner permitting a uniform set of dielectric constants over the entire region of interest. The fields and equations generated from each homogeneous section were then coupled by enforcing tangential field continuity at the transition boundaries of the different dielectric regions. An important aspect of this approach is the use of the unbounded-space Greens function for the treatment of each homogeneous region. Obviously, in a case of highly complex inhomogeneous dielectric region (i.e., a region in which the permittivity is arbitrary functions of position) this approach cannot be used because of lack of an appropriate Green's function.

A new approach is discussed in [36] to model ice aggregate and their melting process denoted as modified version of Fabry and Szyrmer's model 3 (FS3) to determine their scattering characteristics using Generalized Multiparticle Method (GMM) and T-Matrix Method involving a bulk representation at 3 and 35.6 GHz, however, their method do not produce the expected results at millimetre wavelength compared with those obtained using GMM for melting snowflakes.

The point matching technique as described in [96] use an infinite expansion in spherical vector waves of the incident and scattered fields with unknown coefficients. Truncation to a finite number of terms and application of boundary conditions for the representative number of points on the surface of the particle yield simultaneous linear equations for the determination of the unknown coefficients which in turn give the scattering amplitude. An essentially similar method is also used by [97], but with a least squares fitting process of the boundary conditions to yield greater accuracy. Although easy to describe and to understand, the practical implementation and usefulness of this method is limited to nearly spherical particles.

The finite-element method (FEM) as discussed in [19] is a differential equation technique that computes the scattered time-harmonic electric by solving numerically the vector Helmholtz equation subject to the standard boundary conditions. The scatterer is imbedded in a finite computational domain that is discretized into cells called elements, with about 10 to 20 elements per wavelength. The electric field values are specified at the nodes of these elements and are initially unknown. Through the requirement of the boundary conditions, the differential equation is converted into a matrix equation for the unknown node electric field values. This equation is solved using, e.g., standard Gaussian elimination (GE) or one of the

preconditioned iterative method such as the conjugate gradient method (CGM). The computational complexity of the FEM with sparse GE is $O(n^7)$, whereas that of the FEM with the CGM is only $O(n^4)$. The important advantages of the FEM are that it can be applied to arbitrarily shaped and inhomogeneous particles, is simple in concept and implementation, and avoid the singular-kernel problem typical of integral equation methods. However, FEM computations are spread over the entire computational domain rather than the confined to the scatterer itself as in the integral equation methods. This tends to make FEM calculations rather time consuming and limits the maximum size parameter to values less that about 10. Other disadvantage of the FEM with CGM is that computations must be repeated for each new direction of incidence.

Another significant approach of solving electromagnetic waves scattering problem is the Fredholm Integral Method (FIM) [13], [98, 99, 100, 101, 102], formulated in terms of volume integral equation which can be solved approximately by means of a series of successive or iterative approximations known as the Born series approximation. Applying Fourier transforms to the general solution expressed in terms of Green's function (i.e. by solving the point source equation) leaves the volume integral with a non-singular kernel. In 1980 Holt [103] gave an in-depth comparison of the FIM theory and the T-matrix methods. However, the Holt approach could not effectively handle arbitrary shape and inhomogeneous particle due to the limitation in evaluating the second Born approximation term. Our new approach of the FIM implementation proposed in this study has a good potential for evaluating inhomogeneous scatterers if numerical approach is applied and the number of equations to be solved reduces to n^2.

2.8 Summary

In this chapter we presented an overview of the Maxwell macroscopic equations as the basis for the wave theory approach in electromagnetic scattering by dielectric particles. The processes lead to the formation, growth, and precipitation of cloud particles in the atmosphere with emphasis on irregular hydrometeors such as melting snowflakes were highlighted. Followed by the melting layer model use in weather radar to describe the height of the Bright Band.

A short description of available models to evaluate the refractive index of irregular hydrometeors such as melting snowflake consisting liquid water, ice and air are given. A concise overview of effective mixing theories such as Maxwell-Garnett, Bruggeman and Coherent Potential mixing rule were described using the general family formula and appropriate references have been provided for application of these rules and others not mentioned in this study to dielectric or conductor-dielectric mixtures.

An overview of the Mie theory in terms of scattering problems has been given with particular interest in spherical particles and suitable literature have also been provided. We highlighted the theory and progress in T-Matrix Extended Boundary Condition (P.C.Waterman) in terms of its applications in the weather radar and microwave propagation and scattering, the T-Matrix approach supported by freely available codes is now ubiquitous. Furthermore, we gave a short description of another competing method, the Discrete Dipole Approximation, which replaces the scattering bodies with point of dipoles. For electrically small scatterers that are nevertheless compositionally fine grained, this approach is potentially more efficient than the standard Holt FIE method.

Finally, a short description of other techniques were presented with emphasis on Fredholm integral method owing to its distinctive feature in this study. The FIM is not new, rather the task of extending this approach with the main aim of evaluating scattering properties of inhomogeneous scatterers consisting of homogeneous inclusions. An in-depth theoretical overview of the FIM would be covered in chapter 3 and form the theoretical framework of this study.

CHAPTER 3

THEORY OF THE DISCRETE METHOD

3.1 Theoretical overview

Physical laws often can be expressed as differential, integro-differential and integral equations. In particular, scattering problems in differential or integro-differential necessitate additional boundary conditions which complicates the problem to be solved. This constraint does not arise when an integral equation method is used to characterise the scattering problem. Most importantly, the boundary condition of an integral equation is embedded in the formation of the problem [104]. This is particularly appropriate for the theoretical analysis of scattering theory, where

the interaction of electromagnetic waves with the particles may be presented in a somewhat phenomenological form to evaluate the desired scattering functions. In this chapter, we will highlight properties of an integral equation with special interest in Fredholm Integral Equation (FIE) of the second kind [105]. The theoretical expression for the scattering problem for both scalar and electromagnetic cases is discussed briefly. Finally, the formulation of theoretical analysis of the problem statement using FIE approach is introduced.

Fundamentally, an integral equation can be defined as an equation in which the unknown function to be determined appears under the integral sign. A typical form of an integral equation with the unknown function is given [105]

$$u(x) = f(x) + \lambda \int_{\alpha(x)}^{\beta(x)} K(x,t)u(t)\,dt, \tag{3.1}$$

where $K(x,t)$ is called the kernel of the integral equation (3.1), $\alpha(x)$ and $\beta(x)$ are the limits of integration. It can be easily observed that the unknown function $u(t)$ appears under the integral sign. Both the kernel and the function $f(x)$ are usually known functions, and λ is a constant parameter.

There are four major types of integral equations used for solving the unknown function; however, equation (3.3) would be mentioned because of its peculiarity for the solution of inhomogeneous problems which is the focus of this work. The standard form of Fredholm linear integral equation used in this analysis will be treated in § 3.1.2 and it is generally expressed as

$$\phi(x)u(x) = f(x) + \lambda \int_{a}^{b} K(x,t)u(t)\,dt, \tag{3.2}$$

where the limits of integration a and b are constant, the unknown function appears

linearly under the integral sign and $\phi(x) = 1$, then (3.2) becomes

$$u(x) = f(x) + \lambda \int_a^b K(x,t)u(t)\,dt. \tag{3.3}$$

This equation is defined as the non-homogeneous Fredholm linear Integral Equation (FIE) of the second kind. For $\phi(x) = 0$ in equation (3.2) leads to the FIE of the first kind expressed as

$$0 = f(x) + \lambda \int_a^b K(x,t)u(t)\,dt. \tag{3.4}$$

Applying an integral equations method to solve physical problems offers many advantages, few of which are listed below:

1. In a situation where the problem size becomes very large, the cruelty of scaling law prevails, implying that differential equations become very complex and usually require more unknown to be solved [106].

2. The unknown function can often be reduced from volume to surface integral whereas if a differential equation is solved and the unknown permeates the whole space of the object.

3. The Green's function method is appropriate to the boundary condition at hand and is a common approach in solving electromagnetic problems.

4. No boundary condition is required when applying integral equations to solve physical problems.

5. An integral equation method is seen to be very advantageous for numerical calculations.

3.1.1 Integral equation approach to scalar waves scattering

The time-independent Schrödinger differential equation in [22] is used to describe a scalar wave function $\psi(\mathbf{r})$

$$\mathbf{E}\,\psi(\mathbf{r}) = \left[-\frac{\hbar^2}{2m}\nabla^2 + V(\mathbf{r})\right]\psi(\mathbf{r}), \tag{3.5}$$

which can be rewritten as

$$(\nabla^2 + k^2)\psi(\mathbf{r}) = Q, \tag{3.6}$$

where $k = \dfrac{\sqrt{2m\mathbf{E}}}{\hbar}$ is the wavenumber, and $Q = \dfrac{2m}{\hbar^2}\,V(\mathbf{r})\,\psi(\mathbf{r})$ is the forcing function. The general solutions of (3.6) can be expressed as the sum of the homogeneous $\psi_h(\mathbf{r})$ and a particular $\psi_p(\mathbf{r})$ solutions

$$\psi(\mathbf{r}) = \psi_h(\mathbf{r}) + \psi_p(\mathbf{r}). \tag{3.7}$$

The homogeneous part satisfies this equation

$$(\nabla^2 + k^2)\psi_h(\mathbf{r}) = 0, \tag{3.8}$$

and the solution correspond to an incident plane wave $A\,e^{i\mathbf{k}\cdot\mathbf{r}}$. To determine the scattered field that will occur with an object having differing refractive index from the background medium, the particular solution has to be evaluated. The Green's function method can be used. Although the derivation of the Green's function method is given in Appendix B.1, and the general solution of (3.7) can be expressed as

$$\psi(\mathbf{r}) = A\,e^{i\mathbf{k}\cdot\mathbf{r}} + \frac{2m}{\hbar^2}\int G(\mathbf{r},\mathbf{r}')V(\mathbf{r}')\,\psi(\mathbf{r}')d^3r'. \tag{3.9}$$

The particular solution $\psi_p(\mathbf{r})$ of equation (3.7) using the Green's function method for the case of the outgoing wave (scattered wave) can be expressed as [107]

$$G(\mathbf{r}, \mathbf{r}') = \frac{e^{\mathrm{i}k|\mathbf{r}-\mathbf{r}'|}}{4\pi\,|\mathbf{r}-\mathbf{r}'|}. \tag{3.10}$$

Substituting (3.10) into (3.9) gives

$$\psi(\mathbf{r}) = A\,e^{\mathrm{i}\mathbf{k}\cdot\mathbf{r}} + \frac{m}{2\pi\hbar^2}\int \frac{e^{\mathrm{i}k|\mathbf{r}-\mathbf{r}'|}}{|\mathbf{r}-\mathbf{r}'|}V(\mathbf{r}')\,\psi(\mathbf{r}')d^3r'. \tag{3.11}$$

Evidently, equation (3.11) takes the form of (3.1) and the solution of can be solved successfully by means of a series of successive or iterative approximations, known as the Born's or Neumann's series [108].

The zeroth order of the Born approximation is straightforward, $\psi_0(\mathbf{r}) = \phi_{inc}(\mathbf{r}) = A\,e^{\mathrm{i}\mathbf{k}\cdot\mathbf{r}}$, where $\phi_{inc}(\mathbf{r})$ is the incident field. Accordingly, the first approximation $\psi_1(\mathbf{r})$ of the solution of $\psi(\mathbf{r})$ is expressed as

$$\psi_1(\mathbf{r}) = \phi_{inc}(\mathbf{r}) + \frac{m}{2\pi\hbar^2}\int \frac{e^{\mathrm{i}k|\mathbf{r}-\mathbf{r}_1|}}{|\mathbf{r}-\mathbf{r}_1|}V(\mathbf{r}_1)\,\psi_0(\mathbf{r}_1)d^3r_1 = \tag{3.12a}$$

$$\phi_{inc}(\mathbf{r}) + \frac{m}{2\pi\hbar^2}\int \frac{e^{\mathrm{i}k|\mathbf{r}-\mathbf{r}_1|}}{|\mathbf{r}-\mathbf{r}_1|}V(\mathbf{r}_1)\,\phi_{inc}(\mathbf{r}_1)d^3r_1. \tag{3.12b}$$

The second approximation $\psi_2(\mathbf{r})$ for the solution of $\psi(\mathbf{r})$ can be obtained by replacing $\psi_0(\mathbf{r})$ in equation (3.12) by the previously obtained $\psi_1(\mathbf{r})$, which become

$$\psi_2(\mathbf{r}) = \phi_{inc}(\mathbf{r}) + \frac{m}{2\pi\hbar^2}\int \frac{e^{\mathrm{i}k|\mathbf{r}-\mathbf{r}_2|}}{|\mathbf{r}-\mathbf{r}_2|} V(\mathbf{r}_2)\,\psi_1(\mathbf{r}_2) d^3r_2 = \tag{3.13a}$$

$$\phi_{inc}(\mathbf{r}) + \frac{m}{2\pi\hbar^2}\int \frac{e^{\mathrm{i}k|\mathbf{r}-\mathbf{r}_2|}}{|\mathbf{r}-\mathbf{r}_2|} V(\mathbf{r}_2)\,\phi_{inc}(\mathbf{r}_2) d^3r_2 + \frac{m^2}{4\pi^2\hbar^4}\int \frac{e^{\mathrm{i}k|\mathbf{r}-\mathbf{r}_2|}}{|\mathbf{r}-\mathbf{r}_2|} V(\mathbf{r}_2)\, d^3r_2 \int \frac{e^{\mathrm{i}k|\mathbf{r}_2-\mathbf{r}_1|}}{|\mathbf{r}_2-\mathbf{r}_1|} V(\mathbf{r}_1)\,\phi_{inc}(\mathbf{r}_1) d^3r_1. \tag{3.13b}$$

Continuing in this way, we can obtain any desired order; the nth order approximation for the wave function is a series which can be obtained by analogy of inserting lower-order terms into higher ones. The second approximation term is considered to be adequate and well approximated in scattering theory to describe the desired characteristics of the scatterer.

Now that we have used the Born approximation, exploring the far field or asymptotic limits of the wave function can be achieved. In scattering theory $\mathbf{r} >> \mathbf{r}'$, where $\mathbf{r}$ is the observation point of the scattering particle and $\mathbf{r}'$ is inferred to be the characteristic dimension of the scatterer. We may approximate for all points in the integral

$$k\,|\mathbf{r}-\mathbf{r}'| = k\sqrt{r^2 + r'^2 - 2\,\mathbf{r}\cdot\mathbf{r}'} \simeq kr - k\hat{\mathbf{r}}\cdot\mathbf{r}', \tag{3.14a}$$

$$e^{ik|\mathbf{r}-\mathbf{r}'|} = e^{ikr}\; e^{-i\mathbf{k}\cdot\mathbf{r}'}, \tag{3.14b}$$

$$\frac{1}{|\mathbf{r}-\mathbf{r}'|} = \frac{1}{r}\frac{1}{|1-\mathbf{r}\cdot\mathbf{r}'/r^2|} \simeq \frac{1}{r}\left(1 + \frac{\mathbf{r}\cdot\mathbf{r}'}{r^2}\right) \simeq \frac{1}{r}. \tag{3.15}$$

where $\mathbf{k} = k\hat{\mathbf{r}}$. Note that substituting (3.14) and (3.15) into (3.11) gives

$$\psi(\mathbf{r}) = A\, e^{\mathrm{i}\mathbf{k}\cdot\mathbf{r}} + \frac{m}{2\pi\hbar^2}\int \frac{e^{\mathrm{i}kr}\, e^{-\mathrm{i}\mathbf{k}\cdot\mathbf{r}'}}{r}\, V(\mathbf{r}')\psi(\mathbf{r}') d^3r'. \tag{3.16}$$

It is possible from the previous two approximation (3.14), we may write the asymp-

totic form of (3.11) as follows

$$\psi(\mathbf{r}) \approx \exp\left(\mathrm{i}\mathbf{k}_i \cdot \mathbf{r}\right) + \frac{\exp\left(\mathrm{i}kr\right)}{r} f(\theta,\, \varphi), \qquad r \longrightarrow \infty. \tag{3.17}$$

And here the scattering amplitude function $f(\theta, \varphi)$ is given as

$$f(\theta,\, \varphi) = \frac{m}{2\pi\hbar^2} \int \exp\left(-\mathrm{i}\mathbf{k}_s \cdot \mathbf{r}'\right) V(\mathbf{r}')\psi(\mathbf{r}')d^3r', \tag{3.18}$$

where $\mathbf{k}_s$ is the wave vector of scattered wave; the differential and total cross section are given by

$$\frac{d\sigma}{d\Omega} = \left|f(\theta,\, \varphi)\right|^2, \tag{3.19a}$$

$$\sigma_t = \int \left|f(\theta,\, \varphi)\right|^2 d\Omega. \tag{3.19b}$$

All we have done is to rewrite the Schrödinger differential equation (3.5) into an integral form (3.11), which is more suitable and well approximated for the scalar scattering theory problems.

3.1.2 Integral equation approach to EM waves Scattering

The notation of [29] and [109] are followed for the brief description of electromagnetic scattering problem by single particles. Considering a finite scatterer in the form of a single body or fixed aggregate embedded in an infinite, homogeneous, linear, isotropic, and non-absorbing medium. Mathematically, this is equivalent to dividing all space into two mutually disjoint regions, the finite region represents the interior of the scattering object and the infinite region is described as the exterior to the object.

We shall here use the Green's function method which is customary in quantum scattering theory (scalar waves). Here it is adapted for the case of electromagnetic wave. A typical representation of the scattering by the object begins with Maxwell's differential equations that are valid inside and outside of the volume containing dielectric objects. The differential equation in (2.22) is expressed herein as

$$\nabla \times (\nabla \times \mathbf{E}) - k_0^2 \, \mathbf{E} = k_0^2 (n^2 - 1)\mathbf{E}. \tag{3.20}$$

The general solution of the inhomogeneous linear differential equations (3.20) is (a) a complimentary solution of the respective homogeneous equation with the right hand side identically equal to zero and (b) particular solution of the inhomogeneous equation. Thus, the homogeneous equation of part (a) is the Helmholtz vector wave equation (2.15)

$$\nabla \times \nabla \times \mathbf{E} - k^2 \mathbf{E} = 0, \tag{3.21}$$

and describes the field that will exist in the absence of the scattering object, (i.e. the incident field). The physical appropriate particular solution of equation (3.20) must satisfy the scattered field generated by the forcing function. The Green's function method is employed with the derivation given in Appendix B.1 which shows that to evaluate the scattered field $\mathbf{E}$ in equation (3.20), the scattered field is replaced by the free space dyadic Green's function $\bar{\mathbf{G}}(\mathbf{r}, \mathbf{r}')$ while the right hand side of the inhomogeneous equation is also replaced by a three dimensional Dirac delta function $\delta(\mathbf{r}, \mathbf{r}')$ or point source. This modification leads to a new differential equation [107]

$$\nabla \times \nabla \times \bar{\mathbf{G}}(\mathbf{r}, \mathbf{r}') - k_0^2 \bar{\mathbf{G}}(\mathbf{r}, \mathbf{r}') = -\bar{\mathbf{I}}\delta(\mathbf{r}, \mathbf{r}'). \tag{3.22}$$

The solution of the equation (3.22) consisting of the dyadic Green's function and

Dirac delta function is given in [110] and [111]

$$\bar{\mathbf{G}}(\mathbf{r},\mathbf{r}') = (\bar{\mathbf{I}} + k_0^{-2}\nabla\nabla)G(\mathbf{r},\mathbf{r}'), \tag{3.23}$$

where $G(\mathbf{r},\mathbf{r}') = \dfrac{\exp(ik\,|\mathbf{r}-\mathbf{r}'|)}{4\pi\,|\mathbf{r}-\mathbf{r}'|}$ is the three dimensional free space Green's function, $\bar{\mathbf{I}}$ is the unit dyadic. It is worth noting that the dyadic component essentially projects out longitudinal components in the far field, which automatically ensure that the far field is transverse, so having only two components.

The general solution of (2.22) for the case of the electric field $\mathbf{E}(\mathbf{r})$ in integral form after rigorous analysis is given in (2.20)

$$\mathbf{E}(\mathbf{r}) = \mathbf{E}_i(\mathbf{r}) + \int_V \bar{\mathbf{G}}(\mathbf{r},\mathbf{r}')\left\{k_0^2(n^2-1)\mathbf{E}(\mathbf{r}') + \nabla\times\left[(1-\mu^{-1})\nabla'\times\mathbf{E}(\mathbf{r}')\right]\right\}\mathrm{d}^3r', \tag{3.24}$$

where $\gamma(\mathbf{r}) = k_0^2(n^2-1)$ is the polarizability and n the refractive index of the scattering object. It is clear from equation (3.24) that the integral extends over the volume of the scatterer. In the case of dielectric particles (i.e. non magnetic particles $\mu = 1$), the integral equation reduces to the form

$$\mathbf{E}(\mathbf{r}) = \mathbf{E}_i(\mathbf{r}) + \int_V \bar{\mathbf{G}}(\mathbf{r},\mathbf{r}')k^2(n^2-1)\mathbf{E}(\mathbf{r}')\mathrm{d}^3r'. \tag{3.25}$$

The incoming or incident plane wave $\mathbf{E}_i(\mathbf{r})$ can be defined in dyadic notation as:

$$\mathbf{E}_i(\mathbf{r}) = \bar{\mathbf{J}}_i\exp(i\mathbf{k}\cdot\mathbf{r}), \tag{3.26}$$

where $\bar{\mathbf{J}}_\lambda = \bar{\mathbf{I}} - \hat{\mathbf{k}}_\lambda\hat{\mathbf{k}}_\lambda$ is the projection dyadic relative to the incident field direction, $\hat{\mathbf{k}}_\lambda$ is a unit vector along k_λ and the subscript λ could be referred as incident i or scattered s . If we assume the refractive index of the scatterer $n \longrightarrow 1$ and $\mu \approx 1$,

then equation (3.24) becomes

$$\mathbf{E}(\mathbf{r}) = \mathbf{E}_i(\mathbf{r}), \tag{3.27}$$

which means the electric field is apparently equal to the incident field. The problem of non-linear equations are more convenient to solve in differential equation form as discussed in [106] and [112], however, this is not considered in this study.

3.2 Definition of the research problem

The theoretical definition of research problem is presented in this section especially in relation to some assumptions that have to be included to satisfactorily characterize electromagnetic waves scattering by homogeneous scatterer for studying inhomogeneous (melting irregular hydrometeors) particles.

If one assumes that scattered wave from a sphere will behave as an outgoing spherical wave, for large distance from the scattering particle, then it is possible to express the electric field at some point in space $\mathbf{r}$ by [113]

$$\begin{aligned} &\mathbf{E}(\mathbf{r}) = \mathbf{E}_i(\mathbf{r}) + \mathbf{E}_s(\mathbf{r}), \\ &\mathbf{E}(\mathbf{r}) \approx \exp\left(\mathrm{i}\,\mathbf{k}_i \cdot \mathbf{r}\right) + \frac{\exp(\mathrm{i}k_0 r)}{r}\,\mathbf{F}(\mathbf{k}_s,\,\mathbf{k}_i) + O\left(\frac{1}{r^2}\right). \end{aligned} \tag{3.28}$$

The $\mathbf{k}_i$ is the incident wave vector and $\mathbf{k}_s$ is the scattered wave vector and $\mathbf{F}$ is the scattering function which describes the scattering behaviour of the particle. Different methods can be employed to obtain this function. One of these has already been discussed in § 2.7.1 for the case of Mie theory.

However as discussed in § 2.3, the formation of irregular hydrometeors in the melt-

ing layer are relatively complex and the techniques discussed briefly in § 2.7 are not satisfactory. The FIM technique has been applied to the case of spheroids and ellipsoids [98]. Nevertheless, melting snowflake can not really be modelled as such geometric bodies since it is demonstrated that many scattering models, including spherical and spheroidal models, do not adequately describe the aggregate snowflakes that are observed [114]. As a result of this difficulty we proposed a new approach to the FIM for evaluation microwave scattering by irregular hydrometeors with solid inclusions randomly distributed (such as melting snowflakes consisting of different dielectric constants).

We assume a plane electromagnetic wave incident on a single or fixed aggregate scatterer with simple harmonic time dependence at angular frequency ω. For simplicity we suppressed the time factor $\exp(-\mathrm{i}\omega t)$ in all field quantities. Considering a homogeneous dielectric scatterer scenario and can be formulated using the dyadic EM wave equation. Substituting (3.26) into (3.25) we obtain

$$\mathbf{E}(\mathbf{r}) = \bar{\mathbf{J}}_i \exp\left(\mathrm{i}\mathbf{k}_i \cdot \mathbf{r}\right) + \int \bar{\mathbf{G}}(\mathbf{r}, \mathbf{r}') k_0^2 (n^2 - 1) \mathbf{E}(\mathbf{r}') \mathrm{d}^3 r', \tag{3.29}$$

where $\mathbf{r}$ and $\mathbf{r}'$ are position vectors respectively, with $\mathbf{r}'$ within the volume of the scatterer and $\mathbf{r}$ observation point in space. $\bar{\mathbf{G}}$ is the dyadic Green's function given in Appendix B.1 and defined as

$$\bar{\mathbf{G}}(\mathbf{r}, \mathbf{r}') = \left[\bar{\mathbf{I}} + \frac{\nabla\nabla}{k_0^2}\right] \frac{\exp(\mathrm{i}k_0 |\mathbf{r} - \mathbf{r}'|)}{4\pi |\mathbf{r} - \mathbf{r}'|}, \tag{3.30}$$

using the asymptotic behaviour of $\bar{\mathbf{G}}(\mathbf{r}, \mathbf{r}')$ as $r \longrightarrow \infty$, it is possible to deduce the total electric field $\mathbf{E}(\mathbf{r})$ in the far field

$$\mathbf{E}(\mathbf{r}) \approx \bar{\mathbf{J}}_i \exp\left(\mathrm{i}\mathbf{k}_i \cdot \mathbf{r}\right) + \frac{\exp(\mathrm{i}k_0 r)}{r} \bar{\mathbf{F}}(\mathbf{k}_s, \mathbf{k}_i) + O\left(\frac{1}{r^2}\right), \tag{3.31}$$

which is of the same form as (3.28) and where the dyadic scattering amplitude $\bar{\mathbf{F}}(\mathbf{k}_s, \mathbf{k}_i)$ is definite as

$$\bar{\mathbf{F}}(\mathbf{k}_s,\, \mathbf{k}_i) = \bar{\mathbf{J}}_s \cdot \int_V \exp(-\mathrm{i}\, \mathbf{k}_s \cdot \mathbf{r})\gamma(\mathbf{r})\mathbf{E}(\mathbf{r})\mathrm{d}^3 r. \tag{3.32}$$

Now can we see that the scattering function is dependent only on the electric field within the volume of the scatterer. This formulation does not actually require any knowledge of the field outside the scatterer since the integration in (3.32) is only throughout the volume of the scatterer. Therefore, we are able to compute the electric field inside the scattering particle, it is possible to obtain the dyadic scattering amplitude function $\bar{\mathbf{F}}$.

The field equation (3.29) is an integral equation with a singular kernel which makes it exceedingly demanding to evaluate. In what follows, a method is proposed to deal with the singularity effect analytically, leaving an integral equation with a non-singular kernel. Hence, pre-multiplying (3.29) by $\exp(-\mathrm{i}\mathbf{k}_1 \cdot \mathbf{r})\gamma(\mathbf{r})$, where $\mathbf{k}_1$ is an arbitrary vector and integrating throughout the volume of the scattering particle gives [113]

$$\begin{aligned} \int \exp(-\mathrm{i}\mathbf{k}_1 \cdot \mathbf{r})\gamma(\mathbf{r})\mathbf{E}(\mathbf{r})\mathrm{d}^3 r = \\ \bar{\mathbf{J}}_i \int \exp\left\{\mathrm{i}(\mathbf{k}_i - \mathbf{k}_1) \cdot \mathbf{r}\right\} \gamma(\mathbf{r})\mathrm{d}^3 r + \\ \iint \mathrm{d}^3 r\; \mathrm{d}^3 r' \exp(-\mathrm{i}\mathbf{k}_1 \cdot \mathbf{r})\bar{\mathbf{G}}(\mathbf{r}, \mathbf{r}')\gamma(\mathbf{r}')\mathbf{E}(\mathbf{r}'), \end{aligned} \tag{3.33}$$

with $\gamma(\mathbf{r}) = k_0^2(n^2 - 1)$ the polarizability.

Carrying out a Fourier transform on (3.29), which is square integrable inside the

scatterer, it is possible to avoid the singularity and it is expressed in [101]

$$\mathbf{E}(\mathbf{r}) = \int \bar{\mathbf{C}}(\mathbf{k}_2) \exp(\mathrm{i}\mathbf{k}_2 \cdot \mathbf{r}) \, \mathrm{d}^3 k_2. \tag{3.34}$$

It is noted that (3.34) does not give any representation of the field outside the scatterer, but it does coincide with true field inside the scatterer. Hence, substituting (3.34) into (3.33) gives

$$\int \mathrm{d}^3 k_2 \, \bar{\mathbf{K}}(\mathbf{k}_1, \, \mathbf{k}_2) \, \bar{\mathbf{C}}(\mathbf{k}_2)) = \bar{\mathbf{J}}_i \, U(\mathbf{k}_1, \, \mathbf{k}_i), \tag{3.35}$$

where

$$U(\mathbf{k}_1, \, \mathbf{k}_i) = \int \gamma(\mathbf{r}) \exp\left[-\mathrm{i}(\mathbf{k}_1 - \mathbf{k}_i) \cdot \mathbf{r}\right] \mathrm{d}^3 r, \tag{3.36}$$

the first Born term and in effect the spatial Fourier transform of the polarizability $\gamma(\mathbf{r})$ of the scatterer. The $\bar{\mathbf{K}}$ term can be expressed as

$$\begin{aligned} \bar{\mathbf{K}}(\mathbf{k}_1, \, \mathbf{k}_2) = \bar{\mathbf{I}} \, U(\mathbf{k}_1, \, \mathbf{k}_2) - \int \mathrm{d}^3 r \int \mathrm{d}^3 r' \\ \cdot \exp(-\mathrm{i} \, \mathbf{k}_1 \cdot \mathbf{r}) \gamma(\mathbf{r}) \bar{\mathbf{G}}(\mathbf{r}, \mathbf{r}') \gamma(\mathbf{r}') \exp(\mathrm{i} \, \mathbf{k}_2 \cdot \mathbf{r}'), \end{aligned} \tag{3.37}$$

is the kernel of the FIM and this is known to be remarkably stable. It can be expressed as

$$\bar{\mathbf{K}}(\mathbf{k}_1, \, \mathbf{k}_2) = \bar{\mathbf{I}} \, W(\mathbf{k}_1, \, \mathbf{k}_2) - \bar{\mathbf{Z}}(\mathbf{k}_1, \, \mathbf{k}_2), \tag{3.38}$$

where $\bar{\mathbf{K}}(\mathbf{k}_1, \mathbf{k}_2)$ is the non-singular kernel, $\bar{\mathbf{Z}}(\mathbf{k}_1, \mathbf{k}_2)$ correspond to the second Born series terms respectively. In the case of homogeneous scatterers, $W(\mathbf{k}_1, \, \mathbf{k}_2)$ is a simple pointwise multiplication of th first Born term $U(\mathbf{k}_1, \mathbf{k}_2)$ with the dielectric

constant given in [13]

$$W(\mathbf{k}_1,\, \mathbf{k}_2) = \int \exp\left[-\mathrm{i}(\mathbf{k}_1 - \mathbf{k}_2)\cdot \mathbf{r}\right] \gamma(\mathbf{r})\varepsilon(\mathbf{r})\mathrm{d}^3 r, \tag{3.39}$$

and

$$\bar{\mathbf{Z}}(\mathbf{k}_1,\, \mathbf{k}_2) = \frac{1}{8\pi^3 k_0^2} \lim_{\varepsilon\to 0} \int \frac{p^2\, \mathrm{d}^3 p}{p^2 - k_0^2 - i\varepsilon} \left[\bar{\mathbf{I}} - \hat{\mathbf{p}}\hat{\mathbf{p}}\right] U(\mathbf{k}_1, \mathbf{p}) U(\mathbf{p}, \mathbf{k}_2). \tag{3.40}$$

Substituting (3.34) into (3.33) leads to expressing the dyadic scattering function given in [98]

$$\bar{\mathbf{F}}(\mathbf{k}_s,\, \mathbf{k}_i) = \frac{1}{4\pi}\, \bar{\mathbf{J}}_s \cdot \int \mathrm{d}^3 k_2\, U(\mathbf{k}_s, \mathbf{k}_2)\, \bar{\mathbf{C}}(\mathbf{k}_2). \tag{3.41}$$

Equations (3.37) and (3.41) are the exact solution of the coupled Fredholm integral equations which together are use to determine the scattering amplitudes. They have the important property that $\bar{\mathbf{K}}$ is non-singular and (3.37) is solved by evaluating the integral by numerical quadrature. This has the effect of reducing the integral equation to matrix equations, which can easily be solved using any of the established factorization methods. This reduction is equivalent to describing the internal field in terms of a finite number of linear elements.

Evaluation of (3.36) which is known as the first Born term is straight forward. However, the $\bar{\mathbf{Z}}$ term known as the second Born approximation term is more complex to evaluate. Holt et.al [98],[101] calculates the $\bar{\mathbf{Z}}$ by expanding the first Born terms appearing under the phase integral into a series and then performed contour integration of the infinite radial phase integral as explained in [115] and [116]. This leads to the reduction of the integral into two angular integrations which are evaluated numerically. Detailed description of the derivation and evaluation of the Born terms are omitted for brevity and are expressly described in previous work

of [98], [103] and [113].

We need to use a new approach in this study which is directly in contrast with the FIM method description given by Holt et.al [98] and it would be treated in the next section.

3.3 Adapting FIM theory to Discrete Method

The method already discussed in § 3.2 is based on scattering from homogeneous bodies such as spheroids and ellipsoids is adapted to account for our new approach that we called the Discrete Method (DM) since we propose to employ a direct spatial integration rather than using the numerical integration of expansion in a set of polynomial proposed by Holt et al [98]. In this way, the scattering problem for the inhomogeneous particle can be formulated using equation (3.28) considering discretizing the inhomogeneous scattering particle into homogeneous dielectric cells.

3.3.1 Theoretical analysis of the first Born's term

We consider a finite homogeneous domain of three-dimensional regular lattice field discretized into uniform cubes known as cells or grid points. In order to validate the new proposed approach we consider solid shapes such as sphere with refractive index different from that of the finite domain as a result of already existing exact solution (Mie theory).

The evaluation of first Born term given in (3.36) using our proposed method is simple and straight forward with the discretization of the lattice field. We express

the U term as a summation over the cells according to their weighted contents given as follows

$$U(\mathbf{k}_n, \mathbf{k}_m) = \sum_j U_j(\mathbf{k}_n, \mathbf{k}_m), \tag{3.42}$$

hence,

$$\begin{aligned} U_j(\mathbf{k}_n, \mathbf{k}_m) &= \exp\left[-\mathrm{i}(\mathbf{k}_n - \mathbf{k}_m)\cdot\mathbf{r}_j\right]\ \gamma(\mathbf{r}_j) \\ &\cdot \int_{r\subset V_j} \exp\left(-\mathrm{i}(\mathbf{k}_n - \mathbf{k}_m)\cdot\mathbf{r}_j\right)\cdot(\mathbf{r}-\mathbf{r}_j)\mathrm{d}^3 r = \\ &\exp\left[-\mathrm{i}(\mathbf{k}_n - \mathbf{k}_m)\cdot\mathbf{r}_j\right]\ \gamma(\mathbf{r}_j)\ U_0(\mathbf{k}_n, \mathbf{k}_m) = \\ &= \exp(-\mathrm{i}\Delta\mathbf{k}_{n,m}\cdot\mathbf{r}_j)\ \gamma(\mathbf{r}_j)\ \Delta v. \end{aligned} \tag{3.43}$$

where V_j is the interior of the j_{th} cell, $U_0(\mathbf{k}_n, \mathbf{k}_m)$ well approximated to be the elementary cell volume Δv, $\gamma(\mathbf{r})$ the polarizability/cells and $\mathbf{r}_j$ is the centre of the j_{th} cell. Clearly, the integral is the Fourier transform of the weighted cell, and is a spatially invariant function of $\mathbf{k}_n - \mathbf{k}_m$. Note that the integral part of (3.43) after some manipulation is well approximated by the elementary cell volume dv, and $\mathbf{k}_n$ and $\mathbf{k}_m$ are expressed as

$$\begin{aligned} \mathbf{k}_n = \mathbf{k}_m &= |\mathbf{k}_n|\,(\sin\theta_n\cos\phi_n,\ \sin\theta_n\sin\phi_n,\ \cos\theta_n), \\ |\mathbf{k}_n| &= \mathrm{m}k_0, \end{aligned} \tag{3.44}$$

where $|\mathbf{k}_n|$ is the internal wave number, m the complex refractive index of the scatterer, $\mathbf{r}$ is a position vector which indicates location of cells or grid points in the regular lattice field (j_{th} cell), $\mathbf{k}_n$ and $\mathbf{k}_m$ are array of internal wave vectors, n and m represent the dimensions of the internal wave vectors, $\Delta\mathbf{k}_{n,m} = \mathbf{k}_n - \mathbf{k}_m$ are the distances between the array of pivot vectors, $\exp(-\mathrm{i}\Delta\mathbf{k}_{n,m}\cdot\mathbf{r})$ is the phase shift for each grid point in the 3-dimensional regular lattice field and $U(\mathbf{k}_n, \mathbf{k}_m)$ is the algebraic sum of the evaluated cells within the scattering particle according to their weighted contents.

The distances between pair of array of internal vectors $(\mathbf{k}_n - \mathbf{k}_m)$ appear like a mesh structure for a grid point as shown in Figure 3.1. This is the same for all other grid points within the lattice field. This approach simplifies the evaluation of the first Born term in (3.43) and $\Delta\mathbf{k}_{n,m}$ can be expressed in matrix form as:

$$\Delta\mathbf{k}_{n,m} = \begin{bmatrix} \mathbf{k}_{1,1} & \mathbf{k}_{1,2} & \cdots & \mathbf{k}_{1,m} \\ \mathbf{k}_{2,1} & \mathbf{k}_{2,2} & \cdots & \mathbf{k}_{2,m} \\ \vdots & \vdots & \ddots & \vdots \\ \mathbf{k}_{n,1} & \mathbf{k}_{n,2} & \cdots & \mathbf{k}_{n,m} \end{bmatrix}. \tag{3.45}$$

The matrix form of (3.45) is illustrated in Figure 3.1 showing the distance between the internal wave vectors for a grid point with lines in a two-dimensional configuration.

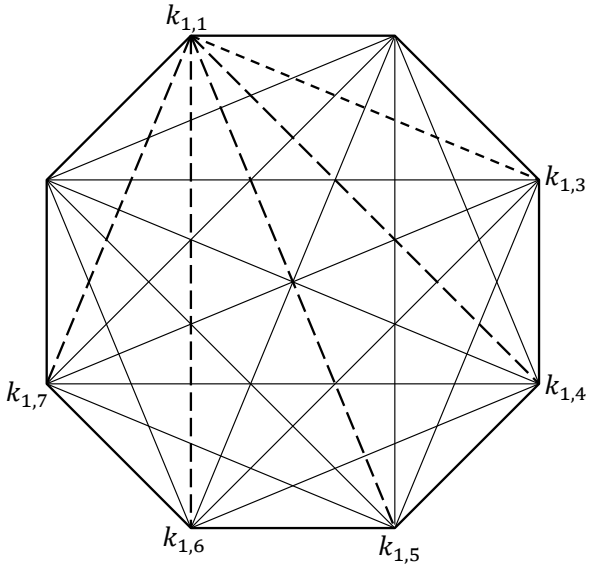

Figure 3.1: Geometry of a cross-sectional view of grid point in a mesh like structure showing the distance between array of internal wave vectors for evaluating first Born term with attention to $\Delta\mathbf{k}_{n,m}$.

Note that the array of the internal waves vectors $\mathbf{k}_n$ and $\mathbf{k}_m$ are identical, so

that the leading diagonal elements in (3.45) become zero and the phase shift $\exp(-\mathrm{i}\Delta\mathbf{k}_{n,m} \cdot \mathbf{r}) = 1$. The lower triangular matrix elements are conjugate of the correspondent upper elements. Hence, the number N_p of elements required has been reduced to the upper triangular matrix elements and it is

$$Np = \frac{n(n+1)}{2}.$$

By virtue of the theory of the U-term described, it is noted that (3.42) is easy to evaluate as a result of reusing numerical values for a grid point in other cells and this is achieved due to the uniform discretization of the lattice field into grid points (cubes).

The $W(\mathbf{k}_n, \mathbf{k}_m)$ function follows the same analytical procedure except for the addition of extra term, $\varepsilon(\mathbf{r})$. In relation to the generic theoretical approach, it is just a simple pointwise multiplication of the dielectric constant of the grid points $\varepsilon(\mathbf{r})$ within the scatterer as a function of position $\mathbf{r}$ by the first Born series term in equation (3.42). Fortunately each of the cells or grid points are homogeneous. Therefore, $W(\mathbf{k}_n, \mathbf{k}_m)$ function can be expressed as

$$W(\mathbf{k}_n, \mathbf{k}_m) = \sum_{\mathbf{r}_j} \exp(-\mathrm{i}\Delta\mathbf{k}_{n,m} \cdot \mathbf{r}_j) \;\; \gamma(\mathbf{r}_j)\, \varepsilon(\mathbf{r}_j)\, \Delta v, \tag{3.46}$$

or, alternatively as

$$W(\mathbf{k}_n, \mathbf{k}_m) = \sum_{\mathbf{r}_j} U_j(\mathbf{k}_n, \mathbf{k}_m)\varepsilon(\mathbf{r}_j). \tag{3.47}$$

3.3.2 Theoretical analysis of the second Born's term

We use the same assumption of uniform discretization of the regular lattice field for the evaluation of the second Born approximation. We begin the theoretical analysis by adapting equation (3.40), expanding the U terms that appear under the integral and expressing it as a summation over the cells.

$$Z(\mathbf{k}_n,\, \mathbf{k}_m) = \frac{1}{8\pi^3 k_0^2} \int_\Omega \int_0^\infty \frac{p^4 \,\mathrm{d}\Omega \,\mathrm{d}p}{p^2 - k_0^2 - i\varepsilon} [\bar{\mathbf{I}} - \hat{\mathbf{p}}\hat{\mathbf{p}}]\, U_j\left(\mathbf{k}_n, \mathbf{p}\right) U_i\left(\mathbf{p}, \mathbf{k}_m\right). \tag{3.48}$$

For brevity, we expressed the U terms in the same way as equation (3.43)

$$U_j(\mathbf{k}_n, \mathbf{p}) = \gamma(\mathbf{r}_j) \exp\left(-i(\mathbf{k}_n - \mathbf{p}) \cdot \mathbf{r}_j\right) U_0(\mathbf{k}_n, \mathbf{p}), \tag{3.49}$$

and

$$U_i(\mathbf{p}, \mathbf{k}_m) = \gamma(\mathbf{r}_i) \exp\left(-i(\mathbf{p} - \mathbf{k}_m) \cdot \mathbf{r}_i\right) U_0(\mathbf{p}, \mathbf{k}_m). \tag{3.50}$$

Substituting (3.49) and (3.50) into (3.48) and taking summation over $\mathbf{r}_j$ and $\mathbf{r}_i$ leads to expressing the Z-term in a discretized version of the U terms

$$\begin{aligned} \bar{Z}(\mathbf{k}_n,\, \mathbf{k}_m) = \frac{1}{8\pi^3 k_0^2} \sum_j \sum_i \gamma(\mathbf{r}_j)\gamma(\mathbf{r}_i) \int_\Omega \int_0^\infty e^{[-\mathrm{i}(\mathbf{k}_n - \mathbf{p})\cdot \mathbf{r}_j]} \\ \cdot\, e^{[-\mathrm{i}(\mathbf{p} - \mathbf{k}_m)\cdot \mathbf{r}_i]}\, U_0(\mathbf{k}_n, \mathbf{p})\, U_0(\mathbf{p}, \mathbf{k}_m) \frac{p^4 \,\mathrm{d}\Omega \,\mathrm{d}p}{p^2 - k_0^2 - i\varepsilon} [\bar{\mathbf{I}} - \hat{\mathbf{p}}\hat{\mathbf{p}}]. \end{aligned} \tag{3.51}$$

The notation $[\bar{\mathbf{I}} - \hat{\mathbf{p}}\hat{\mathbf{p}}]$ has the representation

$$\bar{\mathbf{I}} - \hat{\mathbf{p}}\hat{\mathbf{p}} = \begin{pmatrix} 1 - y^2\cos^2\phi & -y^2\cos\phi\sin\phi & -xy\cos\phi \\ -y^2\cos\phi\sin\phi & 1 - y^2\sin^2\phi & -xy\sin\phi \\ -xy\cos\phi & -xy\sin\phi & y^2 \end{pmatrix}, \tag{3.52}$$

we have used the following: $\cos\theta = x$, $\sin\theta = y$ and

$$\begin{aligned} \sin^2\theta + \cos^2\theta &= 1, \\ y^2 + x^2 &= 1, \end{aligned} \tag{3.53}$$

where

$$y^2 = 1 - x^2. \tag{3.54}$$

By separation of the radial exponential terms in the U-terms in equation (3.51) and rearranging the terms, the $\bar{\mathbf{Z}}$ term is further simplified to the form expressed as

$$\begin{aligned} Z(\mathbf{k}_n,\, \mathbf{k}_m) = \frac{1}{8\pi^3 k_0^2} \sum_j \sum_i \gamma(\mathbf{r}_j)\gamma(\mathbf{r}_i)\ \exp\left(-\mathrm{i}\mathbf{k}_n \cdot \mathbf{r}_j\right)\ \exp\left(\mathrm{i}\mathbf{k}_m \cdot \mathbf{r}_i\right) \\ \cdot \int_\Omega \int_0^\infty \cdot \exp\left[\mathrm{i}(\hat{\mathbf{p}} \cdot (\mathbf{r}_j - \mathbf{r}_i)p\right]\, U_0(\mathbf{k}_n, \mathbf{p})\, U_0(\mathbf{p}, \mathbf{k}_m) \\ \cdot \frac{p^4\, \mathrm{d}\Omega\, \mathrm{d}p}{p^2 - k_0^2 - i\varepsilon} [\bar{\mathbf{I}} - \hat{\mathbf{p}}\hat{\mathbf{p}}], \end{aligned} \tag{3.55}$$

where $\mathbf{k}_n$, $\mathbf{k}_m$ are array of internal wave vectors respectively, $\mathbf{p}$ the array of pivot vector, $\gamma(\mathbf{r}_j)$ and $\gamma(\mathbf{r}_i)$ are the polarizabilities given as $k_0^2(\varepsilon - 1)$ with respect to distinct cells in the regular 3-dimensional lattice field.

The aim is to evaluate the integral over p by contour integration. The largest contribution to this integral occurs close to the pole so that the U_0 factors in the term are well approximated. Now, we have to deal with the integral over p, expressed as

$$\int_\Omega \int_0^\infty U_0(\mathbf{k}_n, \mathbf{p})\, U_0(\mathbf{p}, \mathbf{k}_m)\ \exp(i\beta p) \frac{p^4\, \mathrm{d}\Omega\, \mathrm{d}p}{p^2 - k_0^2 - i\varepsilon}, \tag{3.56}$$

where $\beta = \hat{\mathbf{p}} \cdot (\mathbf{r}_i - \mathbf{r}_j)$ is the relative phase of the cells measured in the direction

of the pivot vector. The problem arises if we wish to directly evaluate the integral (3.56) over p by means of contour integration. The behaviour of the integrand on the imaginary axis needs to be considered carefully. For a cubic cell, U_0 takes the form of a three dimensional sinc function, and there are considerable difficulties in obtaining a convergent integral analytically.

Now, we may consider a more radical approach in which it is argued that the contribution of these terms should not depend critically on the shape of the cubic cell, but is much more strongly dependent on its volume. Accordingly, we consider instead, substituting U_0 with U_s, defined as the function for a sphere of equal volume to the basic cubic cell. We need to do this approximation because of the singularity in the domain of integration, but noticed that it is not possible to use the cubic cell as discussed [117]. We only need to consider how this term behaves at large imaginary p, hence we expressed the U_0 factors as

$$U_0 \approx U_s = 4\pi\rho^3 \frac{J_{\frac{3}{2}}(p\rho)}{(p\rho)^{\frac{3}{2}}}, \tag{3.57}$$

where $J\left(3/2, \rho p\right)$ is the half order Bessel function, the relationship of the radial part of (3.57) to the basic cubic cell characteristic length can be approximated as

$$abc \approx \frac{4\pi\rho^3}{3}, \qquad \text{if } a = b = c, \qquad a^3 \approx \frac{4\pi\rho^3}{3}, \tag{3.58}$$

where a, b, c are the dimensions of the cubic cell and the equivalent volume radius ρ is expressed as

$$\rho = a\left(\sqrt[3]{\frac{3}{4\pi}}\right). \tag{3.59}$$

When the argument $p\rho$ in (3.57) is very small (i.e. zero of the Fourier transform of the content of the sphere), the half order Bessel function tends to 1/3, so

that the term is equal to the cell volume. In (3.57) we have neglected the offset contribution of $\mathbf{k}_n$ and $\mathbf{k}_m$. It can be justified by considering an expansion in infinite series of higher order cylinder functions. It may be assumed that $p\rho$ is so small for fundamental cell that the higher terms may be neglected. Note that substituting (3.57) into (3.56) introduces integrals of product of Bessel functions of half order. It is not possible to apply a closed form analytical solution to evaluate this integral as described in G.N.Watson [115, p. 429]. The problem of the Z-term integral for paired spherical cells is that we need to evaluate the radial part of the Z integral. This can be expressed as

$$I_{k_0} = \lim_{\varepsilon \longrightarrow 0+} \frac{1}{\rho^3} \int_0^\infty \frac{J_\nu^2(p\rho)}{p^3} \frac{p^4 \exp(i\beta p)}{p^2 - k_0^2 - i\varepsilon} \, dp, \tag{3.60}$$

where $v = \frac{3}{2}$ is the order of the Bessel function. The position of the main pole is close to the real axis as shown in Figure 3.4 for the problem of interest. Care need to be exercised with regards to the signs of the residues because of the direction of traversing the contour. A further simplification is that if the cell sizes are small enough with respect to the wavelength, the expansion of the Bessel functions involving the separation vector in wavenumber space can be truncated to the first term as the rest are negligible [115]. Let us consider the following integral

$$I_1 = \lim_{\varepsilon \longrightarrow 0+} \frac{1}{\rho^3} \int_0^\infty J_\nu^2(\rho \, k_0 \, p') \frac{p' \exp(i\beta k_0 p')}{p'^2 - 1 - i\varepsilon} \, dp', \tag{3.61}$$

where

$$p' = \frac{p}{k_0}. \tag{3.62}$$

Hence, comparing coefficients of (3.60) and (3.61), we can write I_{k_0} as

$$\begin{aligned} I_{k_0} &= \frac{1}{k_0^2}\, I_1, \\ &= \frac{1}{k_0^2}\,\frac{1}{\rho^3}\int_0^\infty J_\nu^2(\rho\, k_0\, p')\,\frac{p'\exp(i\beta\, k_0\, p')}{p'^2-1}\,\mathrm{d}p'. \end{aligned} \tag{3.63}$$

Then, substituting (3.63) into (3.55) leads to expressing the Z-term as

$$\begin{aligned} Z(\mathbf{k}_n,\,\mathbf{k}_m) = \frac{1}{8\pi^3 k_0^2}\,\frac{4\pi}{N_m}\,\frac{16\,\pi^2\,\rho^6}{\rho^3}\sum_j\sum_i \gamma(\mathbf{r}_j)\gamma(\mathbf{r}_i)\;\exp\left(-\mathrm{i}\mathbf{k}_n\cdot\mathbf{r}_j\right)\;\exp\left(\mathrm{i}\mathbf{k}_m\cdot\mathbf{r}_i\right) \\ \cdot\,[\bar{\mathbf{I}}-\hat{\mathbf{p}}\hat{\mathbf{p}}]\int_0^\infty J_\nu^2(\rho\, k_0\, p')\,\frac{p'\,\exp(i\beta k_0 p')}{p'^2-1}\,dp'. \end{aligned} \tag{3.64}$$

Equation (3.64) is the normalised form of the integral required in evaluating the contribution of the Z integral, which is the product of the Fourier transforms of the scatterer content $k_0^2(\varepsilon-1)$ and therefore, a double volume integral over pairs of points. This can be re-expressed as the sum of a more elementary integral involving pairs of identically sized cells. Knowing how to calculate this integral for an arbitrarily separated pair of cells, the entire Z integral can be expressed as the sum of all such pair-wise contributions.

The function (3.60) depends on two parameters, $\rho\, k_0$ and β, where ρ is the radius of the equivolume spherical cell. By definition there is a singularity close to the real axis, which makes direct evaluation of the integral by numerical means somehow problematic. Integrals of this type were considered early in the history of analysis of Bessel functions, and particularly by Hankel integral method [115, p.429]. In many cases, such integrals of products of Bessel functions have a closed form solution involving Bessel functions and Hankel functions evaluated at the pole. In our case, the pure exponential factor in the integrand can be expressed in terms of Bessel functions of half-order. Unfortunately the approach taken by Hankel

and others [115, 116] cannot be applied essentially because of the power of p in the integrand being odd. In fact, it is not possible to use symmetry arguments to extend the integral to the negative axis. An alternative approach which still involves contour integration method would be to integrate along a quandrantal contour which goes from zero to real infinity, then anticlockwise around a quarter circle and then returning along the imaginary axis. The attractiveness of this scheme would be that the integral along the imaginary axis has no poles and decreases monotonically. However, investigations found that although there is a dominant exponential factor, the residual factor is not close to polynomial form because of the denominator terms in the integrand, and fast quadrature schemes do not work well.

A more workable solution was found by using a weighting function to the radial integral (3.60). This takes the form,

$$\int_0^\infty J_\nu^2\left(k_0\,\rho\,p'\right)\,w(p')\,\frac{p'\,\exp(i\beta k_0 p')}{p'^2-1}\,dp'. \tag{3.65}$$

The conditioning weighting function $w(p')$ can be expressed as

$$w(p') = \frac{1}{1+\exp(-(\alpha\,p')^2)}, \tag{3.66}$$

where p' in (3.66) is complex, given as

$$p' = \frac{1}{\alpha}\sqrt{(2n-1)\pi\,i}, \tag{3.67}$$

and

$$\sqrt{i} = \exp\left(\frac{i\pi}{4}\right). \tag{3.68}$$

Expanding the right hand side of (3.68) using Euler's formula leads to

$$\sqrt{i} = \frac{1+i}{\sqrt{2}}, \tag{3.69}$$

hence, p' can be expressed as

$$p' = \frac{1}{\alpha}\sqrt{(2n-1)\pi}\,\frac{(1+i)}{\sqrt{2}} \qquad n = 1, 2, 3, 4, \cdots, N. \tag{3.70}$$

Now the weighting function on the real axis, $w(p') \approx \frac{1}{2}$ near the origin as shown in Figure 3.2, but rapidly increases to 1. The function approximates the desired integral (3.63) as α increases. Since the integral is small anyway near the origin, the result is accurate even for modest values of α. The function w on the real axis, where $p' = x$ takes this form

$$w(x) = \frac{1}{1 + \exp\left(-\alpha^2\, x^2\right)}, \tag{3.71}$$

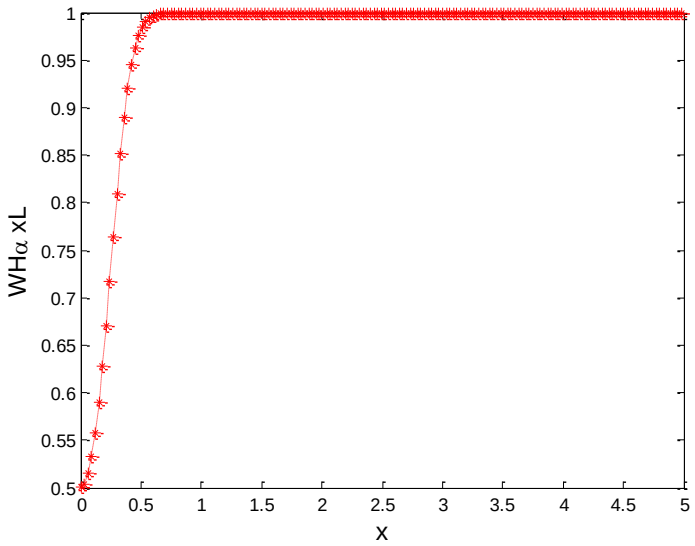

Figure 3.2: The weighting factor w as a function of $\Re(p')$ for $\alpha = 4.0$

on the imaginary axis, where $p' = iy$, it takes this form

$$w(y) = \frac{1}{1 + \exp\left(\alpha^2\, y^2\right)}, \tag{3.72}$$

For small y, thus $w \approx \frac{1}{2}$ it decreases very rapidly as shown in Figure 3.3. Even though the integral of the original integration (3.60) might increase exponentially in one direction of the other, w increases it quickly. We are assured that on the arc, the real axis tends to infinity and the integrand is vanishingly small.

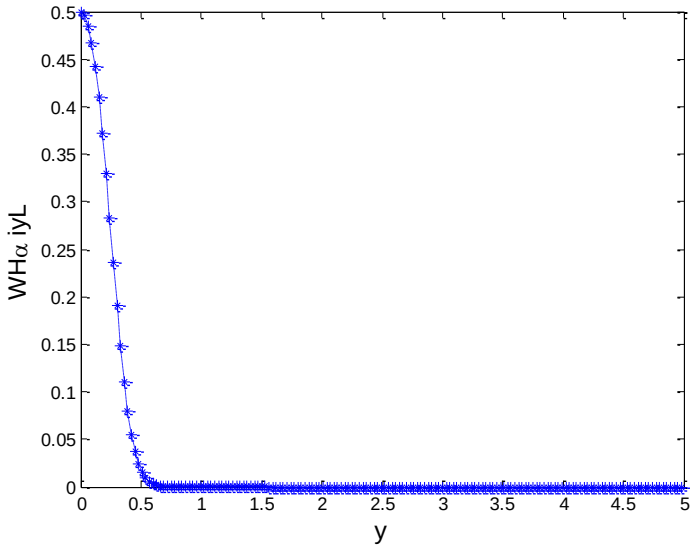

Figure 3.3: The weighting factor w as a function of $\Im(p')$ for $\alpha = 4.0$

This integral (3.60) is reduced relatively to the unweighted one by a slight amount, because the integrand is very small near the origin. If necessary, the correction can in anywise easily be corrected because the integrand has very simple behaviour away from the pole. Correspondingly, along the positive imaginary axis the weighting function very rapidly tends to zero, and apart from a similar very small contribution near the origin, the weighted integral on the imaginary axis becomes negligible. It can be verified that the integrand on the quarter circle diminishes

sufficiently rapidly to be neglected towards infinity along the real axis as discussed. As a result, therefore, the desired integral can be expressed accurately as a sum of residues. There is only one problem with this prescription, which is that the weighting function itself introduces new singularities, in fact an infinity of them along the line $x = y$ as shown in Figure 3.4, where the complex coordinate is $p' = x + iy$. However, experimental results show that the number of weighting function poles, $np' \geq 100$ are sufficient to relatively perform the integration.

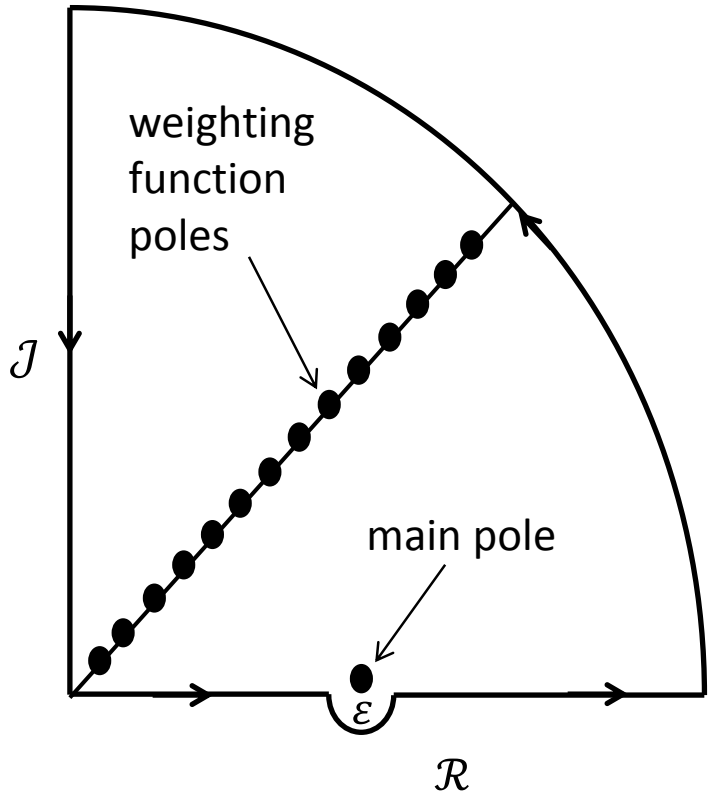

Figure 3.4: Geometry of a semi circle split into two equal half with the top half enclosing the poles at near real axis and the weighting function poles at $x = y$ for the evaluation of the second Born term.

Although it is necessary to sum typically hundreds of residues to obtain convergence, the regularity of the spacing of the poles makes the sum typically scalable in relation to the cell size, and by considering the sum of the residues as a function in its own right, it has been found that for a wide range of parameters ρ and β, the residue sum can be approximated piecewise as a function of ρ and β. Figure 3.5 depict the conditioning weighting function poles without the normalised integral

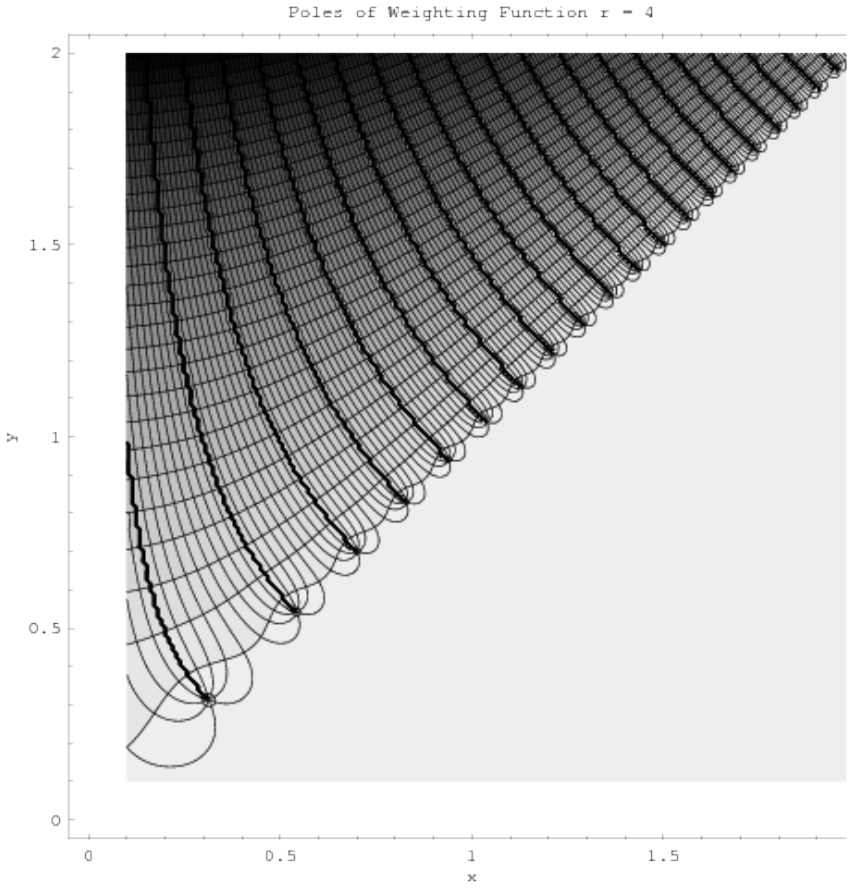

Figure 3.5: The conditioning weighting function poles at $x = y$.

An exception to this finding, however, occurs when the phase separation parameter β is small. For this regime it appears that the summation of the residues fails to converge, and the only viable alternative appears to directly model the function. Numerical experimentation established that in this regime the function

has excellent scaling properties with respect to cell size (when the cell is small) so that a universal function of one parameter can effectively be established. Because the function has a real symmetric peak, and an antisymmetric imaginary part that also decays rapidly, the primary model for the function was a Gaussian for the real part and the derivative of a Gaussian for the imaginary part. In practice this was refined by fitting quartic functions to the argument of the exponential factors.

The conditioning weighting function suppresses the integrand a little at small values, but to a very high accuracy kills the integrand on the imaginary axis, suppressing the effect of the Bessel functions. The weighting function introduces an infinite sequence of poles as shown in Figure 3.4 along the $x = y$ line whose residues have to be summed. But for larger β this turns out to be a well behaved function that can also be interpolated. By breaking up the range appropriately, good approximations that scale simply with the cell size parameter are obtained using quartic polynomial segments. No attempt is made to force continuity in value or derivatives between adjacent segments has been made. The graph of the weighted integrand including poles at $p = k_0$ and at $x = y$.

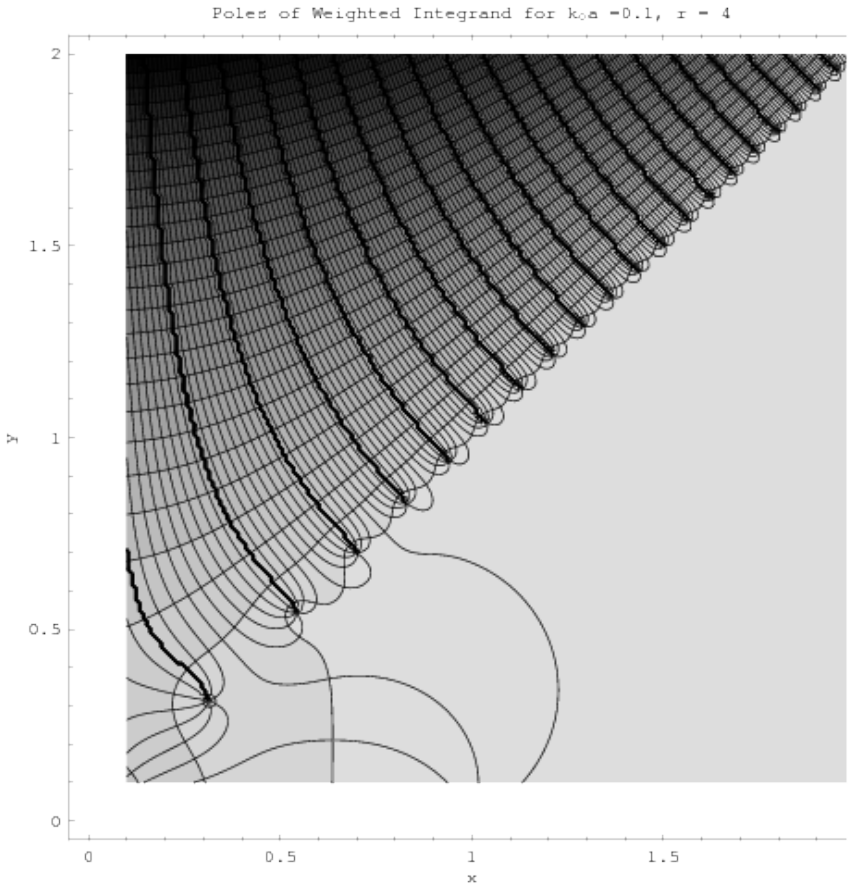

Figure 3.6: The conditioning weighted integrand including poles at $p = k_0$ and at $x = y$

Looking at the graphs of both functions, one could suggest that the effect of introducing the conditioning weighting function does not really affect the original integral. Finally, the Z-term including the conditioning weighting function is summarised as

$$Z(\mathbf{k}_n,\, \mathbf{k}_m) = \frac{1}{2\pi^2 k_0^2\, N_m}\, 12\pi\, \Delta v \sum_j \sum_i \gamma(\mathbf{r}_j)\gamma(\mathbf{r}_i)\ \exp\left(-\mathrm{i}\mathbf{k}_n \cdot \mathbf{r}_j\right)\ \exp\left(\mathrm{i}\mathbf{k}_m \cdot \mathbf{r}_i\right) \cdot [\bar{\mathbf{I}} - \hat{\mathbf{p}}\hat{\mathbf{p}}] \int_0^\infty J_\nu^2(\rho\, k_0\, p')\, \frac{p'\, \exp(i\beta k_0 p')}{p'^2 - 1}\, dp', \tag{3.73}$$

where $16\pi^2\rho^3 = \dfrac{4\pi\rho^3}{3} \times 12\pi = 12\pi \times \Delta v$ and the number of integral over p is given

as N_m term.

In chapter 4, we would apply (3.73) according to the relationship between β and ρk_0 for the code level implementation of the Z-term for each cell pair.

3.3.3 Analysis of the non-singular Kernel and Amplitude function

For the theory of non-singular kernel we multiply equation (3.46) by a unit dyadic, thus leads to expressing the FIM kernel as subtracting the dyadic form of (3.46) from (3.55), one can write the non-singular kernel as

$$\bar{\mathbf{K}}(\mathbf{k}_n, \mathbf{k}_m) = \bar{\mathbf{I}} W(\mathbf{k}_n, \mathbf{k}_m) - \bar{\mathbf{Z}}(\mathbf{k}_n, \mathbf{k}_m). \tag{3.74}$$

Now it is possible to evaluate the unknown solution vector in the form of dyadic Fourier coefficient $\bar{\mathbf{C}}_m$, we simplified (3.74) which reduces to a linear block matrix equation with dyadic elements. This takes the form

$$\begin{aligned} \sum_{n,m} \bar{\mathbf{K}}(\mathbf{k}_n, \mathbf{k}_m)\,(w_m \bar{\mathbf{C}}_m) &= \bar{\mathbf{J}}_i\, U(\mathbf{k}_n, \mathbf{k}_i), \\ \sum_{n,m} \bar{\mathbf{K}}(\mathbf{k}_n, \mathbf{k}_m)\,\bar{\mathbf{Y}}_m &= \mathbf{J}\bar{\mathbf{U}}_n, \end{aligned} \tag{3.75}$$

and

$$\begin{aligned} \mathbf{k}_n &= k_n(\sin\theta_n \cos\phi_n,\ \sin\theta_n \sin\phi_n,\ \cos\theta_n), \\ \mathbf{k}_i &= k_0(\sin\theta_i \cos\phi_i,\ \sin\theta_i \sin\phi_i,\ \cos\theta_i), \\ k_n &= \mathrm{m} k_0, \end{aligned} \tag{3.76}$$

where $\mathbf{k}_n$ is the internal array wave vectors, $w_m = \frac{4\pi}{N_m}$ is the formal numerical integration weighting factor, N_m the number of integral over p, $\mathbf{k}_i$ is the incident

wave vector, m is the refractive index of scatterer, $\bar{\mathbf{C}}_m$ is the unknown solution vector to be evaluated with elements in dyadic form and $\bar{\mathbf{J}}_i = [\bar{\mathbf{I}} - \hat{\mathbf{k}}_i\hat{\mathbf{k}}_i]$ is the projection vector along the incident field direction with elements in dyadic form, $U(\mathbf{k}_n, \mathbf{k}_i)$ is also a first Born term with respect to array of internal wave vectors and incident wave vector but with same theoretical approach and can be expressed as

$$U(\mathbf{k}_n, \mathbf{k}_i) = \sum_j U_j(\mathbf{k}_n, \mathbf{k}_i), \tag{3.77}$$

where

$$\begin{aligned} U_j(\mathbf{k}_n, \mathbf{k}_i) &= \exp\left[-\mathrm{i}(\mathbf{k}_n - \mathbf{k}_i)\cdot\mathbf{r}_j\right]\ \gamma(\mathbf{r}_j)\ U_0(\mathbf{k}_n, \mathbf{k}_i)), \\ &= \exp(-\mathrm{i}\Delta\mathbf{k}_{n,i}\cdot\mathbf{r}_j)\ \gamma(\mathbf{r}_j)\ \Delta v, \end{aligned} \tag{3.78}$$

and the U_0 term in (3.78) is approximated to the elementary cell volume, hence the theory of the distance between the array of internal wave vectors and the incident wave vector ($\Delta\mathbf{k}_{n,i} = \mathbf{k}_n - \mathbf{k}_i$).

The block matrix form of equation (3.75) is given by

$$\begin{bmatrix} \bar{\mathbf{K}}_{1,1} & \bar{\mathbf{K}}_{1,2} & \cdots & \bar{\mathbf{K}}_{1,m} \\ \bar{\mathbf{K}}_{2,1} & \bar{\mathbf{K}}_{2,2} & \cdots & \bar{\mathbf{K}}_{2,m} \\ \vdots & \vdots & \ddots & \vdots \\ \bar{\mathbf{K}}_{n,1} & \bar{\mathbf{K}}_{n,2} & \cdots & \bar{\mathbf{K}}_{n,m} \end{bmatrix} \begin{bmatrix} \bar{\mathbf{Y}}_1 \\ \bar{\mathbf{Y}}_2 \\ \vdots \\ \bar{\mathbf{Y}}_m \end{bmatrix} = \begin{bmatrix} \mathbf{J}\bar{\mathbf{U}}_1 \\ \mathbf{J}\bar{\mathbf{U}}_2 \\ \vdots \\ \mathbf{J}\bar{\mathbf{U}}_n \end{bmatrix}, \tag{3.79}$$

and

$$\Delta\mathbf{k}_{n,i} = \begin{bmatrix} \mathbf{k}_1 - \mathbf{k}_i \\ \mathbf{k}_2 - \mathbf{k}_i \\ \vdots \\ \mathbf{k}_n - \mathbf{k}_i \end{bmatrix}, \tag{3.80}$$

where $\bar{\mathbf{Y}}_m = \dfrac{4\pi}{N_m} \times \bar{\mathbf{C}}_m$ is the multiplication of the formal weighting factor and

unknown Fourier coefficient vector, and $\mathbf{J}\bar{\mathbf{U}}_n$ is the right hand side vector in the form of dyadic.

After some mathematical manipulation, we write (3.41) as a summation over cells and multiply by scattered direction projection vector in dyadic form

$$\bar{\mathbf{F}}(\mathbf{k}_s, \mathbf{k}_i) = \bar{\mathbf{J}}_s \sum_m U_j(\mathbf{k}_s, \mathbf{k}_m)\bar{\mathbf{Y}}_m, \tag{3.81}$$

hence

$$\begin{aligned} \mathbf{k}_m &= k_m(\sin\theta_m \cos\phi_m,\ \sin\theta_m \sin\phi_m,\ \cos\theta_m), \\ \mathbf{k}_s &= k_0(\sin\theta_s \cos\phi_s,\ \sin\theta_s \sin\phi_s,\ \cos\theta_s), \\ k_m &= \mathrm{m}k_0, \end{aligned} \tag{3.82}$$

where $\mathbf{k}_m$ is the internal array wave vectors, $\mathbf{k}_s$ is the scattered wave vector, m is the refractive index of scatterer, $\bar{\mathbf{Y}}_m$ is the solution vector including formal weighting factor in dyadic form, and $\bar{\mathbf{J}}_s = [\bar{\mathbf{I}} - \hat{\mathbf{k}}_s\hat{\mathbf{k}}_s]$ is the dyadic projection vector in the scattered field direction.

Clearly, the theory of the first Born term $U(\mathbf{k}_s, \mathbf{k}_m)$ appearing under the summation in (3.81) is slightly different from (3.42) but followed the same procedure given in (3.80) and is defined as

$$U(\mathbf{k}_s, \mathbf{k}_m) = \sum_j U_j(\mathbf{k}_s, \mathbf{k}_m), \tag{3.83}$$

where

$$\begin{aligned} U_j(\mathbf{k}_s, \mathbf{k}_m) &= \exp\left[-\mathrm{i}(\mathbf{k}_s - \mathbf{k}_m)\cdot\mathbf{r}_j\right]\ \gamma(\mathbf{r}_j)\ U_0(\mathbf{k}_s, \mathbf{k}_m)), \\ &= \exp(-\mathrm{i}\Delta\mathbf{k}_{s,m}\cdot\mathbf{r}_j)\ \gamma(\mathbf{r}_j)\ \Delta v. \end{aligned} \tag{3.84}$$

Note that the U_0 term in (3.84) is also well approximated to the elementary cell volume, and the distance between array of pair vectors ($\Delta\mathbf{k}_{s,m} = \mathbf{k}_s - \mathbf{k}_m$) are

based on scattered wave vector and array of internal wave vectors respectively and can be expressed in column vector form as

$$\Delta\mathbf{k}_{s,m} = \begin{bmatrix} \mathbf{k}_s - \mathbf{k}_1 \\ \mathbf{k}_s - \mathbf{k}_2 \\ \vdots \\ \mathbf{k}_s - \mathbf{k}_m \end{bmatrix}. \tag{3.85}$$

Both equations (3.75) and (3.81) are coupled Fredholm integral equation which together determine the scattering amplitude function which confirm the validity of the our theoretical analysis, and are similar to the previous method described in [98]. Other scattering properties can easily be obtained once the dyadic scattering amplitude function is evaluated.

The scattering amplitude considering incident and scattered fields polarization are defined by

$$\begin{aligned} f_{\parallel}(0) &= \hat{\mathbf{e}}_{\parallel} \cdot \bar{\mathbf{F}}(\mathbf{k}_s, \mathbf{k}_i) \cdot \hat{\mathbf{e}}_x, \\ f_{\perp}(0) &= \hat{\mathbf{e}}_{\perp} \cdot \bar{\mathbf{F}}(\mathbf{k}_s, \mathbf{k}_i) \cdot \hat{\mathbf{e}}_y, \end{aligned} \tag{3.86}$$

and

$$\begin{aligned} f_{\parallel}(\pi) &= \hat{\mathbf{e}}_{\parallel} \cdot \bar{\mathbf{F}}(\mathbf{k}_s, \mathbf{k}_i) \cdot \hat{\mathbf{e}}_x, \\ f_{\perp}(\pi) &= \hat{\mathbf{e}}_{\perp} \cdot \bar{\mathbf{F}}(\mathbf{k}_s, \mathbf{k}_i) \cdot \hat{\mathbf{e}}_y. \end{aligned} \tag{3.87}$$

The description of the electric polarization vectors given in (3.86) and (3.87) view with $x\,z$ as the horizontal plane or the laboratory bench top (scattering plane) shown in Figure 3.7. The $\hat{\mathbf{e}}_{\perp} = \hat{\mathbf{e}}_y$, is always perpendicular to the scattering plane. The parallel polarization vector $\hat{\mathbf{e}}_x$ in the scattered wave direction is $\hat{\mathbf{y}} \times \hat{\mathbf{k}}_s$ using the geometry of Figure 3.7.

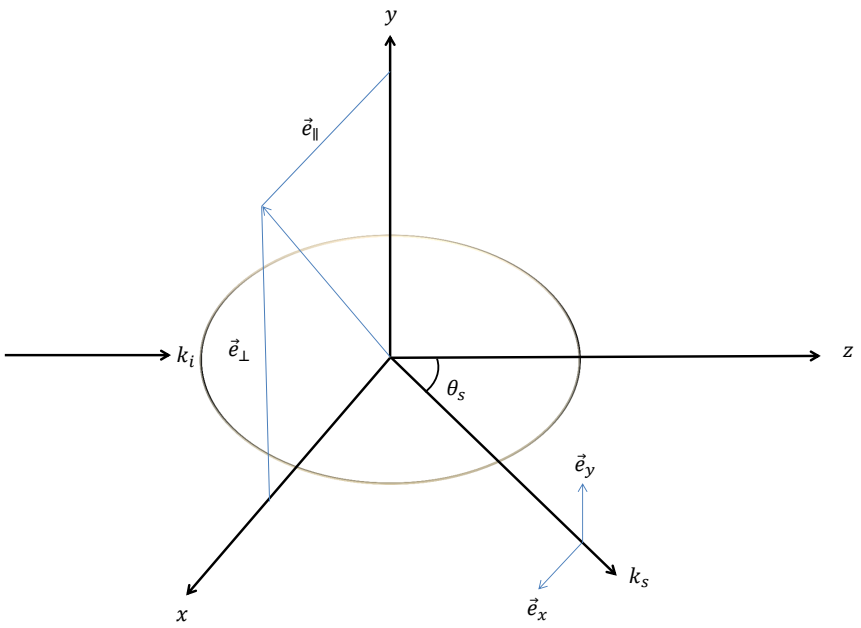

Figure 3.7: Geometry of scattering particle defining the electric polarization components

Therefore, the scattered wave vector is given as

$$\hat{\mathbf{k}}_s = \hat{\mathbf{z}}\cos\theta + \hat{\mathbf{x}}\sin\theta, \tag{3.88}$$

and

$$\begin{aligned} \hat{\mathbf{e}}_x &= (\hat{\mathbf{y}} \times \hat{\mathbf{z}})\cos\theta + (\hat{\mathbf{y}} \times \hat{\mathbf{x}})\sin\theta, \\ &= \hat{\mathbf{x}}\cos\theta - \hat{\mathbf{z}}\sin\theta. \end{aligned} \tag{3.89}$$

So in the incident field direction, the electric polarization vectors are

$$\begin{aligned} \hat{\mathbf{e}}_{\parallel} = &\quad (1,0,0), \\ \hat{\mathbf{e}}_{\perp} = &\quad (0,1,0), \end{aligned} \tag{3.90}$$

and the electric polarization components of of the scattered field are given as

$$\begin{aligned} \hat{\mathbf{e}}_x = &\quad (\cos\theta_s,\ 0, -\sin\theta_s), \\ \hat{\mathbf{e}}_y = &\quad (0, 1, 0), \end{aligned} \tag{3.91}$$

where θ_s is the scattering angle. The forward and back scattering amplitude functions as given in (3.86) and (3.87) represent vertical and horizontal polarizations respectively.

3.4 Summary

The basis and significance of integral equations has highlighted with special consideration given to the Fredholm Integral Equation of the second kind which was adapted for the overview and form the theoretical framework of this work.

We demonstrated the efficiency of a new theoretical approach known as the discrete method of evaluating the first Born term by filling the modelled arbitrary homogeneous scatterer with cubic or spherical cells according to their weighted contents.

The discrete method discussed in § 3.3.1 for the evaluation of the first Born term proved inconsistent in the theory of the Z function. In the course of the Z function analysis, many techniques were employed such as Hankel Integrals method, one involving the auxiliary function which involves sine, cosine and exponential integrations, and the other consisting of partial expansion. However, these methods were also deficient to handle the effect of the discontinuity in the domain of integration. In order to deal with this ill condition, we explored a completely different

approach by expanding the U_0 functions under the radial integral. This expansion leads to simplifying the radial integral by applying a scaling factor k_0^2. In order to evaluate the modified radial integral in the calculation of the Z function, the ratio of β and ρk_0 were considered for the evaluation of the Z pair function. Thus, the main approach explored here was the introduction of a weighting function which only slightly affects the integral on the real line, but strongly attenuates the integral on the imaginary axis. However, the weighting function introduces poles on the lines $x = y$ in the complex plane. These are simple poles, but the real part integrand itself has only one pole.

The theories of the non-singular kernel, and the dyadic scattering amplitude function discussed were straight forward. The code level implementation of our new approach would be introduced and covered in chapter 4.

CHAPTER 4

IMPLEMENTATION OF THE DISCRETE METHOD ALGORITHM

4.1 Introduction

This chapter deals with the implementation of the code for the computation of the angular dependent scattering of irregular dielectric particles using the new FIM approach discussed in chapter 3. An initial development of the algorithm focuses on scattering by spherical particle. Since exact solutions (Rayleigh and Mie theory) are readily available, this implementation will serve the purpose of validating the accuracy of the model. The block diagram that summarizes the program structure and logic flow is depicted in Figure 4.1.

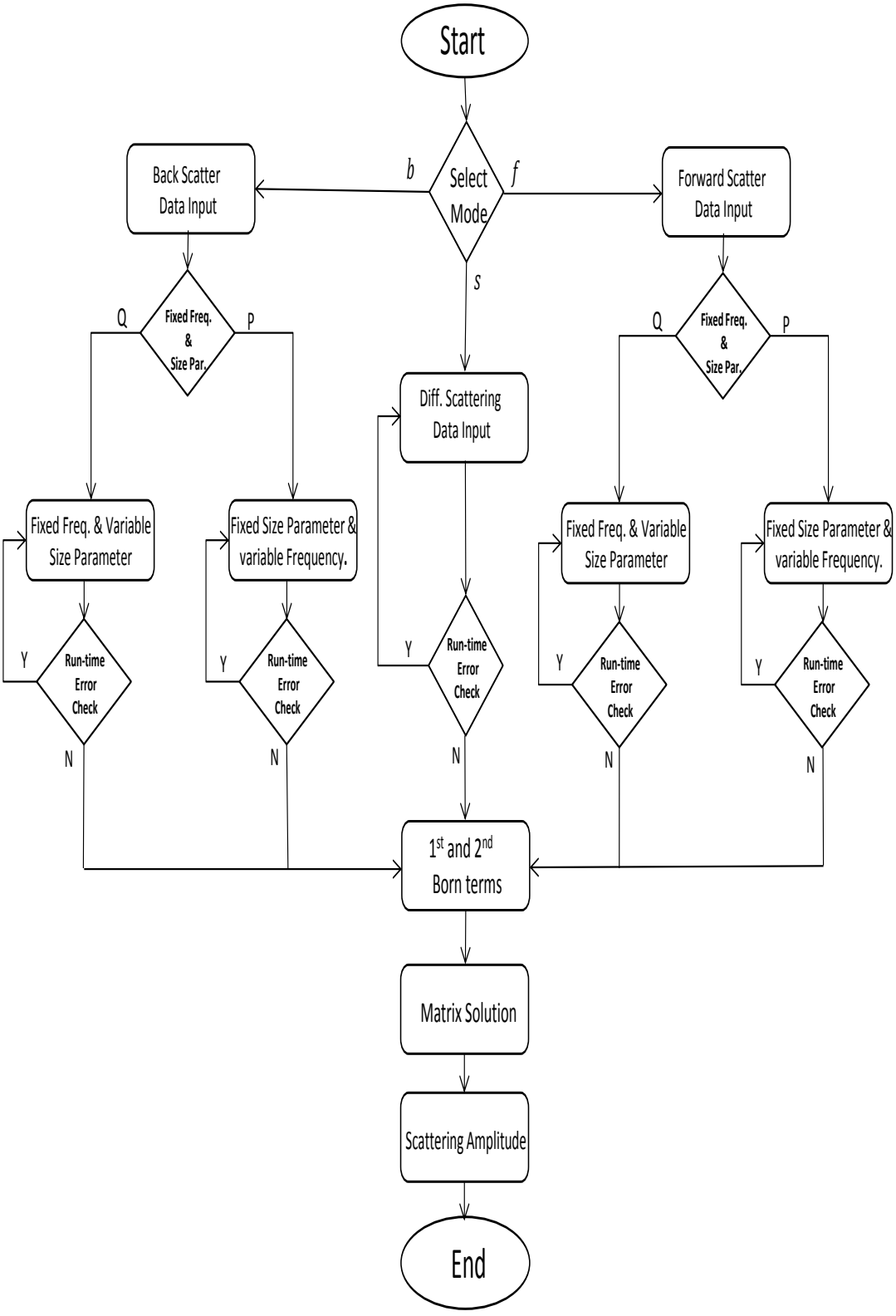

Figure 4.1: Flow-chart of Fredholm Integral Equation Algorithm.

4.1.1 Computational procedures of the FIM model

The computer program is written in FORTRAN 95 language with version 6.10 FTN95 Silverfrost compiler on a 64 bit machine considering double precision for the numerical results. The procedures are separated into sub-programs and modules for the evaluation of amplitude functions for variable scattering angles θ_s through a volume integral known as Fredholm Integral Equation of the second kind.

The Discrete Method algorithm is designed to give the user a range of flexibility to select different program modes for the evaluation of the scattering functions such as varying and fixed angles. In the case of a fixed angle, forward and back scattering are computed. It is important to note that the desired program mode is selected at the beginning with the following key input parameters:

1. The number N_{pol} of the polar and N_{az} of the azimuth angles required to evaluate the array of unit vectors within one cell

2. The incident wave propagation direction defined by the values of these two angles θ_i and ϕ_i

3. The number of grid points or cells along each lattice dimension

4. The refractive index of the scattering particle to be evaluated

5. The size parameter of the scatterer

6. The frequency in GHz

7. The shape of the scattering particle to be evaluated.

As discussed in § 3.2, a plane electromagnetic wave is incident on the scatterer,

and its direction of propagation is defined using the polar θ_i and the azimuth ϕ_i angles (where i stands for incident). For the case of sphere, change in direction of the incident wave does not affect the scattering properties due to symmetry of the sphere. However, for other shapes different incident directions result in scattering characteristics that depends on the orientation and the position of the scatterer relatively to the incident direction.

In this work, an array of N_{pol} polar angles and an array N_{az} azimuth angles are generated and used for retrieving Cartesian unit vectors using a spherical coordinates system. The number unit vectors generated is $N_{pol} \times N_{az}$. These arrays are used as internal wave vectors ($\mathbf{k}_n$ and $\mathbf{k}_m$) within each cell. The same type of vectors are also used to generate the unit vector $\mathbf{p}$ outside the cells (array of pivot vectors) in the Fourier domain.

The size parameter and the frequency are used to evaluate the physical size of the scatterer (diameter). Since the algorithm has been developed for a general shape, the physical size of the scattering particle is used to determine the principal axes of the scatterer (a, b, c). In the case of sphere, once the scatterer diameter is known, the actual dimensions of the finite domain is evaluated by multiplying the diameter by a dimensionless margin. Instead, the physical dimension of the lattice filed for other shapes such as spheroids, cylinder, circular plate, and rod, is calculated with the principal axes with maximum dimension.

It is important to note that thorough error checks are carried out during parameters input, and at different stages of program execution to ensure that the numerical results are satisfactory.

4.2 Born's terms implementation

The code implementation of the first and second Born terms discussed in § 3.3, and other related functions are presented in this section. Pseudo-code is used to illustrate the implementation of the Born terms.

4.2.1 Evaluation of the first Born term

In order to implement the numerical computation of the U-term given in (3.43), we expressed it as a summation over all the cells within the lattice field as described in [118]. The algorithm is developed in such a way that it can be used to evaluate all the cases in which the U-term is involved: $U(\mathbf{k}_n, \mathbf{k}_m)$, $U(\mathbf{k}_n, \mathbf{k}_i)$ and $U(\mathbf{k}_s, \mathbf{k}_m)$. The U-terms $U(\mathbf{k}_n, \mathbf{k}_i)$ and $U(\mathbf{k}_s, \mathbf{k}_m)$ are used for the K matrix equation (3.77) and dyadic scattering amplitude (3.84) respectively. The same algorithm is used also to compute the W-term (3.46) if the condition flag is set as shown in the algorithm 4.1.

The input parameters to calculate all the U-term functions are the following:

1. Origin of the scattering particle within 3-dimensional structure (the value is zero for scatterer centred at the origin and non zero for offset origin)
2. Physical dimension of the scatterer (i.e. principal axes)
3. Actual size of the 3-dimensional lattice field
4. Wavenumber (k_0)
5. Complex dielectric constant ε relative to grid points in the lattice field

6. physical cubic cell dimensions within the lattice field

7. Array of internal wave vectors ($\mathbf{k}_n$ and $\mathbf{k}_m$)

8. External wave vectors ($\mathbf{k}_i$ and $\mathbf{k}_s$)

9. Status flag to evaluate different U-terms

Algorithm 4.1 Numerical implementation of the U-term algorithm

```
1: procedure UMAT(U, W)
2:     for l = 1 : xmax do                          ▷ lattice field dimension along x
3:         for n = 1 : ymax do                      ▷ lattice field dimension along y
4:             for m = 1 : zmax do                  ▷ lattice field dimension along z
5:                 γ ← Γ(l, n, m)                   ▷ array of evaluated polarizability/cell
6:                 if γ == 0 then Cycle             ▷ terminate loop and goto line 4
7:                     φ ← exp(−iΔk · r)            ▷ phase shift/cell
8:                     if present(W) then
9:                         DU ← φ ∗ γ(r_j) ∗ Δv
10:                        U ← U + DU
11:                        W ← W + DU ∗ ε(r_j)
12:                    else
13:                        U ← U + φ ∗ γ(r_j) ∗ Δv
14:                    end if
15:                end if
16:            end for
17:        end for
18:    end for
19: end procedure
```

For brevity, only some of the input parameters are shown in this algorithm 4.1, and the U and W are returned as output on exit for the case of $\mathbf{k}_n$ and $\mathbf{k}_m$, while for all other cases, only the U term is returned.

It is necessary to point out that the scatterer is modelled using cells of shape of standard ellipsoid (5.1) inscribed within the regular lattice with no touching edges. All the volume of the scatterer is populated with the ellipsoids according to their weighted contents. Their weighted contents is related to the value of polarizability

per cell $\gamma(\mathbf{r}_j)$. The polarizability is set to $\gamma(\mathbf{r}_j) = k_0^2(\varepsilon(\mathbf{r}_j) - 1)$ for $\mathbf{r}$ inside the ellipsoid (5.1) otherwise, outside the ellipsoid, $\gamma(\mathbf{r}_j) = 0$.

The coordinates of phase reference centre of the lattice field (midpoint) is evaluated and the origin of the modelled particle is chosen to be at this point for convenient purpose. However, offsetting the origin of a spherical particle can be used to evaluate the scattering properties of slightly non-spherical particles as proposed by [18] and [86]. For $\gamma(\mathbf{r}_j) = 0$, the calculation of the U-term is not performed for the cell $\mathbf{r}_j$, while for $\gamma(\mathbf{r}_j) \neq 0$ the program proceed to evaluate the Fourier transform of the polarizability for each cell times their elementary volume. Finally, the U-term is summed for all the cells. The W-term given in (3.46) is evaluated as the product of the U-term and the complex dielectric constant for each cell and the W-term summed for all the cells in the lattice field. Comparison of our discrete method with the approach proposed by Holt et.al (exact method) is depicted in the curves shown in Figures 4.2 - 4.5.

The initial validation and testing of this model was carried out by evaluating the first Born term in (3.43), and compared with the exact method (3.36) proposed by Holt et.al [98]. Numerical results with different number of pivots are shown in Figures 4.2 - 4.5 and they suggest a good agreement. However, slight ripple effects can be noticed in the curves. This is due to the process of filling the volume of the modelled scatterer with an ellipsoid inscribed in the cubic cells, and we have verified that this effect is amplified as the size parameter increases. Another reason is numerical integration errors due to the discretization process.

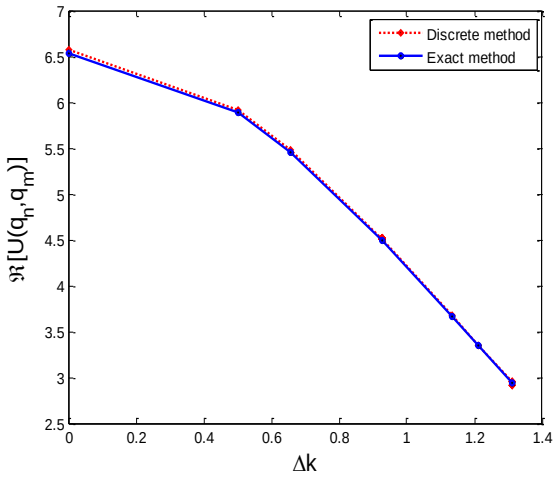

Figure 4.2: Comparison of First Born term using Discrete and Exact methods Number of iteration over angles $\theta = 3$ and $\phi = 4$.

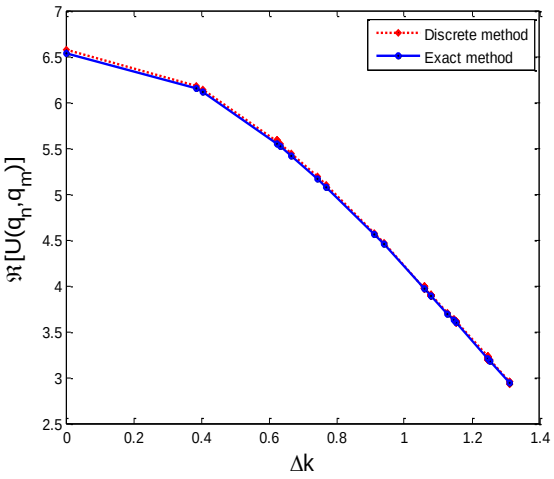

Figure 4.3: Comparison of First Born term using Discrete and Exact methods Number of iteration over angles $\theta = 4$ and $\phi = 6$.

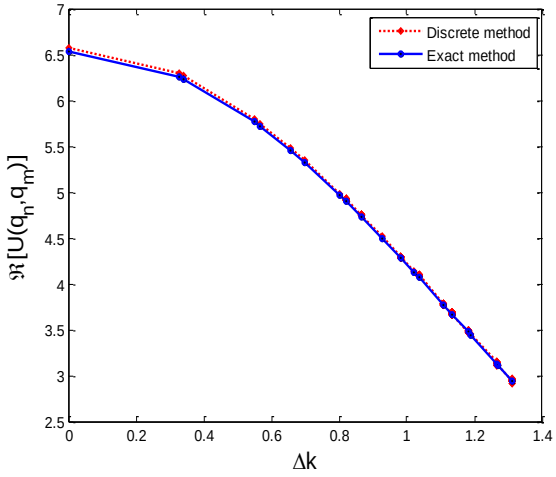

Figure 4.4: Comparison of First Born term using Discrete and Exact methods Number of iteration over angles $\theta = 5$ and $\phi = 6$.

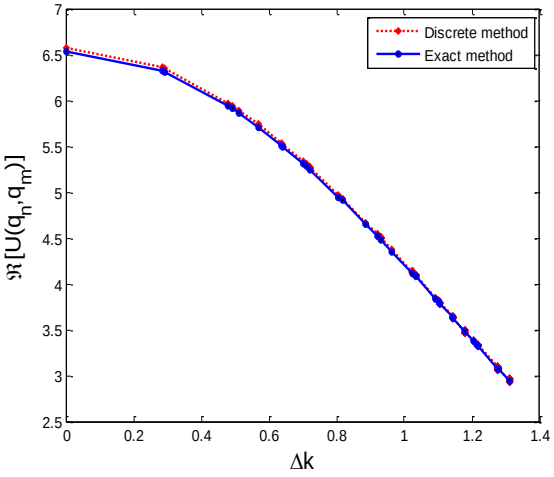

Figure 4.5: Comparison of First Born term using Discrete and Exact methods Number of iteration over angles $\theta = 6$ and $\phi = 6$.

4.2.2 Implementation of the second Born term

The code level implementation of the Z-term equation (3.73) is presented. A well thought out approach is considered in evaluating Z-term numerically. We adopted the same procedure of discretization of the finite lattice field into cells or grid points and then evaluate their equivalent spherical cell radius. This approach is employed because we have verified that using the cubic cells as the domain of integration generate singularities in the radial part of the Z-term. In particular, this was due to the odd power of p as discussed in § 3.3.2. The input parameters to this algorithm 4.2 are not shown for brevity in the pseudo-code, but listed below:

- Array of pivot vector $\mathbf{p}$
- Array of the internal wave vectors $\mathbf{k}_n$ and $\mathbf{k}_m$
- Wavenumber k_0
- cell or grid point dimension
- polarizability per cells in the lattice field according to their weighted contents $\gamma(\mathbf{r}_{i,j})$

An initial numerical evaluation of the Z-function has been performed for a pair of electrically small spherical cells. In this case U-terms are well approximated as Bessel functions of the half order $4\pi\,\rho^3\,J(3/2,\,\rho p)$, where ρ is the spherical equivalent radius as discussed in 3.3.2. When the cells are distinct, the integral (3.55) to be evaluated includes an exponential factor $\exp(i\beta p)$ which becomes exponentially large along the imaginary axis of the complex plane, such that a closed-form analytical solution as in Hankel integrals discussed in G.N.Watson [115, p.430] and [116] is not possible due to odd number of p in the integrand. It

is noteworthy to highlight some of the steps taken in the numerical evaluation of the Z-term (see algorithm 4.2)

1. Variables initialization and work space arrays allocation

2. Evaluation of unit vectors in pivot directions, and their projection matrices

3. Evaluation of the total weight of the Z-term involving the formal weighting function allowing for 4π angle integral and the weighting factor from formal integration

4. Evaluation of the physical coordinates of phase reference centre as a function of the cell and lattice field dimensions

5. Evaluation of cubic or spherical cells position in the discretized lattice field according to their weighted contents for $\gamma(\mathbf{r}_j)$ and $\gamma(\mathbf{r}_i)$

6. A function to approximate the integral contribution for a pair of spherical cells. The inputs of the function Zpair are the size parameter $\rho\, k$ and β which is the relative phase of the cells measured in the direction of the pivot vector

7. Phase shifts evaluation with respect to internal wave vector $\mathbf{k}_n$ and $\mathbf{k}_m$including phase factor due to $\mathbf{r}_j$ and $\mathbf{r}_i$

8. Steps 1 to 7 are used to compute the Z-term for a pair. The summation over all cells give the desired Z-term

Algorithm 4.2 Numerical implementation of the second Born term

procedure ZMAT($\bar{\mathbf{Z}}$)
  $ka \leftarrow \rho\, k_0$ ▷ cell size parameter
  for $j = 1 : J$ **do**
    $\gamma_j \leftarrow \Gamma(jx, jy, jz)$ ▷ polarizability per jth cells
    if $\gamma_j == 0$ **then** Cycle ▷ do not process empty cells

      for $i = 1 : I$ **do**
        $\gamma_i \leftarrow \Gamma(ix, iy, iz)$ ▷ polarizability per ith cells
        if $\gamma_i == 0$ **then** Cycle ▷ do not process empty cells

          $\phi_j \leftarrow exp(i\mathbf{k}_n \cdot \mathbf{r}_j)$ ▷ phase shift per jth cells
          $\phi_i \leftarrow exp(-i\mathbf{k}_m \cdot \mathbf{r}_i)$ ▷ phase shift per ith cells
          $\beta \leftarrow \hat{\mathbf{p}} \cdot (\mathbf{r}_j - \mathbf{r}_i)$ ▷ relative phase of cells in the dir. of $\hat{\mathbf{p}}$

          $Zp \leftarrow \text{Zpair}(\beta,\, ka) * w_f$ ▷ Z-term for a pair of spher. cells
          $Zc \leftarrow Zp * \gamma_i * \gamma_j * \phi_i * \phi_j$
          $\bar{\mathbf{Z}} = \bar{\mathbf{Z}} + \left|\bar{\mathbf{I}} - \hat{\mathbf{p}}\hat{\mathbf{p}}\right| * Zc$

        end if
      end for
    end if
  end for
end procedure

Require: $\beta,\ ka$ ▷ Input parameters
Ensure: Zp ▷ Output parameter
procedure ZPAIR($\beta,\ ka$)
  Initialize Fitting Parameters (C)
  Truncate the Zpair function
  Evaluate $x \leftarrow \dfrac{\beta}{ka}$
  if $x > 3.0$ **then**
    $Z_p \leftarrow (0.0 + 0.0i)$
    return
  end if

  $P \leftarrow \dfrac{2.0\pi}{3.0} * x, \quad xs \leftarrow x^2, \quad U \leftarrow C(6)$

  for $i = 5 : I : -1$ **do**
    $U \leftarrow U * xs + C(i)$
  end for
  $Z_p \leftarrow (U * \cos(p),\ U * \sin(p))$
end procedure

The Zpair function in algorithm 4.2 approximates the integral contribution for a pair of cells of size parameter, x. The first input parameter β is the relative phase of the cells measured in the direction of the pivot vector. This function suppresses the integrand a little at small values, but to a very high accuracy kills the integrand on the imaginary axis, suppressing the blow-up of the Bessel functions in the upper half plane. Figures 4.6 to 4.8 summarise the contribution of the real, the imaginary axes and the combination of both for the pairwise Z-term function evaluation. Nevertheless, various diagnostic tests were tried in Mathematica to obtain satisfactory results of the integral without ill condition. This approach leads to truncating the implementation of Zpair function if the condition $\beta/ka > 3$ is satisfied and this give rise to relatively stable term in the domain of integration.

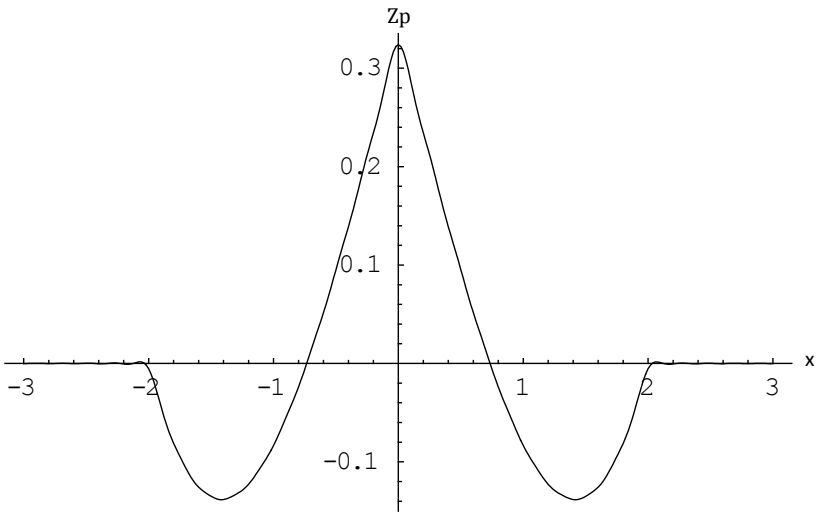

Figure 4.6: The pairwise Z-term numerical integration in the real axis indicates an even function

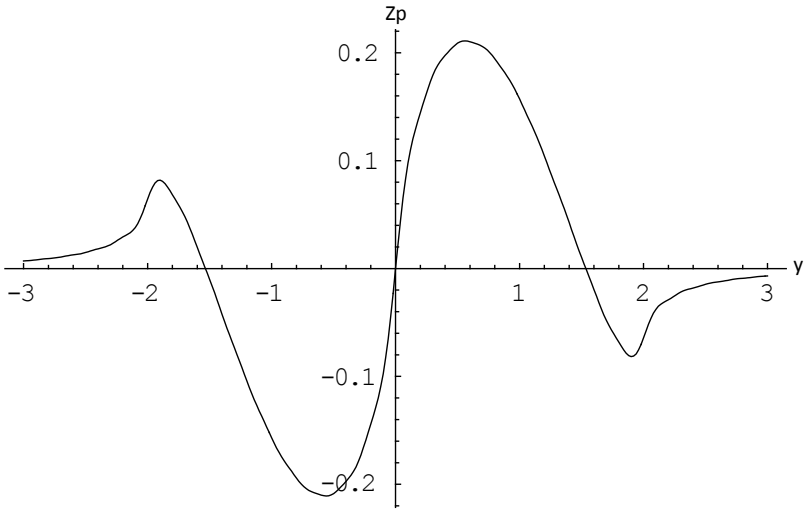

Figure 4.7: The pairwise Z-term numerical integration in the imaginary axis indicates an odd function

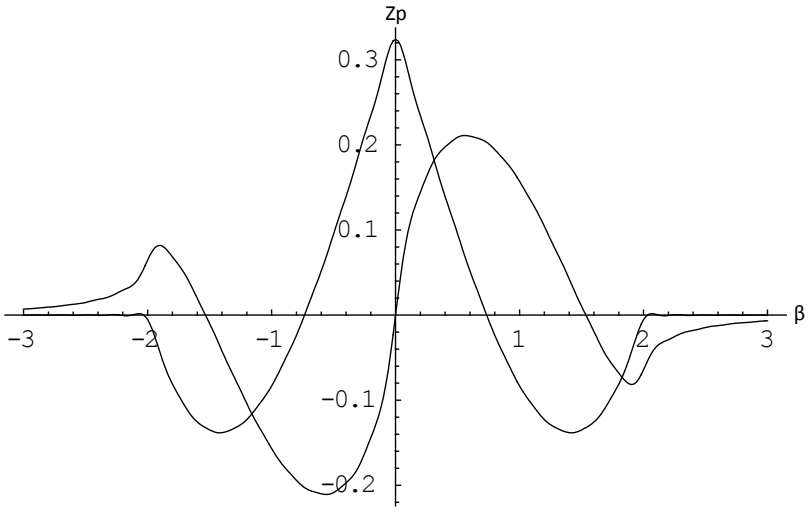

Figure 4.8: The combination of x and y for the pairwise Z-term function

The weighting function discussed in (3.66) introduces an infinite sequence of poles along $\theta = \pm\pi/4$ line whose residues have to be summed. But for larger β this turns out to be a well behaved function that can also be interpolated. The function

returns a complex value, Z_p.

Note that the subscripts j and i represent position of cells in three dimensional space (x, y , z) in the uniformly discretized lattice field and w_f is the total weighting factor for the Z-term function. Thus, empty cells are not processed, this approach speeds up the computation by a factor depending on the number of integration over p. The desired integral is the sum of the residues for the weighting function plus the residue of the pole adjacent to the real axis. However, for very large β values the residue sum turns out to be negligible.

The Z-term algorithm is numerically evaluated as a function of summations over the product of projection matrices in pivot directions, polarizability of ith and jth cells, phase shifts, total weighting factor and the contribution for a pair of spherical cells as a function of the relative phase of the cells measured in the direction of the pivot vector β and size parameter $\rho k_0 \approx ka = x$.

4.3 Description of the non-singular matrix

In order to numerically evaluate (3.79) to obtain the unknown block solution vector $\bar{\mathbf{Y}}_m$ discussed in § 3.3.3, we attempt to factorize the coefficient square block matrix equation (3.79) in dyadic form using block algorithm for LU decomposition described in [119]. However, this approach proved to be inconsistent owing to considerable difficulties in obtaining numerical convergent and stability. Now, we have introduced a more realistic approach in which the coefficient block matrix and the right hand side block vector are expanded to a larger form before applying any of the standard LU factorization methods.

The main input parameters to this algorithm are the non-singular square matrix A(n x n), and the right hand side vector B(n x 1) all in block form, while x(n x 1) represents the unknown solution vector which is returned on exit from the routine. The calculation of the B(n x 1) depends on the incident projection vector using equation (3.52), and the U-term in (3.75) with respect to array of internal wave vector $\mathbf{k}_n$ and external wave vector $\mathbf{k}_i$ is implemented by invoking algorithm 4.1. Thus, this leads to the right hand side vector in (3.79) been expressed in dyadic form.

Firstly, we need to expand coefficient matrix and right hand side vector from dyadic to a complex forms, which becomes A(m x m) and B(m x 1), where m = 3n. Factorization of this kind of complex system does not follow the usual way due numerical error during implementation. Since, the matrix and right hand side are now complex, we can express (3.75) as

$$(A + iC)(x + iy) = (b + id), \tag{4.1}$$

and taking the real and imaginary parts of equation (4.1)), we have

$$\begin{aligned} A \cdot x - C \cdot y &= b, \\ C \cdot x + A \cdot y &= d, \end{aligned} \tag{4.2}$$

which can be written as 2m $\times$ 2m set of real equations,

$$\begin{pmatrix} A & -C \\ C & A \end{pmatrix} \begin{pmatrix} x \\ y \end{pmatrix} = \begin{pmatrix} b \\ d \end{pmatrix}. \tag{4.3}$$

We solved the system coefficient matrix (4.3) by the standard Crout's LU decom-

position with partial pivot algorithm described in [120] to decompose the matrix equation to lower and upper triangular matrices form

$$\begin{pmatrix} a_{1,1} & a_{1,2} & \cdots & a_{1,m} \\ a_{2,1} & a_{2,2} & \cdots & a_{2,m} \\ \vdots & \vdots & \ddots & \vdots \\ a_{m,1} & a_{m,2} & \cdots & a_{m,m} \end{pmatrix} = \begin{pmatrix} 1 & & & \\ l_{2,1} & 1 & & \\ \vdots & \vdots & \ddots & \\ l_{m,1} & l_{m,2} & \cdots & 1 \end{pmatrix} \begin{pmatrix} u_{1,1} & u_{1,2} & \cdots & u_{1,m} \\ & u_{2,2} & \cdots & u_{2,m} \\ & & \ddots & \vdots \\ & & & u_{m,m} \end{pmatrix}. \tag{4.4}$$

The elements of L and U are computed as follows

$$\begin{cases} u_{1j} = a_{1j} \quad (j = 1, 2, \cdots, n) \\ l_{i1} = a_{i1}/u_{11} \quad (i = 2, 3, \cdots, n) \\ u_{kj} = a_{kj} - \sum_{m=1}^{k-1} l_{km} u_{mj} \quad (j = k, k+1, \cdots, n) \\ l_{ik} = (a_{kj} - \sum_{m=1}^{k-1} l_{im} u_{mk})/u_{kk} \quad (i = k+1, k+2, \cdots, n) \\ \qquad\qquad (k = 2, 3, \cdots, n). \end{cases} \tag{4.5}$$

The L and U are created with the same dimension as the expanded coefficient matrix. The leading diagonal elements of the lower triangular matrix are set to 1, then the pivot elements in the column are determined and swap rows to make pivot elements to have greatest magnitude in each column. The aim is to avoid unnecessary division by zero or small number that could lead to ill condition.

The unknown solution can be evaluated using forward/backward substitution approach. The advantage of this method is that the coefficient matrix is factorized

only once and the evaluation of the unknown solution vector is achieved with different right hand side vector without going through the same process. However, more computation time is spent due to the large number of matrix elements. The evaluated solution vector is converted back to dyadic form as shown in the algorithm 4.3.

Algorithm 4.3 Evaluation of the Unknown Fourier Coefficient

Require: A, B ▷ Input
Ensure: Y ▷ Output
procedure KMAT($Y(k_m)$)
  $Cmatrix \leftarrow Kmatrix$ ▷ Matrix expansion dyadic to complex
  $Amatrix \leftarrow Cmatrix$ ▷ Matrix expansion complex to real
  $LU \leftarrow decomposition(A)$ ▷ factorization of A using Crout's method
  $\hat{\mathbf{k}}_i \leftarrow (\sin\theta_i \cos\phi_i, \sin\theta_i \sin\phi_i, \cos\theta_i)$ ▷ incident direction unit vector
  $J_i \leftarrow [\mathbf{I} - \hat{\mathbf{k}}_i \hat{\mathbf{k}}_i]$ ▷ incident projection vector
  $U(k_n, k_\imath) \leftarrow UMAT(k_n,\ k_\imath)$ ▷ evaluation of U-term wrt k_n and $k_\imath$
  for $n = 1 : ncol$ **do**
    for $m = 1 : nrow$ **do**
      $B(m, n) \leftarrow J_\imath * U(k_n, k_\imath)$ ▷ evaluation of rhs vector in dyadic form
    end for
  end for
  for $i = 1 : n$ **do**
    $X(:, i) \leftarrow backsubst.(LU, INDX, B(:, i))$ ▷ solution vector
  end for
  $CX \leftarrow X$ ▷ conversion of solution vector in real form to complex
  $Y \leftarrow CX$ ▷ conversion of solution vector in complex form to dyadic
end procedure

Validation of non-singular matrix algorithm

Each of the sub-program in this algorithm were tested and the numerical results were within acceptable limit. The LU decomposition routine was tested by taking the restored product of lower and upper triangular matrix in comparison with the original coefficient matrix. Excellent agreement was found, and multiplication of solution vector with the original coefficient matrix also suggested good agree-

ment compared with right hand side vector. The maximum residue error in the forward/backward substitution was between 10^{-13} and 10^{-17} depending on the number of pivot vectors.

4.4 Scattering amplitude function

This section deals with the numerical implementation of dyadic scattering amplitude function using equation (3.83) with emphasis on evaluating the amplitude functions for a variable angle. The flag condition FL makes the algorithm flexible to be used for fixed scattering angle, such as forward $\theta_s = 0^o$, or backscattered $\theta_s = 180^o$ and considering size parameter and frequency as the independent variables (see algorithm 4.4).

The input parameters are given as: origin of the scatterer, principal axes of the scattering particle, discretized lattice field dimension, refractive index of the medium. The Fourier coefficient vector in dyadic form $\bar{\mathbf{Y}}$ known as the solution vector obtained from algorithm 4.3, the physical cubic cell dimension and number of points over θ_s and ϕ_s used in this algorithm have already been briefly described in previous sections.

For the case of angular dependent scattering functions, we highlight some external sub-programs used for the code level implementation of this algorithm 4.4:

1. Routine to evaluate outer product of unit vector for each scattered field direction

2. Evaluation of unit dyadic function

3. A sub-program to generate scattering angles θ_s and ϕ_s array using the number of points over polar and azimuth angles

4. Function to retrieving Cartesian unit vectors from the spherical coordinates to evaluate array of internal wave vectors $\mathbf{k}_m$

5. Routine to evaluate the first Born term $U(\mathbf{k}_s, \mathbf{k}_m)$

The U-term function described in equation (3.83) is implemented by invoking algorithm 4.1 with respect to array of internal wave $\mathbf{k}_m$, and external wave vector $\mathbf{k}_s$, or alternatively taking to be the scattered direction vector. The solution vector in dyadic form $\bar{\mathbf{Y}}$ is obtained by the evaluation of algorithm 4.3. The projection vector in dyadic form J_s relative to the scattered direction is evaluated following similar procedure as given in (3.52) except that the unit vector in this case is replaced by $\hat{\mathbf{k}}_s$.

Finally, the amplitude function is evaluated as a summation over the product of the solution vector in dyadic form $\bar{\mathbf{Y}}$ and the U($\mathbf{k}_s$, $\mathbf{k}_m$), and thereafter applying the scattered projection vector factor to the evaluated scattering amplitude for a particular direction to obtain the required function also in dyadic form. For the cases of the forward $\theta_s = 0^0$ and back $\theta_s = 180^0$ differential cross sections as a function of either size parameters or varying frequencies. The same code level implementation procedure is followed for the numerical evaluation of the scattered dyadic amplitude functions.

Algorithm 4.4 Evaluation of the Dyadic Scattering Amplitude Function

```
1: procedure FMAT(F(k_s, k_in))
2:     if (present(FL)) then
3:         switch FL do
4:             case 0                                  ▷ Forward scattering Amplitude
5:                 for i = 1 : 1 do
6:                     θ_s ← (i − 1) ∗ π/180           ▷ Forward scatteing angle θ = 0
7:                     k̂_s ← (sin θ_s cos φ_s, sin θ_s sin φ_s, cos θ_s)   ▷ unit vector scatt.
8:                     J_s ← I − k̂_s k̂_s               ▷ projection vector scattered direction
9:                     U(k_s, k_m) ← UMAT(k_s, k_m)
10:                    for n = 1 : col do
11:                        for m = 1 : row do
12:                            Fsum ← Fsum + Ȳ(m, n) ∗ U(k_s, k_m)
13:                        end for
14:                    end for
15:                    F(i) ← J_s ∗ Fsum               ▷ Applying projection vector factor
16:                end for
17:            case 1                                  ▷ Back scattering Amplitude
18:                for i = 181 : 181 do
19:                    θ_s ← (i − 1) ∗ π/180           ▷ Backscattered angle θ_s = π
20:                    for n = 1 : col do
21:                        for m = 1 : row do
22:                            Fsum ← Fsum + Ȳ(m, n) ∗ U(k_s, k_m)
23:                        end for
24:                    end for
25:                    F(i) ← J_s ∗ Fsum               ▷ Applying projection vector factor
26:                end for
27:    else                                            ▷ Variable angle scattering Amplitude
28:        for i = 1 : Fsize do
29:            θ_s ← (i − 1) ∗ π/180
30:            k̂_s ← (sin θ_s cos φ_s, sin θ_s sin φ_s, cos θ_s)
31:            J_s ← I − k̂_s k̂_s                       ▷ projection vector scattered direction
32:            U(k_s, k_m) ← UMAT(k_s, k_m)
33:            for n = 1 : col do
34:                for m = 1 : row do
35:                    Fsum ← Fsum + Ȳ(m, n) ∗ U(k_s, k_m)
36:                end for
37:            end for
38:            F(i) ← J_s ∗ Fsum                       ▷ Applying projection vector factor
39:        end for
40:    end if
41: end procedure
```

4.5 Summary

The evaluation of the U-term for the Discrete Method has been compared with previous work showing a good agreement for different pivots number and input parameters. We demonstrated a suitable method of implementing the Z-term which involved the inclusion of a conditioning weighting function to avoid singularities in the domain of integration as discussed in chapter 3.

Furthermore, stability and accuracy of core parts of the algorithm were validated separately and the numerical results were satisfactory. The maximum residue error in the lower/upper factorisation of coefficient matrix using Crout's method and forward/backward substitution are negligible.

The algorithm developed to implement the Discrete Method was discussed in this chapter, and will be applied to evaluate scattering amplitude functions of different modelled shapes in chapter 5.

CHAPTER 5

APPLICATION OF THE DISCRETE METHOD TO INHOMOGENEOUS DIELECTRIC SCATTERERS

5.1 Introduction

This chapter deals with the evaluation of angular scattering patterns of ellipsoids and mixed phase hydrometeors modelled as dielectric scatterers containing homogeneous inclusions such as air, ice, and/or liquid water. We start by modelling particles using standard volume equations and applying our approach for known shapes to test the accuracy and stability of our numerical results comparing with

other established methods such as the Mie theory. The modelled particles are filled with cubic or spherical cells according to their weighted contents within the discretized lattice field. Note that an incident plane wave linearly polarized propagating in the $+z$ direction is assumed. The input parameters such as size parameter and refractive index are purposely chosen within Rayleigh and Mie regime, and the C band frequency 5.8 GHz is selected to suit the operating frequency of European weather radar. This gives rise to a ice crystal diameter of approximately 2.0 cm with wavenumber $k_0 \approx 1$.

5.2 Scattering by Ellipsoids

Ellipsoids are of particular interest in the weather radar application since precipitation tends to be represented with this shape. The ellipsoidal shapes are described by the standard equation for the ellipsoid centred at the origin of a Cartesian coordinate system as shown in Figure 5.1

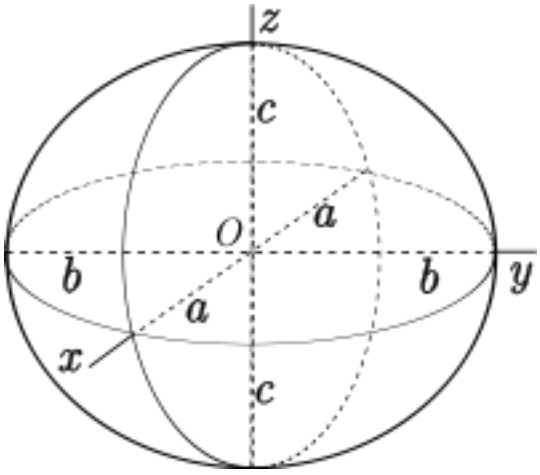

Figure 5.1: Geometry of an ellipsoid with distinct principal axes a, b and c

and expressed as

$$\frac{x^2}{a^2} + \frac{y^2}{b^2} + \frac{z^2}{c^2} \leq 1. \tag{5.1}$$

The points $(a, 0, 0)$, $(0, b, 0)$ and $(0, 0, c)$ lie on the surface and the line segments from the origin to these points are called the semi-principal axes of length x, y, z. Equation (5.1) is used to model different shapes depending on a factor called axial ratio defined as the ratio of the length (or magnitude) of those axes to each other. For $a = b = c$, degenerate to the known case of a sphere. In the case of $a = b < c$ degenerate to prolate spheroid where the axial ratio can be defined as $c/a > 1$, and for the case of oblate spheroid, where $a = b > c$ thus leads to the axial ratio to be less than one. The input parameters to this algorithm are described as:

1. Wavenumber (k_0)

2. Principal axes of the modelled scatterer

3. Dielectric constant of scattering particle (ε)

4. Cubic cell dimension (cd)

5. Coordinates of phase reference centre of the discretized lattice field (rcen)

Algorithm 5.1 Evaluation of the ellipsoid model

Require: $k_0, a, b, c, \varepsilon, cd, rcen$ ▷ Input parameters
Ensure: $\gamma(r)$ ▷ Output:polarizability of cell array

procedure ELLIPSOID($\gamma(r)$)
  for $i = 1 : xmax$ **do**
    for $j = 1 : ymax$ **do**
      for $k = 1 : zmax$ **do**

$$rcs \leftarrow \left(\frac{x^2}{a^2} + \frac{y^2}{b^2} + \frac{z^2}{c^2}\right)$$ ▷ ellipsoid formula evaluation

        if $(rsc \leq 1.0)$ **then** ▷ condition to fill scatterer
          $\gamma(i, j, k) \leftarrow k_0^2(\varepsilon - 1)$ ▷ cells within the scatterer
        else
          $\gamma(i, j, k) \leftarrow 0.0$ ▷ cells outside the scatterer
        end if
      end for
    end for
  end for
end procedure

In order to model a specific shape from the given equation (5.1) above, we need to define the semi-principal axes of the desired scattering particle with the axial ratio at the beginning of implementing algorithm 5.1. Interestingly, the algorithm is designed to account for the centre of the lattice field. The idea behind this approach is to ensure that the modelled particle is positioned so that the origin of the reference system coincides with the coordinates of phase reference centre of the finite three dimensional lattice field. Furthermore, we ensure that the scattering particle is inscribed within the discretized lattice field dimension and does not touch the bounds. The volume of the modelled particle is filled with $\gamma(\mathbf{r}) \neq 0$ if the condition given in equation (5.1) is satisfied and elsewhere equals zero as discussed in chapter 4. This is obviously expected because the refractive index of the surrounding medium is approximately one. For the case of homogeneous scatterers, an important simplification occurs due to uniform dielectric constant in the scattering medium. This technique of modelling solid ellipsoidal particles

can also be applied to inhomogeneous medium such as hybrid scatterers and melting snowflakes since only the distribution of the dielectric constants need to be changed. We demonstrate how efficient and validate our method by applying it to model a sphere with uniform dielectric constant within finite lattice field. Figure 5.2 describes the geometry of the modelled sphere according to their weighted contents of the cubic cells within the finite domain.

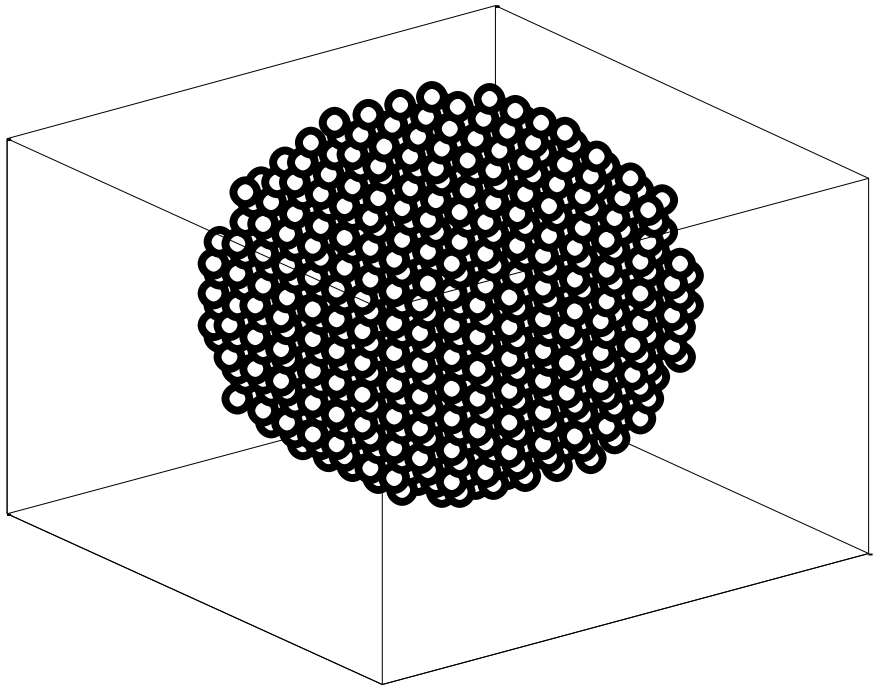

Figure 5.2: Geometry of a modelled solid sphere within the discretized regular lattice field

5.2.1 Scattering by particles small compared with the wavelength

In this section, we consider the scattering of electromagnetic wave by smaller particle (Rayleigh regime). In the low frequency Rayleigh scattering limit where the circumference is less than the wavelength or size parameter, $x << 1$. In the high frequency optical limit, the normalized radar cross section is ≈ 1.The Discrete Method is used to evaluate normalized radar scattering cross scattering, differential and forward scattering cross sections. The stability of our approach is checked in the Rayleigh regime for a sphere by comparison with the exact method using readily available established numerical methods.

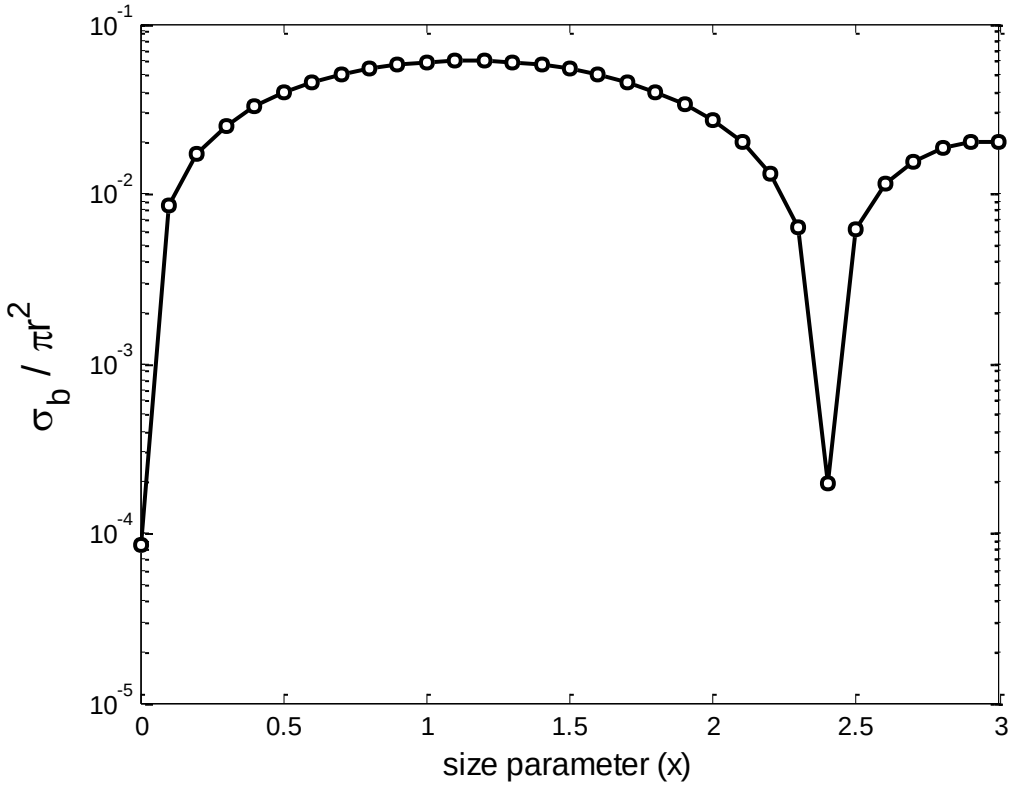

Figure 5.3: Backward scattering cross section against size parameter $n = 1.33$, and frequency = 5.8 GHz.

In Figure 5.3, we demonstrate efficiency of the Discrete Method to calculate the normalized backward scattering known as radar cross section in the weather radar parlance as function of relative frequency or size parameter (calculated by Mie theory). It is evident from the graph that the amplitude function increases with increase in the size parameter to a certain point. Further increase in the size parameter leads to the amplitude to become saturated and gradually decreases with series of peaks and valleys and tends towards where the amplitude function is approximately unity. This point is called the extinction paradox described as twice its geometrical cross-sectional area of the scatterer and this applies only to forward scatter only. In order to visualize this effect, we need to extend the scatterer size parameter far into the Mie regime. The Discrete Method used for this computation suggest similar pattern is followed.

Now, we evaluate the angular dependent scattering function using the Discrete Method for a scatterer with size parameter many times smaller than the wavelength. The size parameters for this computation are chosen to demonstrate the scattering properties in the Rayleigh regime. The curves in Figure 5.4 with $x = 0.1$ show that the forward and backward ratio for both the calculation by the Mie theory and the Discrete Method is virtually identical for the horizontal polarization and fairly similar for vertical polarization. The forward and backward ratio is approximately 1, and this is obviously expected.

We increase the size parameter from $x = 0.1$ to 0.5 in Figure 5.5 and keep other input parameters constant. It is observed that the curves follow the similar pattern as expected but the forward and backward scattering ratio has increased more than one. This is due to the phase shift as the particle size tends towards the Mie regime.

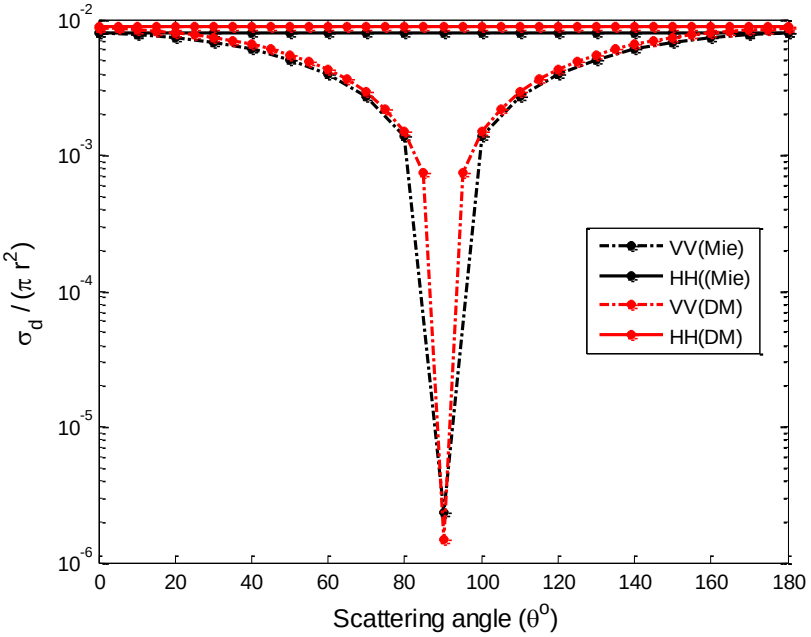

Figure 5.4: Comparison of Discrete Method and Rayleigh theory for the evaluation of normalised differential scattering cross section for a non-absorbing dielectric sphere using the Mie theory code with $x = 0.1$ and $n = 1.33 + 0.0i$

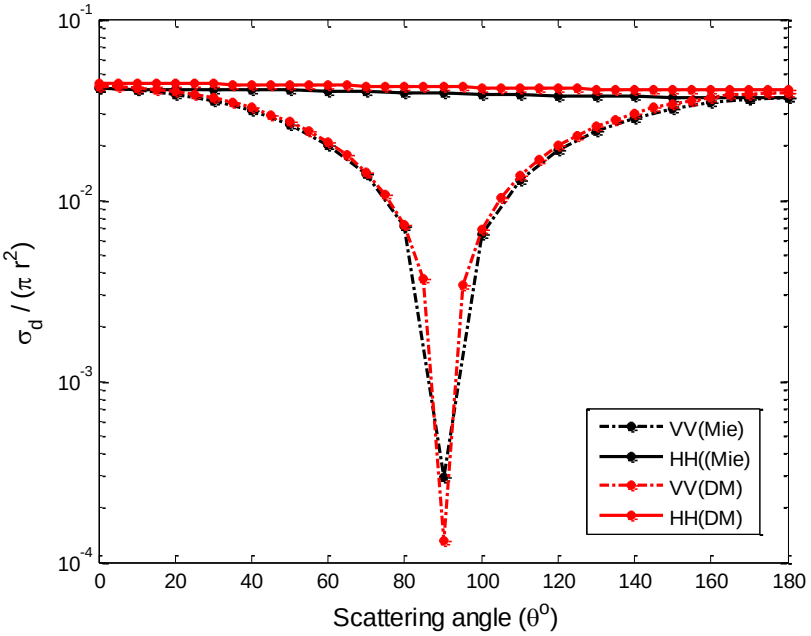

Figure 5.5: Comparison of Discrete Method and Rayleigh theory for the evaluation of normalised differential scattering cross section for a non-absorbing dielectric sphere using the Mie theory code with $x = 0.5$ and $n = 1.33 + 0.0i$

5.2.2 Scattering by spherical particles

Application of the Discrete Method as discussed in this work to evaluate angular scattering functions of the spherical particle is considered first in the past. Spheres have been studied more extensively than has the scattering by any other particle shape. This is partly because, it is the only three dimensional particle for which an analytical closed form solution is readily available and can be easily used to validate new methods. The scattering plane is defined as xz plan contains the vertical and horizontal polarizations is shown in Figure 3.7.

As an example of calculating scattering by sphere we choose a spherical particle of size parameter $x = 1.0$ with an incident wave of 5.8 GHz. At this frequency, we use a refractive index of $1.33 + 0.0i$. The value of the given size parameter corresponds to a scatterer equivalent diameter of about 2.0 cm which is approximately the characteristic length (diameter) of a large ice aggregate. The initial validation is carried out by comparison of the Mie theory and the Discrete Method discussed in this thesis. The numerical results follow similar pattern and in good agreement which is depicted in Figure 5.6. In all graphs the logarithms of the scattering amplitude functions are plotted against the scattering angles which is the independent variable θ_s unless stated otherwise. Perhaps the most significant to note is that the scattering is highly peaked in the forward direction for both cases of polarizations. As the scattering angle increases, the magnitude of the of the vertical polarization decreases to minimum at scattering angle $\theta_s = 90^0$ and increases thereafter to maximum $\theta_s = 180^0$. In the case of the perpendicular polarization decreases gradually to a minimum value $\theta_s = 180^0$. The decrease in the amplitude function magnitude is as a result of phase shift due to interaction of the plane wave with the scattering medium.

However, we notice that the Discrete Method deviates slightly from the Mie theory as shown in Figure 5.6 for the case of the vertical polarization at scattering angle $\theta_s = 90^0$. The reason for this different has not be fully tracked down in the course of this study but it is worth investigating further to account for this effect.

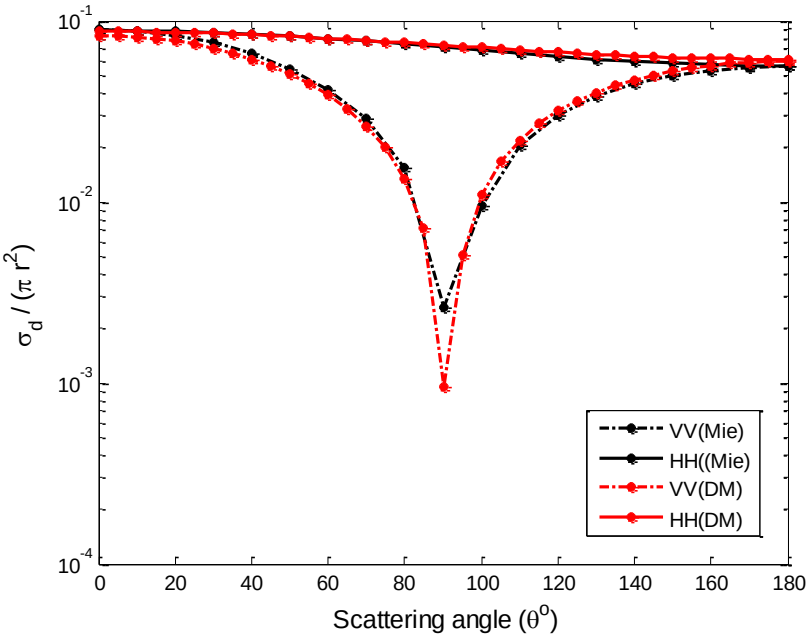

Figure 5.6: Comparison of Mie theory and Discrete Method for the evaluation of normalised differential scattering cross section for a non-absorbing dielectric sphere $x = 1.0$ and $n = 1.33 + 0.0i$

In effect, we know that both polarizations must have the same magnitude at the forward scattering function based on the symmetry. As the size parameter x increases, it expected that a more complex interaction occur between the scatterer and the plane wave and this account for the curves in both polarization modes to change gradually with series of peaks and valleys over the scattering angle. Further test are made including compliance with the law of reciprocity. Specifically, scattering calculation are obtained for spherical particle where the numerical results of the scattered field return in one direction due to an incident plane wave

from another is compared to the scattered field return in the origin incident field direction $+z$. The angular dependent scattering functions obtained from the cases was identical.

From Figure 5.7 it is evident that increasing the size parameter into to the Mie regime using the Discrete Method is virtually identical in comparison with the Mie theory for the curves of the horizontal polarization. But deviate significantly where the dip occurs in the case of vertical polarization. The reason for this break down as the size parameter tends toward 1.5 has not been properly identified and needs to be investigated. This can be attributed either to the evaluation of the scaling factor in the Z-term, the W-term and the non singular matrix K.

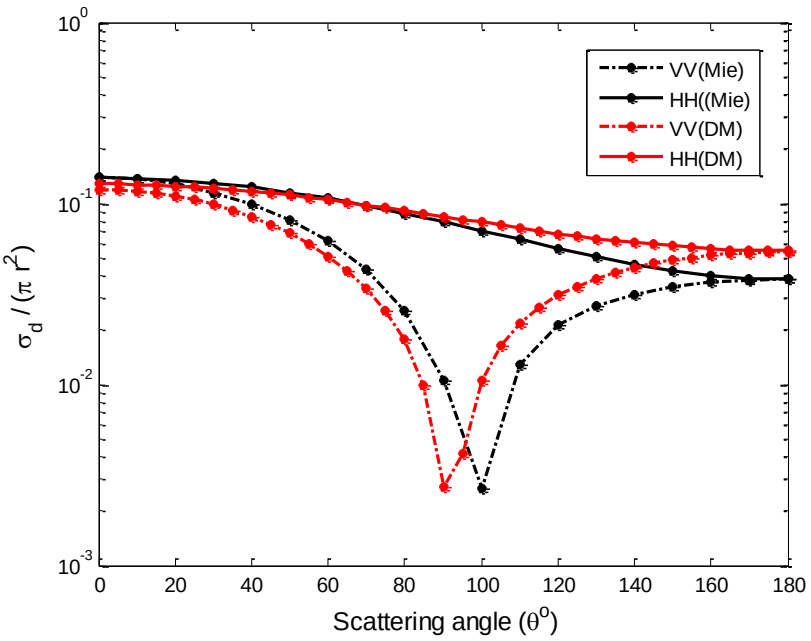

Figure 5.7: Comparison of Mie theory and Discrete Method for the evaluation of normalised differential scattering cross section for a non-absorbing dielectric sphere $x = 1.5$ and $n = 1.33 + 0.0i$

5.3 Scattering by mixed phase hydrometeors

After satisfactory results are obtained from size parameter $x = 1$, we extend the application of the Discrete Method to evaluate the scattering amplitude functions of hybrid irregular hydrometeors modelled as inhomogeneous dielectric particles. In particular, the snowflake aggregate containing of air, ice and/or liquid water is a good representation of such scatterer with mixed dielectric constant.

Firstly, we start by applying Maxwell Garnett two-part mixing formula (2.37) discussed in chapter 2 to dry snowflake modelled as sphere which is a mixture of ice and air. It is important to note that when using effective medium theories to estimate average dielectric constant, considerations must be made as to which component will be the inclusion or the matrix. Significant differences appear with respect to the average dielectric if the two materials are simply interchanged. By this same token, we decide to use a volume of 50% for both components. The ice with refractive index $n = 1.78+0.0i$ is chosen to be the host or background material and the air with refractive index $n = 1.0 + 0.0i$ as the inclusion or guest. The average or effective dielectric constant is obtained to be approximately $\varepsilon \approx 1.839$ which is $n' \approx 1.356$. The input parameters are size parameter $x = 1$, frequency 5.8 GHz.

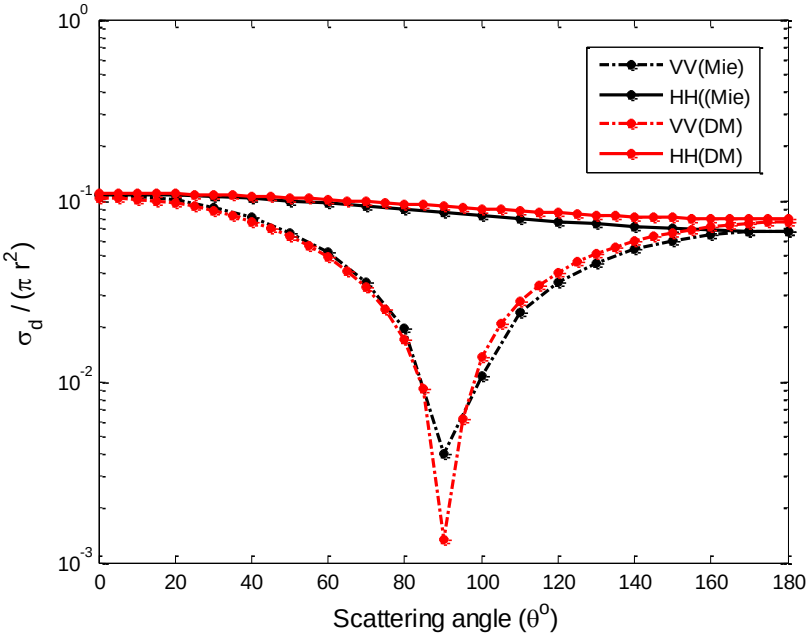

Figure 5.8: Comparison of Mie theory and Discrete Method for the evaluation of normalised differential scattering cross section for a non-absorbing dielectric sphere using Maxwell-Garnett formula for air inclusions in an ice matrix (ice-air mixture) given $x = 1.0$ and $n \approx 1.356 + 0.0i$

Using these parameters listed above, numerical examples are performed to evaluate amplitude function with the Mie theory and the Discrete Method. Remarkably, the curves of the normalized differential scattering cross section shown in Figure 5.8 are virtually identical and in good agreement. The forward and backward ratio for both plots converged reasonably with slight error margin. The amplitude of the forward scattering falls off gradually due to phase shift at the backward direction for the case of the horizontal polarization. However, at the dip, the Discrete Method departs slightly for the vertical polarization in comparison with the Mie theory.

Furthermore, we now use the Discrete Method to evaluate the scattering amplitude function from inhomogeneous particle such as dry snowflake consisting of ice and

air, assuming both with volume fractions of 50%. The scatterer is modelled as a sphere with their dielectric constant evenly distributed in a predefined manner. The input parameters are kept the same as discussed using Maxwell Garnett above for calculation of the differential scattering cross section. The curves in Figure 5.9 shows the relationship using the Discrete Method with Maxwell Garnett mixing formula and without effective medium theory.

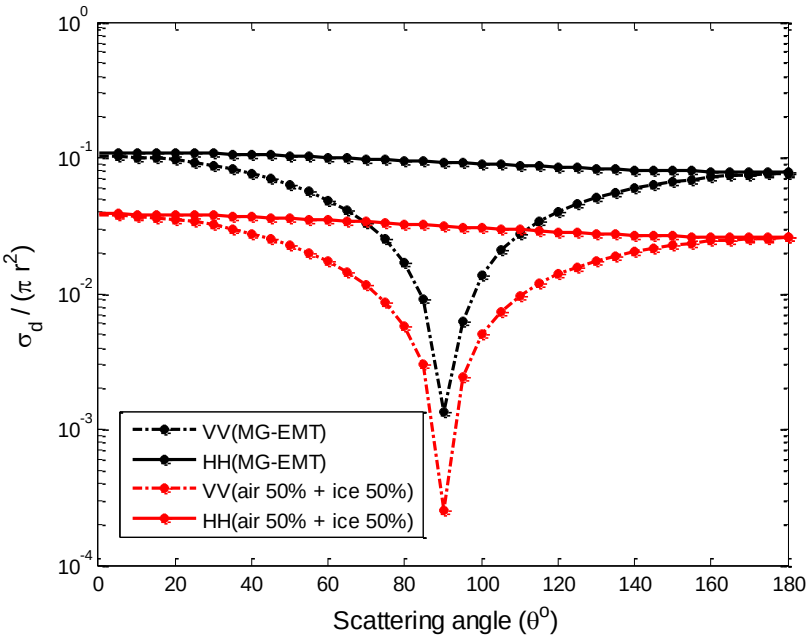

Figure 5.9: Comparison of the Discrete Method for the evaluation of normalised differential scattering cross section for a non-absorbing dielectric sphere with Maxwell Garnett mixing rule and without applying MG EMTs $x = 1.0$ and $n \approx 1.356 + 0.0i$

Although the curves shown in Figure 5.9 follow similar pattern but significantly deviate as expected. The approach of using effective medium theory such as Maxwell Garnett to estimate dielectric constant of the inhomogeneous medium is shown to be insufficient and it is not a linear process as proposed in chapter 2. The reason for this difference has been identified as how the calculations of the Z-term and W-term scale in the homogeneous and inhomogeneous case. In order to verify this

problem, we made the similar assumptions as stated above with volume fraction of 50% mixture.

For ice, $n \approx 1.78$ and the effective refractive index $n' \approx 1.356$. The permittivities are then given as

$$\varepsilon_r \approx 3.168 \qquad \text{and} \qquad \varepsilon_r' \approx 1.839. \tag{5.2}$$

For W, with half of the cells filled, the relative density is $\frac{1}{2}$ so we have a weighting factor

$$\frac{\varepsilon_r \times (\varepsilon_r - 1)}{2} \tag{5.3}$$

and

$$W \approx \frac{3.168 \times 2.168}{2} = 3.43. \tag{5.4}$$

For the effective medium, we have 100% fill, so

$$W' \approx \varepsilon_r' \times (\varepsilon_r' - 1) = 1.839 \times 0.839 = 1.54. \tag{5.5}$$

Similarly we have for Z, the density of the pairs divide by four, hence the scaling factor is expressed as

$$Z \approx (\varepsilon_r - 1)^2 \times \frac{1}{4} = \frac{(2.168)^2}{4} = 1.175, \tag{5.6}$$

and for the effective medium, all cell pairs count, but with smaller polarizabilities γ, so Z' scaling factor is given as

$$Z' \approx 0.839^2 = 0.70 \tag{5.7}$$

The W', Z' and K' are relatively smaller for the effective medium theory approach so the inversion of the equations will give rise to larger amplitudes for the Fourier

Coefficients C. The scaling of the U-term is neutral because it is a factor on both sides for the forward and substitution steps. Looking at the numerical examples in the work, the Discrete Method has a very good potential to be extended to evaluate scattering characteristics of larger size parameters and other inhomogeneous irregular hydrometeors. It is important to note that once the dyadic scattering amplitude functions is evaluated, other particle characteristics such as cross sections and efficiency factors can easily be obtained.

5.4 Summary

We have demonstrated the efficiency of the Discrete Method to evaluate scattering amplitude function for homogeneous and inhomogeneous scatterers up to size parameter $x = 1$. For the inhomogeneous particle such as the dry snowflake. It is evident that our approach is more appropriate to describe the scattering properties compared to the Maxwell Garnett mixing formula. Comparison of the Discrete Method and Mie theory for the forward and backward scattering cross section ratio showed that good agreement is obtained from Rayleigh scattering regime to size parameter $x = 1$ and break down as the size parameter (x) tends toward 1.5.

Numerical results were satisfactory for the evaluation of normalized radar cross section with respect to the size parameter up to 3. Satisfactory result were also achieved using our technique to evaluation the angular dependent scattering amplitude functions for size parameters within the Rayleigh and the Mie regimes. Looking at the numerical examples in this work, the Discrete Method has a very good potential to be extended to evaluate scattering characteristics of large size parameters and other inhomogeneous irregular hydrometeors.

CHAPTER 6

CONCLUSIONS AND FURTHER WORK

A discrete implementation of the Fredholm Integral method for scattering has been presented which can take account of inhomogeneous dielectrics.

The code was implemented in FORTRAN 95 language with version 6.10 FTN95 Silverfrost compiler, which allowed the facility to define types and overloaded operators to be explored, such that a module could be written encapsulating complex dyadic and vector algorithm. This considerably simplified the resulting top level code allowing the structure of the algorithm and its relation to the underlying theoretical equations to be clearly visible.

As in earlier implementation of the method for ellipsoidal and homogeneous scatterer, the most difficult aspect of the implementation is to evaluate the K and Z routines for the pivots. Whereas the earlier implementation relied on truncated expansion in spherical Bessel functions and Gegenbauer polynomials. This Discrete Method, while simple in principle introduces its own particular difficulties. In particular, the simple minded adoption of cubic or cuboid cells introduces new singularities into the required contour integrals involving cell pairs, because of the denominators in the sinc functions. This was overcome by considering spherical cells of the same volume. It is argued that when the discretized cells are sufficiently small, their shape have little effect on the results.

A particular benefit arising from this is that as the cells becomes even smaller relative to the wavelength, the expansion of the Gegenbauer addition formula for the pivot difference vector dependence reduces to a simple dominant term, making the pair trivially just the positional phase dependence on $\mathbf{k}_n$ or $\mathbf{k}_m$. Consequently, evaluation of the pairwise integrals takes place outside the inner loops for the evaluation of the Z terms, reducing the evaluation time by a factor equal to the number of pivots.

The results have been checked to be relatively stable with respect to both the discretization scale and the number of pivots. Unfortunately, it is not yet possible to established precisely the rate of convergence, as the binary choice of inclusion or exclusion of the cells at the scatterer boundary results in the actual volume of the model scattering particle fluctuates according to the number of grid cells adopted. This problem could be addressed at the expense of greater code complexity by attaching partial weighting factors to the boundary cells.

Results have shown that the implementation is reasonably successful from the

Rayleigh regime into the Mie regime, up to size parameters of unity. For ice scatterers, this includes a useful range at C-band which is the predominant band for European Weather radars, and where unity size parameter ka corresponds roughly to a 2.0 cm diameter scatterer. Qualitatively, the results show the typical features that appear in Mie theory mainly. The increase in the forward/backscatter ratio and the infill and migration of the parallel scattering amplitude dip from the exact 90^0 null to angle closer to the backscatter directions.

The surprise was that the implementation appears to break down once the size parameter reaches around 1.5. Considerable effort was devoted to checking the code implementation. In particular, the consistency of the results where frequency can vary while the size parameter is held constant confirms that the scaling factors for the W or Z do not improve the behaviour at large size parameter.

Throughout the process of gathering results the performance of the matrix solution method using LU decomposition was checked, and has always resulted in a maximum error close to machine precision. At present it is not known whether there is a residual 'bug' in the code or whether there is simply a breakdown in assumptions involved in the implementation. There is nothing straightforwardly apparent in either possibility.

Clearly further work is required to try to resolve this problem. It is inherently difficult to visualise the K matrix or find independent ways to verify its evaluation. One possibility however to independently validate the calculation of K would be to apply a 'brute force' numerical integration of the Z term over the dummy pivot p-running from zero to infinity and around the pole at k_0 for the entire U functions rather than pair-wise cell contributions.

Within the range of size parameter for which the implementation has been validated an interesting result has been obtained in which a potential problem arising from the adoption of effective medium theory has been exposed. The first step towards applying the code to an inhomogeneous target has been a hybrid approach. This assumed that the internal wave field could be defined. However, the scattering amplitude is still evaluated by effectively integrating the induced polarization in the scatter interior with respect to the scattered wave term. The two methods give rise to distinctively different results. If the effective medium theory is valid, then there should indeed be an expansion of exponentials with wave vector appropriate to that effective medium, so the hybrid method ought also be valid.

A further possibility is that it may be necessary to take account of the fine scale fluctuating field that the effective would be expected to correlate closely with the permittivity fluctuations and not match the phase variable of the wave scattered wave. Nevertheless, it seems likely that further theoretical development may be required to handle scattering from inhomogeneous targets.

Here also, DDA comparison would also in principle be useful, although for a equivalent level of discretization it would be necessary to handle matrices of order $10^3 - 10^4$ which at present has not proved feasible with resources that were available.

BIBLIOGRAPHY

[1] G. Rees and W. G. Rees, *Physical principles of remote sensing*. Cambridge University Press, 2012.

[2] J. B. Campbell, *Introduction to remote sensing*. CRC Press, 2002.

[3] M. I. Skolnik, "Introduction to radar," *Radar Handbook*, p. 1990, 1962.

[4] T. Oguchi, "Electromagnetic wave propagation and scattering in rain and other hydrometeors," *Proceedings of the IEEE*, vol. 71, no. 9, pp. 1029–1078, 1983.

[5] W. Zhang, J. K. Tervonen, and E. T. Salonen, "Backward and forward scattering by the melting layer composed of spheroidal hydrometeors at 5-100 GHz," *Antennas and Propagation, IEEE Transactions on*, vol. 44, no. 9, pp. 1208–1219, 1996.

[6] F. T. Ulaby, R. K. Moore, and A. K. Fung, *Microwave Remote Sensing*

Active and Passive-Volume III: From Theory to Applications. Artech House, Inc, 1986.

[7] R. L. Fante, "Relationship between radiative-transport theory and maxwells equations in dielectric media," *JOSA*, vol. 71, no. 4, pp. 460–468, 1981.

[8] A. Ishimaru, *Wave propagation and scattering in random media*, vol. 2. Academic press New York, 1978.

[9] A. Ishimaru, "Theory and application of wave propagation and scattering in random media," *Proceedings of the IEEE*, vol. 65, no. 7, pp. 1030–1061, 1977.

[10] M. Born and E. Wolf, *Principles of optics: electromagnetic theory of propagation, interference and diffraction of light*. CUP Archive, 1999.

[11] W. Zhang, "Scattering of radiowaves by a melting layer of precipitation in backward and forward directions," *Antennas and Propagation, IEEE Transactions on*, vol. 42, no. 3, pp. 347–356, 1994.

[12] P. J. Flatau and B. Draine, "Discrete-dipole approximation for scattering calculations," *J. Opt. Soc. Am. A*, vol. 11, p. 1491, 1994.

[13] A. Holt and B. Santoso, "The fredholm integral method. ii. the calculation of scattering amplitudes for potential scattering," *Journal of Physics B: Atomic and Molecular Physics*, vol. 6, no. 10, p. 2010, 1973.

[14] J. M. Garnett, "Colours in metal glasses and in metallic films.," *Proceedings of the Royal Society of London*, vol. 73, no. 488-496, pp. 443–445, 1904.

[15] V. D. Bruggeman, "Berechnung verschiedener physikalischer konstanten von heterogenen substanzen. i. dielektrizitätskonstanten und leitfähigkeiten der mischkörper aus isotropen substanzen," *Annalen der Physik*, vol. 416, no. 7, pp. 636–664, 1935.

[16] H. C. Hulst and H. C. van de Hulst, *Light scattering: by small particles*. Courier Dover Publications, 1957.

[17] M. Kerker, *The scattering of light, and other electromagnetic radiation*. Academic press, 1969.

[18] P. Waterman, "Matrix formulation of electromagnetic scattering," *Proceedings of the IEEE*, vol. 53, no. 8, pp. 805–812, 1965.

[19] M. I. Mishchenko, L. D. Travis, and A. A. Lacis, *Scattering, Absorption, and Emmision of Light by Small Particles*. Cambridge university press, 2002.

[20] H. Lindner, G. Fritz, and O. Glatter, "Measurements on concentrated oil in water emulsions using static light scattering," *Journal of colloid and interface science*, vol. 242, no. 1, pp. 239–246, 2001.

[21] B. K. Wilson, M. R. Behrend, M. P. Horning, and M. C. Hegg, "Detection of malarial byproduct hemozoin utilizing its unique scattering properties," *Optics Express*, vol. 19, no. 13, pp. 12190–12196, 2011.

[22] C. J. Joachain, *Quantum collision theory*. 1975.

[23] V. Twersky, "Rayleigh scattering," *Applied Optics*, vol. 3, no. 10, pp. 1150–1150, 1964.

[24] A. T. Young, "Rayleigh scattering," *Applied Optics*, vol. 20, no. 4, pp. 533–535, 1981.

[25] A. Cox, A. J. DeWeerd, and J. Linden, "An experiment to measure mie and rayleigh total scattering cross sections," *American Journal of Physics*, vol. 70, p. 620, 2002.

[26] C. F. Bohren and D. R. Huffman, *Absorption and scattering of light by small particles*. Wiley. com, 2008.

[27] J. A. Stratton, *Electromagnetic theory*, vol. 33. Wiley. com, 2007.

[28] J. Jackson, *Classical Electrodynamics*. John Wiley & Sons, Inc., New York., 1962.

[29] R. G. Newton, *Scattering theory of waves and particles*. DoverPublications. com, 1982.

[30] B. Thidé, *Electromagnetic field theory*. Upsilon Books Uppsala, 2004.

[31] D. R. DeWalle and A. Rango, *Principles of snow hydrology*. Cambridge University Press, 2008.

[32] A. H. Auer Jr and D. L. Veal, "The dimension of ice crystals in natural clouds," *Journal of the Atmospheric Sciences*, vol. 27, no. 6, pp. 919–926, 1970.

[33] B. Mason, *The physics of clouds*. Clarendon Press Oxford, 1971.

[34] H. R. Pruppacher, J. D. Klett, and P. K. Wang, "Microphysics of clouds and precipitation," 1998.

[35] D. Lamb and J. Verlinde, *Physics and chemistry of clouds*. Cambridge University Press, 2011.

[36] G. Botta, K. Aydin, and J. Verlinde, "Modeling of microwave scattering from cloud ice crystal aggregates and melting aggregates: A new approach," *Geoscience and Remote Sensing Letters, IEEE*, vol. 7, no. 3, pp. 572–576, 2010.

[37] S. Y. Matrosov, "Assessment of radar signal attenuation caused by the melting hydrometeor layer," *Geoscience and Remote Sensing, IEEE Transactions on*, vol. 46, no. 4, pp. 1039–1047, 2008.

[38] L. Liao and R. Meneghini, "On modeling air/spaceborne radar returns in the melting layer," *Geoscience and Remote Sensing, IEEE Transactions on*, vol. 43, no. 12, pp. 2799–2809, 2005.

[39] F. Fabry and I. Zawadzki, "Long-term radar observations of the melting layer of precipitation and their interpretation," *Journal of the atmospheric sciences*, vol. 52, no. 7, pp. 838–851, 1995.

[40] J. Steinert and M. Chandra, "Melting-layer modelling at c-band," *Advances in Radio Science*, vol. 8, no. 16, pp. 285–288, 2010.

[41] W. Zhang, S. I. Karhu, and E. T. Salonen, "Predictions of radiowave attenuations due to a melting layer of precipitation," *Antennas and Propagation, IEEE Transactions on*, vol. 42, no. 4, pp. 492–500, 1994.

[42] L. Raynaud, I. Chenerie, and J. Lemorton, "Modeling of radiowave scattering in the melting layer of precipitation," *Geoscience and Remote Sensing, IEEE Transactions on*, vol. 38, no. 4, pp. 1574–1584, 2000.

[43] F. Fabry and W. Szyrmer, "Modeling of the melting layer. part ii: Electromagnetic," *Journal of the atmospheric sciences*, vol. 56, no. 20, pp. 3593–3600, 1999.

[44] P. L. Smith, "Raindrop size distributions: Exponential or gamma-does the difference matter?," *Journal of Applied Meteorology*, vol. 42, no. 7, pp. 1031–1034, 2003.

[45] C. W. Ulbrich, "Natural variations in the analytical form of the raindrop size distribution," *Journal of Climate and Applied Meteorology*, vol. 22, no. 10, pp. 1764–1775, 1983.

[46] M. N. Sadiku, "Refractive index of snow at microwave frequencies," *Applied optics*, vol. 24, no. 4, pp. 572–575, 1985.

[47] A. H. Sihvola, *Electromagnetic mixing formulae and applications*. No. 47, Iet, 1999.

[48] M. Marzuki, W. L. Randeu, F. Teschl, M. Schonhuber, and W. Harjupa, "Complex permittivity measurements of rainwater in the 0.5–26.5 GHz frequency range," *Geoscience and Remote Sensing Letters, IEEE*, vol. 7, no. 3, pp. 487–490, 2010.

[49] M.-J. Kim, "Single scattering parameters of randomly oriented snow particles at microwave frequencies," *Journal of geophysical research*, vol. 111, no. D14, p. D14201, 2006.

[50] P. J. W. Debye, P. J. W. Debye, and P. J. W. Debye, *Polar molecules*, vol. 172. Dover New York, 1929.

[51] K. S. Cole and R. H. Cole, "Dispersion and absorption in dielectrics i. alternating current characteristics," *The Journal of Chemical Physics*, vol. 9, p. 341, 1941.

[52] L. Klein and C. Swift, "An improved model for the dielectric constant of sea water at microwave frequencies," *Antennas and Propagation, IEEE Transactions on*, vol. 25, no. 1, pp. 104–111, 1977.

[53] P. S. Ray, "Broadband complex refractive indices of ice and water," *Applied Optics*, vol. 11, no. 8, pp. 1836–1844, 1972.

[54] D. H. O. Bebbington, "Complex refractive index of water using debye double relaxation model." Personal Communication, March 1991.

[55] H. J. Liebe, G. A. Hufford, and T. Manabe, "A model for the complex permittivity of water at frequencies below 1 THz," *International Journal of Infrared and Millimeter Waves*, vol. 12, no. 7, pp. 659–675, 1991.

[56] A. H. Sihvola, "How strict are theoretical bounds for dielectric properties of mixtures?," *Geoscience and Remote Sensing, IEEE Transactions on*, vol. 40, no. 4, pp. 880–886, 2002.

[57] T. C. Choy, *Effective medium theory: principles and applications*. No. 102, Oxford University Press, 1999.

[58] W. E. Kohler and G. Papanicolaou, "Some applications of the coherent potential approximation," tech. rep., DTIC Document, 1981.

[59] W. Stiles and F. Ulaby, "Dielectric properties of snow," tech. rep., DTIC Document, 1980.

[60] A. H. Sihvola and J. A. Kong, "Effective permittivity of dielectric mixtures," *Geoscience and Remote Sensing, IEEE Transactions on*, vol. 26, no. 4, pp. 420–429, 1988.

[61] H.-M. Chang and C. Liao, "A parallel derivation to the maxwell-garnett formula for the magnetic permeability of mixed materials," *World*, vol. 1, pp. 55–58, 2011.

[62] L. Kolokolova and B. Å. Gustafsonm, "Scattering by inhomogeneous particles: microwave analog experiments and comparison to effective medium theories," *Journal of Quantitative Spectroscopy and Radiative Transfer*, vol. 70, no. 4, pp. 611–625, 2001.

[63] M. A. Abu-Gabal, A. M. El-Rouby, and I. A. Eshrah, "Simulation of effective dielectric constant for lossless composites using 2d finite difference frequency domain," in *Antennas and Propagation (MECAP), 2010 IEEE Middle East Conference on*, pp. 1–4, IEEE, 2010.

[64] G. Botta, K. Aydin, J. Verlinde, A. E. Avramov, A. S. Ackerman, A. M. Fridlind, G. M. McFarquhar, and M. Wolde, "Millimeter wave scattering from ice crystals and their aggregates: Comparing cloud model simulations with x-and ka-band radar measurements," *Journal of Geophysical Research*, vol. 116, no. D1, p. D00T04, 2011.

[65] P. W. Barber and S. C. Hill, *Light scattering by particles: computational methods*, vol. 2. World scientific, 1990.

[66] B. T. Draine, "The discrete-dipole approximation and its application to interstellar graphite grains," *The Astrophysical Journal*, vol. 333, pp. 848–872,

1988.

[67] M. A. Yurkin and A. G. Hoekstra, "The discrete dipole approximation: an overview and recent developments," *Journal of Quantitative Spectroscopy and Radiative Transfer*, vol. 106, no. 1, pp. 558–589, 2007.

[68] V. Twersky, "Multiple scattering of radiation by an arbitrary configuration of parallel cylinders," *The Journal of the Acoustical Society of America*, vol. 24, no. 1, pp. 42–46, 1952.

[69] V. Twersky, "Multiple scattering by arbitrary configurations in three dimensions," *Journal of Mathematical Physics*, vol. 3, no. 1, pp. 83–91, 1962.

[70] V. Twersky, "Multiple scattering of waves and optical phenomena," *JOSA*, vol. 52, no. 2, pp. 145–169, 1962.

[71] V. Twersky, "Multiple scattering of electromagnetic waves by arbitrary configurations," *Journal of Mathematical Physics*, vol. 8, no. 3, pp. 589–610, 1967.

[72] T. Wriedt, "Mie theory: A review," in *The Mie Theory*, pp. 53–71, Springer, 2012.

[73] T. Wriedt, "A review of elastic light scattering theories," *Particle & particle systems characterization*, vol. 15, no. 2, pp. 67–74, 1998.

[74] W. J. Wiscombe, "Improved mie scattering algorithms," *Applied optics*, vol. 19, no. 9, pp. 1505–1509, 1980.

[75] P. Waterman, "New formulation of acoustic scattering," *The Journal of the acoustical society of America*, vol. 45, no. 6, pp. 1417–1429, 1969.

[76] P. Waterman, "Matrix theory of elastic wave scattering," *The Journal of the Acoustical Society of America*, vol. 60, no. 3, pp. 567–580, 1976.

[77] W. Zheng, "The null field approach to electromagnetic scattering from composite objects: The case with three or more constituents," *Antennas and Propagation, IEEE Transactions on*, vol. 36, no. 10, pp. 1396–1400, 1988.

[78] T. Wriedt, "Review of the null-field method with discrete sources," *Journal of Quantitative Spectroscopy and Radiative Transfer*, vol. 106, no. 1, pp. 535–545, 2007.

[79] P. W. Barber and D.-S. Wang, "Rayleigh-gans-debye applicability to scattering by nonspherical particles," *Applied Optics*, vol. 17, no. 5, pp. 797–803, 1978.

[80] T. Wriedt and A. Doicu, "Formulations of the extended boundary condition method for three-dimensional scattering using the method of discrete sources," *Journal of modern optics*, vol. 45, no. 1, pp. 199–213, 1998.

[81] T. Wriedt, "Using the t-matrix method for light scattering computations by non-axisymmetric particles: superellipsoids and realistically shaped particles," *Particle and Particle Systems Characterization*, vol. 19, no. 4, pp. 256–268, 2002.

[82] M. I. Mishchenko, J. W. Hovenier, and L. D. Travis, *Light scattering by nonspherical particles: theory, measurements, and applications*. Access Online via Elsevier, 1999.

[83] M. I. Mishchenko and L. D. Travis, "T-matrix computations of light scattering by large spheroidal particles," *Optics communications*, vol. 109, no. 1,

pp. 16–21, 1994.

[84] M. I. Mishchenko, L. D. Travis, and D. W. Mackowski, "$< i > t < /i >$-matrix computations of light scattering by nonspherical particles: A review," *Journal of Quantitative Spectroscopy and Radiative Transfer*, vol. 55, no. 5, pp. 535–575, 1996.

[85] P. Waterman, "Symmetry, unitarity, and geometry in electromagnetic scattering," *Physical review D*, vol. 3, no. 4, p. 825, 1971.

[86] P. Barber and C. Yeh, "Scattering of electromagnetic waves by arbitrarily shaped dielectric bodies," *Applied Optics*, vol. 14, no. 12, pp. 2864–2872, 1975.

[87] J. Goodman, B. T. Draine, P. J. Flatau, *et al.*, "Application of fast-fourier-transform techniques to the discrete-dipole approximation," *Opt. Lett*, vol. 16, no. 15, pp. 1198–1200, 1991.

[88] B. T. Draine and P. J. Flatau, "Discrete-dipole approximation for periodic targets: theory and tests," *JOSA A*, vol. 25, no. 11, pp. 2693–2703, 2008.

[89] P. Flatau and B. Draine, "Fast near field calculations in the discrete dipole approximation for regular rectilinear grids," *Opt. Express*, vol. 20, pp. 1247–1252, 2012.

[90] S. B. Singham and C. F. Bohren, "Light scattering by an arbitrary particle: a physical reformulation of the coupled dipole method," *Optics Letters*, vol. 12, no. 1, pp. 10–12, 1987.

[91] G. H. Goedecke, S. G. OBrien, *et al.*, "Scattering by irregular inhomogeneous

particles via the digitized greens function algorithm," *Applied Optics*, vol. 27, no. 12, pp. 2431–2438, 1988.

[92] M. S. Tong and W. C. Chew, "Coupled integral equations for microwave induced elastic wave in elastic media," *Antennas and Propagation, IEEE Transactions on*, vol. 58, no. 7, pp. 2309–2317, 2010.

[93] J. Markkanen, C.-C. Lu, X. Cao, and P. Yla-Oijala, "Analysis of volume integral equation formulations for scattering by high-contrast penetrable objects," *Antennas and Propagation, IEEE Transactions on*, vol. 60, no. 5, pp. 2367–2374, 2012.

[94] L. Auchterlonie and D. Bryant, "Experimental study of millimetre-wave scattering from simulated hailstones in an open resonator," *Microwaves, Optics and Antennas, IEE Proceedings H*, vol. 128, no. 5, pp. 236–242, 1981.

[95] W. Zheng and S. Strom, "The null field approach to electromagnetic scattering from composite objects: The case of concavo-convex constituents," *Antennas and Propagation, IEEE Transactions on*, vol. 37, no. 3, pp. 373–383, 1989.

[96] T. Oguchi, "Scattering properties of oblate raindrops and cross polarization of radio waves due to rain- calculations at 19. 3 and 34. 8 ghz," *Radio Research Laboratories, Journal*, vol. 20, no. 102, pp. 79–118, 1973.

[97] J. Morrison and M.-J. Cross, "Scattering of a plane electromagnetic wave by axisymmetric raindrops," *Bell System Technical Journal*, vol. 53, pp. 955–1019, 1974.

[98] A. Holt, N. Uzunoglu, and B. Evans, "An integral equation solution to

the scattering of electromagnetic radiation by dielectric spheroids and ellipsoids," *Antennas and Propagation, IEEE Transactions on*, vol. 26, no. 5, pp. 706–712, 1978.

[99] A. Holt, "Electromagnetic wave scattering by spheroids: A comparison of experimental and theoretical results," *Antennas and Propagation, IEEE Transactions on*, vol. 30, no. 4, pp. 758–760, 1982.

[100] J. Shepherd and A. Holt, "The scattering of electromagnetic radiation from finite dielectric circular cylinders," *Journal of Physics A: Mathematical and General*, vol. 16, no. 3, p. 651, 1983.

[101] N. Uzunoglu, B. Evans, and A. Holt, "Evaluation of the scattering of an electromagnetic wave from precipitation particles by the use of fredholm integral equations," *Electronics Letters*, vol. 12, no. 12, pp. 312–313, 1976.

[102] N. Uzunoglu and A. Holt, "The scattering of electromagnetic radiation from dielectric scatterers," *Journal of Physics A: Mathematical and General*, vol. 10, no. 3, p. 413, 1977.

[103] A. Holt, "The fredholm integral equation method and comparison with the t-matrix approach," in *Acoustic, Electromagnetic and Elastic Wave Scattering-Focus on the T-Matrix Approach*, vol. 1, pp. 255–268, 1980.

[104] J. L. Volakis and K. Sertel, *Integral equation methods for electromagnetics*. SciTech Pub., 2012.

[105] M. Rahman, *Integral equations and their applications*. WIT Southampton, 2007.

[106] W. C. Chew, M. S. Tong, and B. Hu, "Integral equation methods for electromagnetic and elastic waves," *Synthesis Lectures on Computational Electromagnetics*, vol. 3, no. 1, pp. 1–241, 2008.

[107] M. I. Mishchenko, *Electromagnetic scattering by particles and particle groups: an introduction*. Cambridge University Press, 2014.

[108] E. W. Weisstein, "Fredholm integral equation of the second kind," 2002.

[109] M. I. Sancer, K. Sertel, J. L. Volakis, and P. Van Alstine, "On volume integral equations," *Antennas and Propagation, IEEE Transactions on*, vol. 54, no. 5, pp. 1488–1495, 2006.

[110] M. L. Boas, *Mathematical methods in the physical sciences*. Wiley. com, 2006.

[111] R. Snieder, *A guided tour of mathematical methods for the physical sciences*. Cambridge University Press, 2004.

[112] D. Colton and R. Kress, *Inverse acoustic and electromagnetic scattering theory*, vol. 93. Springer, 2012.

[113] N. K. Uzunoglu, *Theoretical Calculation of Scattering of Electromagnetic Waves from Precipitation Particles.* PhD thesis, University of Essex, 1976.

[114] T. H. Stein, C. D. Westbrook, and J. Nicol, "Fractal geometry of aggregate snowflakes revealed by triple-wavelength radar measurements," *Geophysical Research Letters*, vol. 42, no. 1, pp. 176–183, 2015.

[115] G. N. Watson, *A treatise on the theory of Bessel functions*. Cambridge university press, 1995.

[116] C. Schwartz, "A class of discontinuous integrals involving bessel functions," *Journal of Mathematical Physics*, vol. 23, no. 12, pp. 2266–2267, 1982.

[117] J. G. Van Bladel, *Electromagnetic fields*, vol. 19. John Wiley & Sons, 2007.

[118] F. O. Ngobigha and D. H. Bebbington, "Electromagnetic waves scattering by dielectric ellipsoids applying integral equation approach," in *Radio Science Meeting (Joint with AP-S Symposium), 2014 USNC-URSI*, pp. 227–227, IEEE, 2014.

[119] J. Chen, K. Ji, Z. Shi, and W. Liu, "Implementation of block algorithm for lu factorization," in *Computer Science and Information Engineering, 2009 WRI World Congress on*, vol. 2, pp. 569–573, IEEE, 2009.

[120] W. H. Press, *Numerical recipes in Fortran 77: the art of scientific computing*, vol. 1. Cambridge university press, 1992.

[121] M. Abramowitz and I. A. Stegun, *Handbook of mathematical functions: with formulas, graphs, and mathematical tables*. Courier Dover Publications, 2012.

[122] J. W. Brown, R. V. Churchill, and M. Lapidus, *Complex variables and applications*, vol. 7. McGraw-Hill New York, 1996.

Appendices

APPENDIX A

DERIVATIONS

A.1 Expansion of Vector Spherical Wave Functions

The VSWFs used in Mie theory with respect to spherical scattering particles are adapted from [26, 27] and can be written in spherical coordinates as:

$$\mathbf{M}_{emn} = \frac{-m}{\sin\theta}\sin m\phi\ P_n^m(\cos\theta)z_n(\rho)\hat{\mathbf{e}}_\theta - \cos m\phi\frac{dP_n^m(\cos\theta)}{d\theta}z_n(\rho)\hat{\mathbf{e}}_\phi, \tag{A.1a}$$

$$\mathbf{M}_{omn} = \frac{m}{\sin\theta}\cos m\phi\ P_n^m(\cos\theta)z_n(\rho)\hat{\mathbf{e}}_\theta - \sin m\phi\frac{dP_n^m(\cos\theta)}{d\theta}z_n(\rho)\hat{\mathbf{e}}_\phi, \tag{A.1b}$$

$$\begin{aligned}\mathbf{N}_{emn} = {} & \frac{z_n(\rho)}{\rho}\cos m\phi\ n(n+1)P_n^m(\cos\theta)\hat{\mathbf{e}}_r + \\ & \cos m\phi\frac{dP_n^m(\cos\theta)}{d\theta}\frac{1}{\rho}\frac{d}{d\rho}\left[\rho z_n(\rho)\right]\hat{\mathbf{e}}_\theta - \\ & m\sin m\phi\frac{P_n^m(\cos\theta)}{\sin\theta}\frac{1}{\rho}\frac{d}{d\rho}\left[\rho z_n(\rho)\right]\hat{\mathbf{e}}_\phi,\end{aligned} \tag{A.1c}$$

$$\begin{aligned}\mathbf{N}_{omn} = {} & \frac{z_n(\rho)}{\rho}\sin m\phi\ n(n+1)P_n^m(\cos\theta)\hat{\mathbf{e}}_r + \\ & \sin m\phi\frac{dP_n^m(\cos\theta)}{d\theta}\frac{1}{\rho}\frac{d}{d\rho}\left[\rho z_n(\rho)\right]\hat{\mathbf{e}}_\theta + \\ & m\cos m\phi\frac{P_n^m(\cos\theta)}{\sin\theta}\frac{1}{\rho}\frac{d}{d\rho}\left[\rho z_n(\rho)\right]\hat{\mathbf{e}}_\phi.\end{aligned} \tag{A.1d}$$

The associated Legendre functions are $P_n^m(cos\theta)$ and $z_n(\rho)$ are Bessel functions. Primes denote differentials with respect to the argument of z_n, ρ. Once we have simplified to the spherical case, with plane parallel incident light and $(m = 1)$, we write equation (A.1) in terms of π_n and τ_n

$$\pi_n = \frac{P_n^1(\cos\theta)}{\sin\theta}, \qquad\qquad \tau_n = \frac{dP_n^1(\cos\theta)}{d\theta}$$

$$\mathbf{M}_{e1n} = \qquad\qquad - \sin\phi\ \pi_n z_n \hat{\mathbf{e}}_\theta - \cos\phi\ \tau_n z_n \hat{\mathbf{e}}_\phi, \tag{A.2a}$$

$$\mathbf{M}_{o1n} = \qquad\qquad \cos\phi\ \pi_n z_n \hat{\mathbf{e}}_\theta - \sin\phi\ \tau_n z_n \hat{\mathbf{e}}_\phi, \tag{A.2b}$$

$$\mathbf{N}_{e1n} = n(n+1)\cos\phi\ \sin\theta\ \pi_n \frac{z_n}{\rho}\hat{\mathbf{e}}_r \quad + \cos\phi\ \tau_n \frac{[\rho z_n]'}{\rho}\mathbf{e}_\theta - \sin\phi\ \pi_n \frac{[\rho z_n]'}{\rho}\mathbf{e}_\phi, \tag{A.2c}$$

$$\mathbf{N}_{o1n} = n(n+1)\sin\phi\ \sin\theta\ \pi_n \frac{z_n}{\rho}\hat{\mathbf{e}}_r \quad + \sin\phi\ \tau_n \frac{[\rho z_n]'}{\rho}\mathbf{e}_\theta + \cos\phi\ \pi_n \frac{[\rho z_n]'}{\rho}\mathbf{e}_\phi. \tag{A.2d}$$

A.2 Spherical solution of the scalar wave equation

The derivation and general solution of scalar function ψ which satisfies the following scalar wave equation in spherical coordinates is given as

$$\nabla^2\psi + k^2\psi = 0. \tag{A.3}$$

Now we set the wave equation (A.3) in spherical polar coordinates

$$\frac{1}{r^2}\frac{\partial}{\partial r}\left(r^2\frac{\partial\psi}{\partial r}\right) + \frac{1}{r^2\sin\theta}\frac{\partial}{\partial\theta}\left(\sin\theta\frac{\partial\psi}{\partial\theta}\right) + \frac{1}{r^2\sin^2\theta}\frac{\partial^2\psi}{\partial\phi^2} + k^2\psi = 0. \tag{A.4}$$

We use the standard approach of separating the variables, i.e. we write

$$\psi(r,\,\theta,\,\phi) = R(r)\Theta(\theta)\Phi(\phi). \tag{A.5}$$

Upon substituting Eq. (A.5) into Eq. (A.4) and dividing the entire equation by $\psi(r,\,\theta,\,\phi)$, we obtain

$$\frac{1}{r^2}\frac{1}{R}\frac{\partial}{\partial r}\left(r^2\frac{\partial R}{\partial r}\right)+\frac{1}{r^2\sin\theta}\frac{1}{\Theta}\frac{\partial}{\partial\theta}\left(\sin\theta\frac{\partial\Theta}{\partial\theta}\right)+\frac{1}{r^2\sin^2\theta}\frac{1}{\Phi}\frac{\partial^2\Phi}{\partial\phi^2}+k^2=0. \quad \text{(A.6)}$$

If equation (A.6) is multiplied by $r^2\sin^2\theta$, then we have

$$\left[\sin^2\theta\frac{1}{R}\frac{\partial}{\partial r}\left(r^2\frac{\partial R}{\partial r}\right)+\sin\theta\frac{1}{\Theta}\frac{\partial}{\partial\theta}\left(\sin\theta\frac{\partial\Theta}{\partial\theta}\right)+k^2r^2\sin^2\theta\right]+\frac{1}{\Phi}\frac{\partial^2\Phi}{\partial\phi^2}=0. \quad \text{(A.7)}$$

Since the first three terms in this equation contain the variables r and θ only, the only way (A.7) can be valid is if

$$\frac{1}{\Phi}\frac{d^2\Phi}{d\phi^2}=constant=-m^2. \quad \text{(A.8)}$$

The solution is clearly

$$\Phi(\phi)=e^{im\phi}, \quad \text{(A.9)}$$

with m an integer (in order that the solution is the same for ϕ and $\phi+2\pi$). Substituting (A.8) into (A.7) and upon dividing by $\sin^2\theta$, we obtain

$$\frac{1}{R}\frac{d}{dr}\left(r^2\frac{dR}{dr}\right)+k^2r^2+\frac{1}{\Theta\sin\theta}\frac{d}{d\theta}\left(\sin\theta\frac{d\Theta}{d\theta}\right)-\frac{m^2}{\sin^2\theta}=0. \quad \text{(A.10)}$$

The third and fourth terms in equation (A.10) are only a function of θ (whereas the first two only depend on radial part r), and must therefore be a constant which, for reasons that will be clear later, we write as $n(n+1)$, i.e.

$$\frac{1}{R}\frac{d}{dr}\left(r^2\frac{dR}{dr}\right)+k^2r^2=constant=n(n+1), \quad \text{(A.11)}$$

$$\frac{1}{\Theta \sin\theta}\frac{d}{d\theta}\left(\sin\theta\frac{d\Theta}{d\theta}\right) - \frac{m^2}{\sin^2\theta} = constant = -n(n+1), \tag{A.12}$$

where n is an integer. The selection of the constant here is also for mathematical convenience. With the substitution of $x = \cos\theta$ into (A.12), so that

$$\frac{d}{dx}\left[\left(1-x^2\right)\frac{d\Theta}{dx}\right] + \left[n(n+1) - \frac{m^2}{1-x^2}\right]\Theta = 0. \tag{A.13}$$

The solution of Eq. (A.13) are the associated Legendre polynomials (spherical harmonics of the first kind)

$$\Theta = P_n^m(x) = P_n^m(\cos\theta).$$

We now focus on the radial equation (A.11), we set

$$x = kr, \qquad\qquad R = \frac{Z}{\sqrt{x}} \tag{A.14}$$

where

$$Z = Z_{n+\frac{1}{2}}(x). \tag{A.15}$$

Substituting this into Eq.(A.11) we find that Z satisfies

$$x^2\frac{d^2Z}{dx^2} + x\frac{dZ}{dx} + \left[x^2 - \left(n+\frac{1}{2}\right)^2\right]Z = 0, \tag{A.16}$$

which is Bessel's equation of order $n+\frac{1}{2}$. The solution are $J_{n+1/2}(x)$ and $Y_{n+1/2}(x)$ which, together with the factor $(x)^{1/2}$ means that the solutions for R are the spherical Bessel and Neumann functions, $j_n(x)$ and $y_n(x)$ defined by

$$j_n(x) = \sqrt{\frac{\pi}{2x}}J_{n+1/2}(x), \qquad\qquad y_n(x) = \sqrt{\frac{\pi}{2x}}Y_{n+1/2}(x). \tag{A.17}$$

The functions $j_n(x)$ are regular in every finite domain of the r-plane including the origin, whereas the functions $y_n(x)$ have singularities at the origin $r = 0$ where they become infinite. Hence, we may use $j_n(x)$ but not $y_n(x)$ to represent the wave inside the sphere.

$$R(r) = c_n j_n(x) + d_n y_n(x), \tag{A.18}$$

where c_n and d_n are arbitrary constants. Equation (A.18) represents the solution of (A.11). The general solution of the scalar wave equation can then be expressed as

$$\psi(r,\, \theta,\, \phi) = \sum_{n=0}^{\infty} \sum_{m=-n}^{n} P_n^m(\cos\theta)\, [c_n j_n(x) + d_n y_n(x)]\, (\cos m\phi + i \sin m\phi), \tag{A.19}$$

we note here that $c_n = 1$ and $d_n = i$,

$$j_n(x) + i y_n(x) = \sqrt{\frac{\pi}{2x}} H^{(1)}_{n+1/2}(x) = h^{(1)}_n(x), \tag{A.20}$$

where $H^{(1)}_{n+1/2}$ is the half integral order Hankel function of the first kind. It has the property of vanishing at infinity in the complex plane and is suitable for the representation of the electromagnetic scattering problem. (i.e. scattered wave)

APPENDIX B

DYADIC GREEN'S FUNCTION

B.1 Free-space dyadic Green's function

The dyadic Green's function used in equation (3.23) is related to the scalar Greens function and given in [107]

$$\bar{\mathbf{G}}(\mathbf{r}, \mathbf{r}') = (\bar{\mathbf{I}} + k^{-2}\nabla\nabla)G(\mathbf{r}, \mathbf{r}'), \tag{B.1}$$

where $\mathbf{r}, \mathbf{r}' \in \Re^3, k$ is a positive real number, and the scalar Green's function is expressed as

$$G(\mathbf{r}, \mathbf{r}') = \frac{1}{4\pi}\frac{e^{ik|\mathbf{r}-\mathbf{r}'|}}{|\mathbf{r}-\mathbf{r}'|}, \tag{B.2}$$

$$(\nabla^2 + k^2)G(\mathbf{r}-\mathbf{r}') = -\delta(\mathbf{r}-\mathbf{r}'), \tag{B.3}$$

where $G(\mathbf{r}-\mathbf{r}')$ and $\delta(\mathbf{r}-\mathbf{r}')$ are given by their Fourier transforms as follows:

$$G(\mathbf{r}-\mathbf{r}') = \frac{1}{(2\pi)^3}\int e^{i\mathbf{q}\cdot(\mathbf{r}-\mathbf{r}')}G(\mathbf{q})\,\mathrm{d}^3q, \tag{B.4}$$

$$\delta(\mathbf{r}-\mathbf{r}') = \frac{1}{(2\pi)^3}\int e^{i\mathbf{q}\cdot(\mathbf{r}-\mathbf{r}')}\,\mathrm{d}^3q. \tag{B.5}$$

A substitution of (B.4) and (B.5) into (B.3) leads to

$$\left(\mathbf{q}^2-\mathbf{k}^2\right)G(\mathbf{q}) = 1 \quad \Longrightarrow G(\mathbf{q}) = \frac{1}{\mathbf{q}^2-\mathbf{k}^2}. \tag{B.6}$$

The expression for $G(\mathbf{r}-\mathbf{r}')$ can be obtained by inserting (B.6) into (B.4)

$$G(\mathbf{r}-\mathbf{r}') = \frac{1}{(2\pi)^3}\int \frac{e^{i\mathbf{q}\cdot(\mathbf{r}-\mathbf{r}')}}{q^2-k^2}\,\mathrm{d}^3q, \tag{B.7}$$

$$G(\mathbf{r}-\mathbf{r}') = \frac{1}{(2\pi)^3}\int_0^\infty \frac{q^2\mathrm{d}q}{q^2-k^2}\int_0^\pi e^{iq|\mathbf{r}-\mathbf{r}'|\cos\theta}\sin\theta\,\mathrm{d}\theta\int_0^{2\pi}\mathrm{d}\phi. \tag{B.8}$$

To integrate over angle θ in (B.8) we need to make the variable change $x=\cos\theta$

$$\int_0^\pi e^{iq|\mathbf{r}-\mathbf{r}'|\cos\theta}\sin\theta\,\mathrm{d}\theta = \int_{-1}^1 e^{iq|\mathbf{r}-\mathbf{r}'|x}\,\mathrm{d}x = \frac{1}{iq\,|\mathbf{r}-\mathbf{r}'|}\left(e^{iq|\mathbf{r}-\mathbf{r}'|}-e^{-iq|\mathbf{r}-\mathbf{r}'|}\right). \tag{B.9}$$

Thus, (B.7) becomes

$$G(\mathbf{r}-\mathbf{r}') = \frac{1}{4\pi^2 i\,|\mathbf{r}-\mathbf{r}'|}\int_0^\infty \frac{q}{k^2-q^2}\left(e^{iq|\mathbf{r}-\mathbf{r}'|}-e^{-iq|\mathbf{r}-\mathbf{r}'|}\right)\mathrm{d}q, \tag{B.10}$$

or alternatively expressed as

$$G(\mathbf{r}-\mathbf{r}') = \frac{1}{4\pi^2 i\,|\mathbf{r}-\mathbf{r}'|}\int_\infty^{-\infty} \frac{qe^{iq|\mathbf{r}-\mathbf{r}'|}}{q^2-k^2}\,\mathrm{d}q. \tag{B.11}$$

The integral in (B.11) can be evaluated by the method of residue by closing the contour in the upper half of the q-plane,and this integral is equal to $2\pi i$ times the residue of the integrand at the poles.

Since there are two poles, $q = \pm k$, the integral has two possible values:

The value corresponding to the pole at $q = k$, which lies inside the contour of the upper semi circle becomes

$$G_+(\mathbf{r}, \mathbf{r}') = \frac{1}{4\pi} \frac{e^{ik|\mathbf{r}-\mathbf{r}'|}}{|\mathbf{r} - \mathbf{r}'|}, \tag{B.12}$$

and the value corresponding to the pole at $q = -k$ is written as

$$G_-(\mathbf{r}, \mathbf{r}') = \frac{1}{4\pi} \frac{e^{-ik|\mathbf{r}-\mathbf{r}'|}}{|\mathbf{r} - \mathbf{r}'|}. \tag{B.13}$$

The Green's function $G_+(\mathbf{r}, \mathbf{r}')$ represents an outgoing spherical wave radiated from r' and the function $G_-(\mathbf{r}, \mathbf{r}')$ corresponds to an incoming wave that converges onto r'. Since the scattered waves are outgoing waves, only $G_+(\mathbf{r}, \mathbf{r}')$ is considered for the analysis.

APPENDIX C

THEORETICAL ANALYSIS OF Z-TERM USING HANKEL INTEGRALS METHOD

In the course of this study, many theoretical techniques were explored to analyse the second Born term described in chapter 3 using the Hankel integrals method involving products of integrals Bessel functions discussed in [115, p. 429] and [116]. However, the methods highlighted in this appendix based on Hankel integrals are inadequate to address the core issue of singularity in the domain of integration.

Following the same assumptions of discretizing the regular lattice field into grid points or cells, and modelled the scattering particle by filling it with weighted

contents defined as $k_0^2(\varepsilon - 1)$. For $p = k_0$, thus gives rise to singularity or discontinuity in the contour integral. As a result of the aforementioned reason, the discrete method discussed in § 3.3.1 can not be used to evaluate the U-terms in (3.40).

Unfortunately the approach taken by Hankel and others, cannot be applied essentially because of the power of p in the integrand being odd. This means that it is not possible to use symmetry arguments to extend the integral to the negative axis. The idea is to present these inadequate methods of evaluating the Z-term function and avoid using this kind of integral.

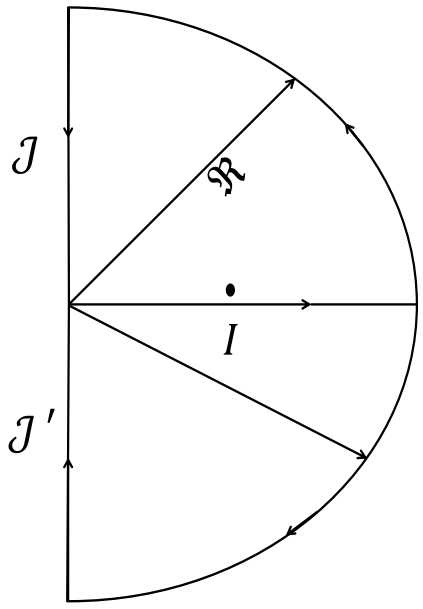

Figure C.1: Geometry of a semi circle split into two equal half with the top half enclosing the pole for the evaluation of the second Born term.

It is worth noting that care need to be exercised with regards to the signs of residues because of the direction of traversing the contours in Figure C.1.

C.1 Hankel integrals combining auxiliary function method

We begin the theoretical analysis by adopting equation (3.40) and expanding the U terms that appear under the integral and expressing it as a summation over cells with other auxiliary functions.

For brevity, we write the U terms as

$$U_j(\mathbf{k}_n, \mathbf{p}) = \gamma(\mathbf{r}_j) \exp\left(-i(\mathbf{k}_n - \mathbf{p}) \cdot \mathbf{r}_j\right) U_0(\mathbf{k}_n, \mathbf{p}), \tag{C.1}$$

and

$$U_i(\mathbf{p}, \mathbf{k}_m) = \gamma(\mathbf{r}_i) \exp\left(-i(\mathbf{p} - \mathbf{k}_m) \cdot \mathbf{r}_i\right) U_0(\mathbf{p}, \mathbf{k}_m). \tag{C.2}$$

Note that for a small size parameter, and where $|k_n| = |k_m| = mk_0$, the U_0 is well approximated by the elementary cell volume. The Z-term now needs to be expressed in terms of the discretized version of U-term

$$\bar{\mathbf{Z}}(\mathbf{k}_n,\, \mathbf{k}_m) = \frac{1}{8\pi^3 k_0^2} \int \frac{p^2}{p^2 - k_0^2} [\bar{\mathbf{I}} - \hat{\mathbf{p}}\hat{\mathbf{p}}] U(\mathbf{k}_n, \mathbf{p})\, U(\mathbf{p}, \mathbf{k}_m)\, \mathrm{d}^3 p, \tag{C.3}$$

then substituting (C.1) and (C.2) into (C.3) and taking summation over r_j and r_i yields:

$$\begin{aligned} \bar{\mathbf{Z}}(\mathbf{k}_n,\, \mathbf{k}_m) = \frac{1}{8\pi^3 k_0^2} \sum_j \sum_i \gamma(\mathbf{r}_j)\gamma(\mathbf{r}_i) \int e^{[-\mathrm{i}(\mathbf{k}_n - \mathbf{p})\cdot \mathbf{r}_j]} e^{[-\mathrm{i}(\mathbf{p} - \mathbf{k}_m)\cdot \mathbf{r}_i]} \\ \cdot U_0(\mathbf{k}_n, \mathbf{p})\, U_0(\mathbf{p}, \mathbf{k}_m) \frac{p^2}{p^2 - k^2} [\bar{\mathbf{I}} - \hat{\mathbf{p}}\hat{\mathbf{p}}]\, \mathrm{d}^3 p. \end{aligned} \tag{C.4}$$

By separation of the radial exponential terms in the U-terms in equation (C.4)

and taking like terms, the $\bar{\mathbf{Z}}$ term is further simplified to the form expressed as

$$\begin{aligned}\bar{\mathbf{Z}}(\mathbf{k}_n,\,\mathbf{k}_m) = \frac{1}{8\pi^3 k_0^2}\sum_j\sum_i \gamma(\mathbf{r}_j)\gamma(\mathbf{r}_i)\ \exp\left(-\mathrm{i}\mathbf{k}_n\cdot\mathbf{r}_j\right)\ \exp\left(\mathrm{i}\mathbf{k}_m\cdot\mathbf{r}_i\right)\\ \cdot\int \exp\left[\mathrm{i}(\hat{\mathbf{p}}\cdot(\mathbf{r}_j-\mathbf{r}_i)p\right]\ U_0(\mathbf{k}_n,\mathbf{p})\,U_0(\mathbf{p},\mathbf{k}_m)\\ \cdot\frac{p^2}{p^2-k^2}[\bar{\mathbf{I}}-\hat{\mathbf{p}}\hat{\mathbf{p}}]\,\mathrm{d}^3p,\end{aligned} \tag{C.5}$$

where $\mathbf{k}_n$, $\mathbf{k}_m$ are array of internal wave vectors respectively, $\gamma(\mathbf{r}_j)$ and $\gamma(\mathbf{r}_i)$ are the polarizabilities given as $k_0^2(\varepsilon-1)$ with respect to distinct cells in the regular 3-dimensional lattice field.

The aim is to evaluate the integral over p by contour integration. The largest contribution to this integral occurs close to the pole so that the U_0 factors in the term are still well approximated by the elementary cell volume (Δv).

Before proceeding, there are some special cases that need to be dealt with considering the following conditions:

1. For identical pair of cells (i.e. $\mathbf{r}_j == \mathbf{r}_i$) or when unit vector ($\hat{\mathbf{p}}$) is orthogonal to the resultant vector of $(\mathbf{r}_j - \mathbf{r}_i)$

2. For distinct cells pair (i.e. $\mathbf{r}_j \neq \mathbf{r}_i$)

Firstly, and simplest to deal with in the conditions highlighted, involves the question of whether the cells labelled i, j involve a distinct or identical pair of cells. Now it can be seen that, generally, when $\mathbf{r}_j \neq \mathbf{r}_i$ the integral is oscillatory along the real axis and may be exponentially small along the appropriate branch of the imaginary axis, but when the integral involves the pairing of a cell with itself or orthogonal to $\hat{\mathbf{p}}$, then $\exp\left[\mathrm{i}(\hat{\mathbf{p}}\cdot(\mathbf{r}_j-\mathbf{r}_i)p\right] = 1$ and (C.5) reduces to the following

form

$$\begin{aligned}\bar{\mathbf{Z}}(\mathbf{k}_n,\,\mathbf{k}_m) = \frac{1}{8\pi^3 k_0^2}\sum_j\sum_i \gamma(\mathbf{r}_j)\gamma(\mathbf{r}_i)\ \exp\left(-\mathrm{i}\mathbf{k}_n\cdot\mathbf{r}_j\right)\ \exp\left(\mathrm{i}\mathbf{k}_m\cdot\mathbf{r}_i\right)\\ \cdot\int\ U_0(\mathbf{k}_n,\mathbf{p})\,U_0(\mathbf{p},\mathbf{k}_m)\frac{p^2}{p^2-k^2}[\bar{\mathbf{I}}-\hat{\mathbf{p}}\hat{\mathbf{p}}]\,\mathrm{d}^3p,\end{aligned} \tag{C.6}$$

now we have to deal with

$$\int_\Omega\int_0^\infty U_0(\mathbf{k}_n,\mathbf{p})\,U_0(\mathbf{p},\mathbf{k}_m)\frac{p^2}{p^2-k^2}[\bar{\mathbf{I}}-\hat{\mathbf{p}}\hat{\mathbf{p}}]\,\mathrm{d}p\,d\Omega. \tag{C.7}$$

In this case the same integral applies for every pairing of a cell with itself, and the problem arises that if we wish to evaluate this by means of contour integration, the behaviour of the integrand on the imaginary axis needs to be considered carefully. For a cubic cell, U_0 takes the form of a three dimensional sinc function, and there are considerable difficulties in obtaining a convergent integral analytically.

Now we may consider a more radical approach in which it is argued that the contribution of these terms should not depend critically on the shape of the cubic cell, but is much more strongly dependent on its volume. Accordingly, we consider instead, substituting for U_0 with U_s, defined as the function for a sphere of equal volume to the basic cubic cell. We also only need to consider how this term behaves at large imaginary p, hence we assign as

$$U_0 \approx U_s = 4\pi\rho^3\frac{J_{\frac{3}{2}}(p\rho)}{\sqrt{p\rho}}, \tag{C.8}$$

and the relationship of the radial part is expressed as

$$abc \approx \frac{4\pi\rho^3}{3}, \qquad a=b=c, \qquad a^3 \approx \frac{4\pi\rho^3}{3}, \tag{C.9}$$

where a, b, c are the dimensions of the cubic cell and the equivalent volume radius ρ is expressed as

$$\rho = a\left(\sqrt[3]{\frac{3}{4\pi}}\right). \tag{C.10}$$

When the argument in (C.8) is small, the half order Bessel function tends to 1/3, so that the term is equal to the cell volume. Neglecting the offset contribution of $\mathbf{k}_n$ and $\mathbf{k}_m$ can be justified by considering an expansion in infinite series of higher order cylinder functions, but it may be assumed that $k_0\rho$ is so small for fundamental cell that the higher term may be neglected. Applying the first condition and note that substituting (C.8) into (C.7), involves integrals of product of Bessel functions of the form [115, p. 429] known as Hankel integrals and expressed as:

$$\begin{aligned} I &= \int_0^\infty \frac{J_\nu(p\rho)\, J_\nu(p\rho)}{\sqrt{p\rho}\,\sqrt{p\rho}} \frac{p^2}{p^2 - k^2}\, dp, \\ &= \frac{1}{\rho}\int_0^\infty J_\nu(p\rho)\, J_\nu(p\rho) \frac{p}{p^2 - k_0^2}\, dp. \end{aligned} \tag{C.11}$$

For brevity, we write

$$\int_0^\infty J_\nu(p\rho)\, J_\nu(p\rho) \frac{p}{p^2 - k_0^2}\, dp = \frac{1}{2}\pi i J_\nu(k_0\rho) H_\nu^{(1)}(k_0\rho), \tag{C.12}$$

where $\nu = n + \frac{1}{2}$ and $n = 1$, with this reduction (C.12) is finite. Note that substituting (C.12) into (C.6) leads to simplification of the Z term to the form expressed as

$$\begin{aligned} \bar{\mathbf{Z}}(\mathbf{k}_n, \mathbf{k}_m) = \frac{4\pi\chi^2}{8\pi^3\rho k_0^2} \sum_j \sum_i \gamma(\mathbf{r}_j)\, \gamma(\mathbf{r}_i)\, \exp\left(-i\mathbf{k}_n \cdot \mathbf{r}_j\right) \\ \cdot \exp\left(i\mathbf{k}_m \cdot \mathbf{r}_i\right) \frac{\mathrm{i}\pi}{2} J_\nu(\rho k_0)\, H_\nu^{(1)}(\rho k_0)\, [\bar{\mathbf{I}} - \hat{\mathbf{p}}\hat{\mathbf{p}}], \end{aligned} \tag{C.13}$$

where $[\bar{\mathbf{I}} - \hat{\mathbf{p}}\hat{\mathbf{p}}]$ is an array of projection vectors in dyadic form, $\hat{\mathbf{p}}$ is a unit vector

and $\chi = 4\pi\rho^3$.

This approach leads to Z-term been expressed as

$$\begin{aligned}\bar{\mathbf{Z}}(\mathbf{k}_n,\, \mathbf{k}_m) = \frac{\mathrm{i}\, 8\rho^6}{k_0} \sum_j \sum_i \exp\left(-i\mathbf{k}_n \cdot \mathbf{r}_j\right) \exp\left(i\mathbf{k}_m \cdot \mathbf{r}_i\right) \\ \cdot\, \gamma(\mathbf{r}_j)\, \gamma(\mathbf{r}_i)\, j_1(\rho k_0)\, h_1^{(1)}(\rho k_0)\, [\bar{\mathbf{I}} - \hat{\mathbf{p}}\hat{\mathbf{p}}],\end{aligned} \tag{C.14}$$

where

$$j_n(\rho k_0) = \sqrt{\frac{\pi}{2\rho k_0}} J_{n+\frac{1}{2}}(\rho k_0), \tag{C.15}$$

and

$$h_n^{(1)}(\rho k_0) = \sqrt{\frac{\pi}{2\rho k_0}} H_{n+\frac{1}{2}}(\rho k_0). \tag{C.16}$$

The notation $[\bar{\mathbf{I}} - \hat{\mathbf{p}}\hat{\mathbf{p}}]$ has the representation

$$\bar{\mathbf{I}} - \hat{\mathbf{p}}\hat{\mathbf{p}} = \begin{pmatrix} 1 - y^2\cos^2\phi & -y^2\cos\phi\sin\phi & -xy\cos\phi \\ -y^2\cos\phi\sin\phi & 1 - y^2\sin^2\phi & -xy\sin\phi \\ -xy\cos\phi & -xy\sin\phi & y^2 \end{pmatrix}, \tag{C.17}$$

where

$$\begin{aligned}\sin^2\theta + \cos^2\theta = 1, \\ y^2 + x^2 = 1,\end{aligned} \tag{C.18}$$

and

$$y^2 = 1 - x^2. \tag{C.19}$$

For a distinct pair of cells, that is when $[\hat{\mathbf{p}} \cdot (\mathbf{r}_j - \mathbf{r}_i)] \lesseqgtr 0$ or $\mathbf{r}_j \neq \mathbf{r}_i$. The angular integral over solid angle (Ω) using a numerically weighted summation result to evaluation of the Z-term differently from identical pair of cells discussed by applying two different approaches.

Now we consider when $[\hat{\mathbf{p}} \cdot (\mathbf{r} - \mathbf{r}')] > 0$. In order to evaluate this condition, the U_0 factors in the terms are well approximated by the cubic cell volume $\Delta v = a^3$, and the integral part of (C.5) is modified to a known function called the axillary function which involves sine, cosine and exponential integrations, as defined in [121, p. 227 - 237]

$$\begin{aligned} F(x) &= \int_0^\infty \frac{\sin(t)}{t+x} dt = \int_0^\infty \frac{e^{-xt}}{t^2+1} dt, \\ F(x) &= C_i(x)\sin(x) - \left[\frac{\pi}{2} - S_i(x)\right]\cos(x). \end{aligned} \tag{C.20}$$

After some manipulation, the infinite radial integral in (C.5) is transformed to the form given by

$$I = \int_0^\infty \frac{\exp(-\beta q)}{q^2 + k_0^2} q^2 dq, \tag{C.21}$$

where $\beta = [\hat{\mathbf{p}} \cdot (\mathbf{r} - \mathbf{r}')]$ and $q = ip$. Further manipulation and scaling of equation (C.21) is carried out as follows

$$I = \int_0^\infty \left[\frac{k_0^2 + q^2}{k_0^2 + q^2} - \frac{k_0^2}{k_0^2 + q^2}\right] \exp(-\beta q) dq, \tag{C.22}$$

and simplifying (C.22) into to the form given as

$$\begin{aligned} I &= \int_0^\infty \exp(-\beta q)\left[1 - \frac{k_0^2}{k_0^2 + q^2}\right] dq, \\ &= \int_0^\infty \exp(-\beta q) dq - \int_0^\infty \frac{k_0^2 \exp(-\beta q)}{k_0^2 + q^2} dq, \end{aligned} \tag{C.23}$$

where the first integral on the right hand side of equation (C.23) becomes

$$\int_0^\infty \exp(-\beta q) dq = \frac{1}{\beta}, \tag{C.24}$$

and the second integral is divided through by a factor of k_0 which yields a similar form of axillary function given in (C.20)

$$\int_0^\infty \frac{k_0^2 \exp(-\beta q)}{k_0^2 + q^2} dq = k_0 \int_0^\infty \frac{\exp(-\beta \alpha k_0)}{\alpha^2 + 1} d\alpha, \tag{C.25}$$

where $\alpha = \dfrac{q}{k_0}$. Combining analysis from both (C.24) and (C.25) gives

$$\begin{aligned} I &= \frac{1}{\beta} - k_0 \int_0^\infty \frac{\exp(-\beta \alpha k_0)}{\alpha^2 + 1} d\alpha, \\ &= \frac{1}{\beta} \left[1 - \beta k_0 F(\beta k_0)\right]. \end{aligned} \tag{C.26}$$

Hence, comparing coefficients of (C.20) and (C.26), it is possible to write $F(\beta k_0)$ as

$$F(\beta k_0) = C_i(\beta k) \sin(\beta k_0) - \left[\frac{\pi}{2} - S_i(\beta k_0)\right] \cos(\beta k_0). \tag{C.27}$$

Substituting equation (C.26) into (C.5) leads to expressing the Z-term as

$$\begin{aligned} \bar{\mathbf{Z}}(\mathbf{k}_n, \mathbf{k}_m) = \frac{4\pi}{8\pi^3 k_0^2} \sum_j \sum_i &\exp(i\mathbf{k}_n \cdot \mathbf{r}_j) \exp(i\mathbf{k}_m \cdot \mathbf{r}_i) \\ &\cdot \gamma(\mathbf{r}_j)\gamma(\mathbf{r}_i) \Delta v^2 \frac{1}{\beta} \left[1 - \beta k_0 F(\beta k_0)\right] [\bar{\mathbf{I}} - \hat{\mathbf{p}}\hat{\mathbf{p}}]. \end{aligned} \tag{C.28}$$

To complete the theory of the Z-term for the distinct pair of cells, we need to consider another case when $\beta = [\hat{\mathbf{p}} \cdot (\mathbf{r} - \mathbf{r}')] < 0$. In this case, the purpose of this approach is to evaluate the integral over p by contour integration as defined in [122, p. 262 - 265]

$$\oint_c f(z) dz = 2\pi i \sum_{k=1}^{n} Res(f, z_k). \tag{C.29}$$

where $Res(f, z_k)$ denotes the residue of f at the singularity z_k. Hence, if f satisfies condition at the pole, then taking the limit as the real axis tends to infinity, the contour integral over the arc vanishes by Jordan's Lemma method as discussed in [122] and we get the value of the improper integral to be evaluated.

Now we need to carry out contour integration by expressing the integral part of (C.5) as

$$I = \int_0^\infty \exp\left[\mathrm{i}(\hat{\mathbf{p}} \cdot (\mathbf{r}_j - \mathbf{r}_i)p\right] U_0(\mathbf{k}_n, \mathbf{p})\, U_0(\mathbf{p}, \mathbf{k}_m) \frac{p^2}{p^2 - k^2} \mathrm{d}p, \tag{C.30}$$

but the U_0 factors in this case also need to be well approximated by the cell volume Δv. This approach reduces the evaluation of equation (C.30) and it is expressed in another form

$$\begin{aligned}
I &= \Delta v^2 \int_0^\infty \exp\left[\mathrm{i}(\hat{\mathbf{p}} \cdot (\mathbf{r}_j - \mathbf{r}_i)p\right] \frac{p^2}{p^2 - k_0^2}\, dp, \\
&= \Delta v^2 \int_0^\infty \exp\left[\mathrm{i}(\hat{\mathbf{p}} \cdot (\mathbf{r}_j - \mathbf{r}_i)p\right] \frac{p^2}{(p + k_0)(p - k_0)}\, dp, \\
&= \lim_{p \to k_0} dv^2 \int_0^\infty \exp\left[\mathrm{i}(\hat{\mathbf{p}} \cdot (\mathbf{r}_j - \mathbf{r}_i)p\right] \frac{(p - k_0)\, p^2}{(p + k_0)(p - k_0)}\, dp, \\
&= 2\pi i \frac{k_0}{2} \exp\left[\mathrm{i}(\hat{\mathbf{p}} \cdot (\mathbf{r}_j - \mathbf{r}_i)k_0\right] \Delta v^2, \\
&= i\pi k_0\, \Delta v^2 \exp\left[\mathrm{i}(\hat{\mathbf{p}} \cdot (\mathbf{r}_j - \mathbf{r}_i)k_0\right].
\end{aligned} \tag{C.31}$$

The Z-term in this case is now evaluated by substituting (C.31) into (3.55) which

leads to the form

$$Z(k_n,\, k_m) = \frac{4\pi}{8\pi^3 k_0^2} \sum_j \sum_i \exp\left(-i\mathbf{k}_n \cdot \mathbf{r}_j\right)\, \exp\left(i\mathbf{k}_m \cdot \mathbf{r}_i\right) \cdot \gamma(\mathbf{r}_j)\gamma(\mathbf{r}_i)\, i\pi k_0^2\, \Delta v^2\, \beta\, [\bar{\mathbf{I}} - \hat{\mathbf{p}}\hat{\mathbf{p}}], \tag{C.32}$$

where $\beta = \exp\left[\mathrm{i}(\hat{\mathbf{p}} \cdot (\mathbf{r}_j - \mathbf{r}_i)p\right]$.

C.2 Hankel integral combining partial expansion method

A class of infinite integral approach given in [116] and [115] have been adapted to express the U terms and avoid the constraints imposed at the domain of integrations. Thus, we expand and express the $U(\mathbf{k}_n, \mathbf{p})$ function in (3.48) as

$$U(\mathbf{k}_n, \mathbf{p}) = \int \gamma(\mathbf{r})\, \exp(i\mathbf{k}_n \cdot \mathbf{r}) \exp(-i\mathbf{p} \cdot \mathbf{r})\, d^3r. \tag{C.33}$$

Note, we expand $\exp(-i\mathbf{p} \cdot \mathbf{r})$ as given in [115, p. 128]

$$\exp(-i\mathbf{p} \cdot \mathbf{r}) = \exp(-ipr\cos\theta),$$

$$\exp(-ipr\cos\theta) = \left(\frac{2\pi}{pr}\right)^{\frac{1}{2}} \sum_{n=0}^{\infty} c_n\, (-i)^n\, J_{n+\frac{1}{2}}(pr)\, P_n(\cos\theta), \tag{C.34}$$

where $P_n(\cos\theta)$ is the Legendre polynomials, $J_{n+\frac{1}{2}}(pr)$ is the half order Bessel function, n is the order of Bessel term to be evaluated and so $c_n = n + \frac{1}{2}$; thus

leads to the expression

$$\exp(-ipr\cos\theta) = \left(\frac{2\pi}{pr}\right)^{\frac{1}{2}} \sum_{n=0}^{\infty} (n+\frac{1}{2})\,(-i)^n\, J_{n+\frac{1}{2}}(pr)\, P_n(\cos\theta), \tag{C.35}$$

of which a detailed proved of this expression is given in [115, p. 127 - 128]. Again, the same analytical procedure is used to expand $U(\mathbf{p}, \mathbf{k}_m)$ and the complete expansion of the U terms thus, leads to Hankel's integrals involving products of Bessel functions.

$$\bar{\mathbf{Z}}(\mathbf{k}_n, \mathbf{k}_m) = \int \sum_{m,n} f(m, r, k_m, p)\, f(n, r', p, k_n) I(m, n, r, r')\, \bar{\mathbf{J}}_p \,\mathrm{d}^3 r\, \mathrm{d}^3 r'\, d^3 p, \tag{C.36}$$

where

$$I(m, n, r, r') = \int_V \sum_{m,n} \frac{p^2\, J_{n+\frac{1}{2}}(pr')\, J_{m+\frac{1}{2}}(pr)}{p^2 - k_0^2 - i\varepsilon}\, \mathrm{d}^3 r\, \mathrm{d}^3 r'\, d^3 p. \tag{C.37}$$

The integral equation (C.37) resemble those expressed in [115, § 13.53] and we use the expansion as investigated by Hankel's by applying contour integration to the integrand to obtain

$$I(m, n, r, r') = \begin{cases} \dfrac{1}{2}\, i\pi\, k_0\, J_n(k_0 r') H_m(k_0 r) & \text{if } r \geq r' > 0 \\ \dfrac{1}{2}\, i\pi\, k_0\, H_n(k_0 r') J_m(k_0 r) & \text{if } r' > r \end{cases} \tag{C.38}$$

For the problem of interest, the poles are close to the real axis which results in the right hand side of equation (C.38) being expressed as the product of a Bessel function of the first kind and a Hankel functions.

Taking into consideration the existence of the discontinuity in the domain of integration, the contour integral is carried out in a semicircle split into two half

with the pole in one half. The Hankel functions in (C.38) are evaluated with one goes up the imaginary axis ($r \geq r'$) and the other down ($r' > r$), based on the conditions described in [116] these parts cancel out completely. Care need to be exercised with regards to the signs of residues because of the direction of traversing the contours.

The mathematical expression of $f(m, r, k_m, p)$ and $f(n, r', p, k_n)$ functions given in (C.37) are similar and can be expressed as

$$f(m, r, k_m, p) = \int \sum_{m=0} \exp(-\mathbf{k}_m \cdot \mathbf{r}) \gamma(\mathbf{r}) P_m \cos\theta \, \mathrm{d}^3 r, \tag{C.39a}$$

$$f(n, r', p, k_n) = \int \sum_{n=0} \exp(\mathbf{k}_n \cdot \mathbf{r}') \gamma(\mathbf{r}') P_n \cos\theta \, \mathrm{d}^3 r'. \tag{C.39b}$$

Combining the expansion through (C.37) to (C.39) again we solve the second Born series term by evaluating integral by method of numerical quadrature and can be expressed as

$$\bar{\mathbf{Z}}(\mathbf{k}_n, \mathbf{k}_m) = \sum_{m,n,p} f(m, r, k_m, p) \, f(n, r', p, k_n) \, I(m, n, r, r') \, [\mathbf{I} - \hat{\mathbf{p}} \, \hat{\mathbf{p}}]. \tag{C.40}$$

APPENDIX D

LIST OF PUBLICATIONS

The following papers have been presented in workshop and published in conference proceedings.

F.O. Ngobigha, and D.H.O. Bebbington. Scattering of electromagnetic waves by offset spherical particles. In *Second International Conference on Telecommunications and Remote Sensing (ICTRS 2013)*, Netherlands, 11-12 July 2013.

F.O. Ngobigha, and D.H.O. Bebbington. Theoretical Analysis and Evaluation of Scattering Characteristics by Inhomogeneous Particles using Fredholm Integral Equation Approach : A Workshop of UK Festival of Radio Science URSI, 18 September 2013, University of Birmingham.

Bebbington, David H O and Ngobigha, Felix O and Carrea, Laura. Advances in polarimetric radar scattering - modelling and analysis. In: Scattering, Clouds and Climate: A Short Workshop of Exploration, 24-25 March 2014, University of Oxford.

F.O. Ngobigha, and D.H.O. Bebbington. Electromagnetic waves scattering by dielectric ellipsoids applying integral equation approach. *Radio Science Meeting (Joint with IEEE AP-S Symposium), 2014 USNC-URSI*, Memphis, TN, USA, 6-11 July 2014.

F.O. Ngobigha, D.H.O. Bebbington, and C. Laura. Discrete numerical approach to the Fredholm Integral Method for evaluating microwave scattering by irregular dielectric particles. Ready to be submitted to *IEEE-APS* Transaction.